

**Molecular Characterisation of Primary Wool Follicle
Initiation in Merino Sheep**

Hayley Ann McGrice BBiotech (HONS)

June, 2009

This thesis is submitted in partial fulfilment of the award of PhD in the
Discipline of Agricultural and Animal Science, School of Agriculture, Food and
Wine,
University of Adelaide, South Australia

Table of Contents

Abstract	ii
Declaration	iv
Acknowledgements	v
Abbreviations	vii
Chapter 1 Introduction and Literature Review	2
1.1 Introduction	2
1.2 Structure and Development of the Wool Follicle	4
1.2.1 Structure and Function of Mammalian Skin	4
1.2.2 Wool Follicle Types	5
1.2.2.1 Primary Follicles	6
1.2.2.2 Secondary and Secondary-Derived Follicles	6
1.2.2.3 Secondary to Primary Ratio (S/P ratio)	8
1.2.3 Molecular Basis of Primary Follicle Neogenesis	8
1.2.3.1 First Dermal Signal: Formation of the Epidermal Placode	9
1.2.3.2 First Epidermal Signal: Formation of the Dermal Condensate	13
1.2.3.3 Down growth of the epidermal placode	13
1.2.3.4 Formation of the dermal papilla	14
1.2.3.5 Formation of the Follicle Bulb	14
1.2.3.6 Inner Root Sheath (IRS)	15
1.2.3.7 Outer Root Sheath (ORS)	16
1.2.3.8 Follicle Accessory Structures	16
1.2.3.8.1 Sebaceous Gland	16

1.2.3.8.2	Sweat Glands (Primary Follicles Only)	17
1.2.3.8.3	Arrector Pili Muscle (Primary Follicles Only).....	17
1.3	Stem Cells in the Skin	17
1.3.1	Embryonic vs Adult Stem Cells	18
1.3.2	Epidermal Stem Cells	19
1.3.3	Dermal Stem Cells.....	19
1.3.4	Division and Maintenance of Stem Cell Populations	20
1.3.5	Location of Stem Cells in the Hair/Wool Follicle.....	21
1.3.5.1	Mechanisms of Follicle Initiation: Reaction Diffusion Theory vs. Founder Cell Theory.....	22
1.3.5.2	Dermal Condensates: Proliferation, Migration or Both?.....	24
1.4	Summary	25
1.5	Project Aims and Hypothesis	26
Chapter 2	General Materials and Methods	28
2.1	Materials	28
2.2	Foetal Tissue Collection	28
2.3	RNA isolation and purification	28
2.4	Estimation of RNA concentration and assessment of RNA integrity	29
2.5	RT-PCR of isolated RNA for cDNA production	29
2.6	Optimisation of PCR conditions for isolation of sheep cDNA sequences.....	30
2.7	Analysis of PCR products by agarose gel electrophoresis.....	30
2.8	Preparation of PCR template and automated sequencing	31
2.9	Optimisation of quantitative RT-PCR reaction conditions.....	31
Chapter 3	Foetal Skin Series and Histology	34
3.1	Introduction	34

3.2	Specific Methods.....	34
3.2.1	Matings.....	34
3.2.2	Generation of Foetal Skin Series	34
3.2.3	Crown Rump Length Measurements	35
3.2.4	Processing, Embedding and Sectioning.....	36
3.2.5	Haematoxylin and Eosin Staining.....	37
3.2.6	SacPic Staining	38
3.2.7	Histology Images	39
3.2.8	Statistical Analysis	39
3.3	Results	40
3.3.1	Foetal Measurements	40
3.3.1.1	Foetal Data Comparison with a Previous Study	43
3.3.2	Histological Characterisation.....	45
3.4	Discussion.....	48
3.4.1	Foetal Sample Series	48
3.4.2	Histological Characterisation.....	51
3.5	Conclusion.....	52
Chapter 4	: Quantitative PCR Analysis of Whole Skin.....	54
4.1	Introduction	54
4.1.1	Normalisation of qRT-PCR data: geNorm.....	55
4.1.2	Candidate Genes for qPCR Analysis of Wool Follicle Initiation.....	56
4.1.2.1	Actin-based Fibroblast Migration	56
4.1.2.2	Skin Stem Cell Markers	56
4.1.2.3	Cell Proliferation	58
4.1.2.4	Tumor Necrosis Factor Signalling in Hair Follicle Development.....	59
4.1.2.5	Sonic Hedgehog Signalling in Hair Follicle Development.....	60

4.2	Aim.....	62
4.3	Specific Methods.....	62
4.3.1	qRT-PCR	62
4.3.2	geNorm Analysis and Normalisation of qPCR data	63
4.3.3	Statistical Analysis of Relative Expression Patterns.....	64
4.4	Results	64
4.4.1	RNA extractions	64
4.4.2	geNorm Analysis.....	66
4.4.3	Gene Expression Analysis.....	70
4.4.3.1	Migration Markers.....	70
4.4.3.2	Stem Cell Markers	72
4.4.3.3	Proliferation Markers	74
4.4.3.4	Tumor Necrosis Factor Signalling Pathway Members.....	76
4.4.3.5	Sonic Hedgehog Signalling Pathway	82
4.4.3.6	Gene Expression Correlations	84
4.5	Discussion	85
4.5.1	Gene Expression Analysis of Candidate Migration Markers	87
4.5.2	Gene Expression Analysis of Candidate Stem Cell Markers	88
4.5.3	Gene Expression Analysis of Candidate Cell Proliferation Markers.....	89
4.5.4	Ectodysplasin Signaling During Primary Wool Follicle Initiation	90
4.5.5	Gene expression analysis of Sonic Hedgehog and Patched-1 during primary follicle development	94
4.5.6	Differences in Gene Expression between the Midside and Rump	95
4.6	Conclusion.....	97
Chapter 5	: Laser Capture Microdissection of Foetal Sheep Skin	99
5.1	Introduction	99

5.2	Aim.....	100
5.3	Specific Methods.....	100
5.3.1	Frozen tissue sectioning and fixation.....	100
5.3.2	Haematoxylin and Eosin staining of frozen sections for laser capture microdissection	100
5.3.3	Laser Capture Microdissection Protocol	101
5.3.4	RNA extraction from laser captured tissue	102
5.3.4.1	TRIZOL and RNAqueous Micro Extraction Protocols	102
5.3.4.2	Qiagen RNeasy Micro Extraction Kit	103
5.3.5	Estimation of RNA quality and quantity	103
5.3.6	Reverse Transcription of RNA	104
5.3.7	Cells Direct One-Step Kit	104
5.4	Results	104
5.4.1	Optimisation of Sectioning and Staining for Laser Capture Microdissection.....	104
5.4.2	Optimisation of RNA extraction and RT-PCR of Laser Capture Microdissected Material	107
5.4.3	Optimisation of Slide Type for Laser Pressure Catapulting.....	112
5.4.4	Laser capture microdissection and qRT-PCR analysis of follicle regions vs. non-follicle regions of foetal sheep skin.	116
5.5	Discussion	121
5.6	Conclusion.....	129
Chapter 6	General Discussion	131
6.1	Introduction	131
6.2	Future Work	145
6.3	Conclusion.....	147

Appendix I: General Solutions, Buffers and Stains.....	149
Appendix II: Primers.....	153
References.....	155

Abstract

Primary wool follicles are initiated in the skin of sheep foetuses at approximately day 50 of gestation as the result of complex reciprocal molecular interactions between the mesenchyme and overlying epithelium. The lifetime wool production potential and fibre diameter of the Merino sheep is dependent on the total number of follicles initiated *in utero*. Understanding the molecular events that surround primary wool follicle initiation may provide approaches to enhance or manipulate this process in order to maximise the profitability of wool production enterprises.

In order to study the morphological and molecular changes occurring during early wool follicle development, a foetal skin series spanning primary follicle initiation was generated. Foetal skin was sampled from the shoulder, midside and rump of four foetuses at 8 time points between day 43 and day 68 of gestation. Histological characterisation of the shoulder skin samples revealed that primary epidermal placodes emerged at around day 53, dermal condensates were visible from day 57 and downgrowth of the follicle began at day 68. An equation relating age of the foetus (day of gestation post AI) and crown-rump length, specific to Merino foetuses, was developed for use in future studies of this nature.

Molecular markers of fibroblast migration, epidermal and dermal stem cells and cell proliferation were selected to test the hypothesis that dermal condensates are initiated at discrete sites beneath the epidermis as a result of a combination of migration and arrangement of multipotent pre-papilla cells. Quantitative reverse transcription polymerase chain reaction (qRT-PCR) analysis of *RAC1* and *RHOa* (migration markers), *β 1-integrin* and *alkaline phosphatase* (stem cell markers), *proliferative nuclear cell antigen* and *cyclinB1* (proliferation markers), *patched-1*, selected tumor necrosis factor (TNF) signalling molecules and eleven reference genes was conducted using midside and rump skin samples from each of four foetuses from the 8 time points. geNorm analysis of the reference and target genes revealed that the migration markers *RAC1* and *RHOa* along with *GAPDH* were the most stably

expressed genes in this sample series. Significant changes in mRNA expression were detected for *β1-integrin*, *alkaline phosphatase*, *patched-1* and the TNF members *EDA*, *EDAR*, *TROY* and *TRAF6*. Many of these significant differences in expression coincided with key morphological events. Significant differences in expression were also detected between the midside and rump samples for numerous transcripts.

Laser capture microdissection (LCM) was implemented for analysis of the target transcripts within particular structures of foetal sheep skin. Frozen tissue sectioning, staining, LCM, RNA extraction and cDNA synthesis were optimised for qRT-PCR analysis of endogenous controls and selected TNF transcripts. Several RNA extraction methods and reverse transcription approaches were trialled to ensure optimum extraction and reverse transcription efficiency for this tissue type. Exogenous mRNA transcripts were also incorporated prior to RNA extraction and reverse transcription to track reaction efficiency between samples. A comparison of different slide types revealed that laser pressure catapulting from membrane slides was an absolute requirement for foetal skin tissue studies. Follicle regions (including the epidermal placode and dermal condensate) and the adjacent non-follicle regions were laser captured from foetal skin, and the mRNA expression levels of *patched-1* and selected TNF members was compared. Preliminary qRT-PCR analysis using this technique revealed that *EDAR*, *TROY* and *PTCHI* mRNA levels were higher in the follicle regions than the non-follicle regions.

The TNF signalling pathway appears to play an important role in primary wool follicle initiation and patterning at different sites on the body. Spatial differences in expression of some of these regulators may be involved in initiating different types of follicles. The molecular events surrounding primary wool follicle initiation also show a high degree of conservation between sheep, humans, and mice. Considering the high degree of DNA sequence conservation as well as the histological, signalling and cycling similarities between sheep and humans, sheep may represent a better model for the study of human hair follicle initiation and disease than the currently used mice and rat models.

Declaration

This work contains no material which has been accepted for the award of any other degree or diploma in any university or other tertiary institution and, to the best of my knowledge and belief, contains no material previously published or written by another person, except where due reference has been made in the text.

I give consent to this copy of my thesis, when deposited in the University Library, being made available for loan and photocopying, subject to the provisions of the Copyright Act 1968.

Date

Hayley Ann McGrice

Acknowledgements

First and foremost I would like to thank Australian Wool Innovation for their scholarship and research funding. Without your financial support this thesis would not have been possible.

A loud and resounding thank you must go to my supervisors Dr Cynthia Bottema, Dr Greg Natrass and Prof Philip Hynd. Cindy you were always there for me and I can't thank you enough for everything you have done for me over the last four years. The speed at which you read and returned my chapters to me was absolutely amazing and the lengths that you went to in order to support me during my PhD candidature were above and beyond the call of duty, so thank you, from the bottom of my heart. To my technical supervisor Greg, thank you for listening to and answering my silly questions over and over again and for all your advice and assistance in the lab, especially in the large scale qRT-PCR experiment design and undertaking. The chats we had over a quite beer on a Friday afternoon were probably the most valuable in terms of understanding and interpreting the "disco" science. Phil, thank you for nurturing my love of writing on the whiteboard, you have a unique gift for helping people to build and get excited about crazy hypotheses. Your wordsmith skills were also greatly appreciated when writing the conference abstracts and of course, this thesis. The three of you were an excellent supervision team and I greatly appreciate all your support.

Special thanks to Dr Simon Bawden for initially creating the project, awakening my interest in wool research and for your continued guidance and advice during an extremely challenging PhD candidature. Thank you also to Dr Stephanie Dunn and Clive McLaughlin from the SARDI molecular team for your technical advice, assistance and friendship, I think we had about as much fun as anyone could have in a molecular lab!

To Dr Michelle Hebart and A.Prof Wayne Pitchford, thank you a thousand times over for your assistance with the statistical analysis and interpretation, stats are not my strong point and I definitely could not have done this without you.

A special mention must also go to Natasha Edwards, Dr Melanie McDowall, and the Roseworthy wool group. Thank you for all your friendship, laboratory assistance and constructive feedback when preparing conference presentations as well as helping me to build explanations for the results along the way.

To all the farm staff at Turretfield Research Centre, thank you for your expertise and assistance with the animal sampling and for your friendship.

To my best friend and office buddy Dr Rebecca Forder, we laughed and we cried together as we rode the PhD rollercoaster. Thank you for being an excellent shoulder to cry on, an open sympathetic ear, someone to laugh with and an excellent role model when it came to finishing this thesis. Thanks also for assisting me with the tissue collection and for your help with the thesis formatting, not to mention the baby sitting that helped get me over the line. On that note, thank you also to Nana Sue and Uncle Gary John for your assistance with Colby care; babies and thesis writing do not mix! I could not have done this without the Forder's.

Thank you also to Tone for being there for me during the emotionally challenging animal sampling and for putting up with the stress fuelled outbursts at various times along the way. Twas a long PhD road for us both!

Last but by no means least, special thanks goes to my Mum and Kylie, you guys were there for me when everything went wrong, you both helped me get back on my feet, and for that I will forever be in your debt. I nearly gave it all up and it was your support and strength that got me through the roughest patch of my life. Thank you for all the babysitting too mum, you're a class 1A mum and Nana.

Thank you all from the bottom of my heart!

Abbreviations

°C	degrees Celsius
μl	microlitres
μm	micrometres
ACTB	β-Actin
ALP	Alkaline phosphatase
BCC	basal cell carcinoma
BMP	bone morphogenic proteins
bp	base pairs
CAT	chloramphenicol transferase
CD34	CD34 antigen
Cdc42	Cell Division Cycle related family member 42
cDNA	complementary DNA
CDK-1	cyclin dependent kinase 1
CIDR	controlled internal releasing device
cm	centimetres
COLL3AIII	collagen type 3AIII
CoV	coefficient of variation
CRL	crown rump length
C _t	cycle threshold
CYC B1	cyclin B1
d	day
EDA	ectodysplasin A1
EDAR	ectodysplasin A1 receptor
EDARADD	ectodysplasin A1 receptor death domain
EDTA	ethylenediaminetetraacetic acid

EM	epithelial:mesenchymal
FD	fibre diameter
FGF	Fibroblast growth factor
FGFR	FGF receptor
GAPDH	glyceraldehyde 3-phosphate dehydrogenase
GLI1	GLI family zinc finger 1
GSP	gene specific primers
GTP	guanosine-5'-triphosphate
hrs	hours
IKK	I κ B kinase complex
IRS	inner root sheath
KRT5	keratin-5
LCM	laser capture microdissection
LEF/TCF	lymphoid enhancer-binding factor/T cell factor
LPC	laser pressure catapulted
LUC	luciferase
mA	milliamps
MIB-1	mind bomb-1
mins	minutes
mM	millimolar
mm	millimetres
NF- κ β	nuclear factor-kappa-beta
ng	nanograms
nm	nanometres
nmol	nanomoles
OCT	optimal cutting temperature
oligo dTVN	oligonucleotide dTNV combination

PALM	photo-activated localisation microscopy
PCNA	proliferative cell nuclear antigen
PBS	phosphate buffered saline
PCR	polymerase chain reaction
PTCH1	patched-1
qRT-PCR	quantitative reverse transcriptase PCR
RAC1	ras-related C3 botulinum toxin substrate 1
RHOa	Ras homolog gene family, member A
RLT buffer	RNeasy lysis buffer
RO	reverse osmosis
RPL19	Ribosomal protein large 19
RT	remnant tissue
SAS	statistical analysis software
sec	seconds
SEM	standard error of the mean
SHH	sonic hedgehog
S:P ratio	secondary to primary ratio
TE buffer	Tris-EDTA buffer
TGF- β 2	Transforming growth factor –beta 2
TNF	Tumor necrosis factor
TRAF	Tumor necrosis factor associated factors
TROY	tumor necrosis factor receptor superfamily, member 19
V	volts
WNT	wingless-type
XEDAR	X-linked ectodysplasin receptor
YWHAZ	tyrosine 3-monooxygenase /tryptophan 5-monooxygenase activation protein, zeta polypeptide

This thesis is dedicated to my mum Jan and my daughter Colby

Thank you for teaching me the value of education mum,

may I instil the same important values in Colby.

Chapter One

Introduction and Literature Review

Chapter 1 Introduction and Literature Review

1.1 Introduction

Australia is the world's largest producer of wool, with wool exports valued at AUD \$2.64 billion in 2005/2006. The Australian sheep flock of over 100 million sheep is composed of over 88% Merino, 9% crossbred and 3% other breeds (as at 1st January, 2007) and produced 461 million kg of greasy wool during this financial year. Wool is natural, biodegradable, naturally flame resistant and absorbent, and accounted for 1.9% of total world fibre use in 2006 (The Woolmark Company, 2006, AWTA Ltd., 2006).

The major determinants of wool value are average fibre diameter, staple strength and clean fleece weight, all of which have a strong genetic component. In order to maximise the profits from their annual clip, the main objective of many wool producers is to decrease the average fibre diameter whilst maintaining or increasing clean fleece weight. This can be achieved by increasing follicle density as there is a strong negative genetic correlation between fibre diameter and follicle density (-0.65 ± 0.12), and clean fleece weight has a positive genetic correlation of 0.35 ± 0.19 with follicle density in fine wool Merinos (Barton et al., 2001). Staple strength, the second most important determinant of wool value, has a heritability of 0.4 (Hynd, 1995) and a positive genetic correlation of 0.27 with fibre diameter, as determined in the CSIRO fine wool flock (Swan et al., 1995). Wool clips with a staple strength of <30 N/ktex are consistently discounted at sale (Greeff et al., 1995).

There are three types of wool follicles: primary, secondary and secondary-derived or branched follicles. A strong negative correlation between fibre diameter and the ratio of secondary to primary follicles (S:P ratio) has been previously shown (Purvis and Swan, 1997), indicating that the total number of secondary and secondary-derived follicles is the main contributor to the variation observed in fibre diameter, follicle density and clean fleece weight.

Follicle formation occurs only once in any mammal's lifetime. At birth, the entire follicle population has been initiated and normally does not change thereafter (Hocking Edwards et al., 1996). Previous attempts to induce follicle formation in adult sheep skin have failed (Thomas, 2002), indicating that there is either a limited number of follicle inductive cells in the skin (e.g. stem cells), or that the molecular signals required to initiate follicle formation are developmentally regulated and active only during foetal development.

Over the last two decades, a significant amount of research has been devoted to identifying and characterising the signalling molecules involved in human, mouse and rat hair follicle development and cycling (Stenn and Paus, 2001; Millar, 2002; Botchkarev and Paus, 2003). This type of research is highly relevant to the sheep industry because there is morphological conservation in skin appendage initiation amongst mammals. Therefore, sheep can be considered as a relevant model for human hair research. Although several key signals regulating hair and/or wool follicle formation remain unknown or are only partially characterised, recent studies have led to an explosion of information regarding signalling in the developing follicle, perhaps providing the opportunity for pharmaceutical or nutritional intervention. The development of an agricultural pharmaceutical or food additive that could possibly increase the number of follicles initiated and/or increase follicle branching could greatly increase the profits of wool producers.

Given the relationship between the number of follicles initiated during neogenesis (initiation of a new hair/wool follicle from an undifferentiated epithelium) and the key determinants of wool value, the focus of this thesis is primary follicle initiation. Primary follicle initiation was chosen as the focus of this project, as opposed to secondary follicle initiation for two reasons: (1) the number, size and spacing of primary follicles is thought to be important in the establishment of the follicle pattern, and (2) the dynamic change from an undifferentiated epithelium to a complex and organised array of primary follicles provides a more simplified model of the molecular signals utilised in wool follicle initiation. The

relevant literature on the structural characterisation, signalling pathways and stem cell involvement in primary hair/wool follicle initiation will be reviewed, current to 2006.

1.2 Structure and Development of the Wool Follicle

1.2.1 Structure and Function of Mammalian Skin

The skin is the largest and one of the most important organs in mammals. It protects the animal from external injury, receives sensory impulses, excretes various substances, and assists in thermo-regulation (Bloom and Fawcett, 1962). The epidermis (or surface epithelium) and dermis (or corneum) are the two main layers of the skin (Figure 1-1). The epidermis is completely devoid of blood vessels and consists of a multi-layered epithelium that is self renewing for the life of the animal, a process mediated by multipotent stem cells that reside at the basal layer (section 1.3.2 and Figure 1-5). The dermis underlies the epidermis and consists of a loose connective tissue composed of fibrous protein, collagen, elastin and reticulin. Blood vessels, nerves and lymphatics traverse through the dermis providing nourishment and sensation to the overlying epidermis (Montagna and Parakkal, 1974). Beneath the dermis is a loose layer of connective tissue known as the hypodermis, which in places is known to transform into subcutaneous fatty tissue in places. In vertebrate embryos, the epidermis differentiates from the surface ectoderm and the dermis is derived from blocks of tissue called somites, formed from the mesoderm (Thomas, 2002). The surface of contact between the mature dermis and epidermis is uneven and the two can only be separated enzymatically (Bloom and Fawcett, 1962).

NOTE:
This figure is included on page 5
of the print copy of the thesis held in
the University of Adelaide Library.

Figure 1-1_ The structure of mammalian skin (Alonso and Fuchs, 2003b)

1.2.2 Wool Follicle Types

The stages of development of wool follicles were first described in detail by Hardy and Lyne (1956), a publication that is routinely referred to in most published work regarding hair and wool follicles. Wool follicles are initiated relatively late in embryonic development at discrete body sites as the result of interactions between the ectoderm and mesoderm (Hardy, 1992; Powell et al., 1998). Two distinct follicle types form within the dermis, primary and secondary, determined by their order of initiation and distinguished histologically by their associated accessory structures (Hocking Edwards et al., 1996). Primary follicles initiate first, then secondary follicles, followed by branching of the already formed secondary follicles to form secondary-derived follicles. Both primary and secondary follicles form a sebaceous gland from the epithelial lining of the follicle (section 1.2.3.8.1). Primary follicles are distinguished from secondary follicles by the presence of a sweat (eccrine) gland (section

1.2.3.8.2) and an *arrector pili* muscle (section 1.2.3.8.3) that exclusively form with this follicle type (Figure 1-2).

NOTE:
This figure is included on page 6
of the print copy of the thesis held in
the University of Adelaide Library.

Figure 1-2 *Diagrammatic representation of primary, secondary and secondary-derived wool follicles (Hardy and Lyne, 1956)*

1.2.2.1 Primary Follicles

Primary follicles are the first to form in the skin of sheep foetuses and have been reported to be visible from day 40 of gestation (Hocking Edwards, 1999). Primary follicle primordia have also been reported to appear in the midside of the skin at approximately day 60 (Hardy and Lyne, 1956), and in overlapping waves of initiation from days 65-70 (Moore and Moore, 2001). Minor genetic variation between the animals measured in these experiments can account for the slight differences in reported follicle initiation timing. Regardless, it is undisputed that initiation of follicles in sheep skin occurs 30-40 days before the emergence of a mature wool fibre (Fraser, 1954), visible on the anterior region of the foetus at approximately days 90-100.

1.2.2.2 Secondary and Secondary-Derived Follicles

Secondary follicle primordia appear in the skin between days 70-80 but do not begin to branch until approximately day 100 (Hardy and Lyne, 1956; Hocking Edwards, 1999). The primordium of secondary-derived follicles develops from the side of either a secondary

follicle or another secondary-derived follicle in that bundle, all of the fibres of which emerge from a common orifice with their parent secondary follicle (Short, 1955). The incidence of secondary-derived follicle branching in the fine wool Merino is very high.

By birth, all secondary and secondary-derived (branched) follicles are present in the skin but only 16-33% are producing a fibre at this time (Schinckel, 1955; Short, 1955). Fraser (1954) reported that 5-25% of secondary follicles are producing a fibre at birth. Therefore, it has been well established that the secondary follicle population matures to the point of producing fibres after birth. Secondary and secondary-derived follicles mature in two anterior to posterior waves, one wave reaching its peak just before birth and the second, two to four weeks after birth. Until recently, it was assumed that the follicles continued to branch until birth. However, the S/P ratio of Merino foetuses has been reported to peak at day 126 with a higher S/P ratio than samples taken at day 143 (Hocking Edwards et al., 1996; Hocking Edwards, 1999). Furthermore, the potential S/P ratio at birth is rarely achieved at older ages (Schinckel, 1955) indicating that there is significant regression in the number of secondary-derived follicles established *in-utero*, compared to those that mature to produce a fibre.

Secondary follicle initiation and branching is adversely effected by maternal under-nutrition and physiological stresses including high ambient temperature and maternal hypoxia late in pregnancy (Fraser, 1954; Short, 1955; Schinckel and Short, 1961; Hocking Edwards, 1999). Since the secondary follicles initiated late in pregnancy have a lower fibre diameter, the consequences of poor herd management during this time (day 70 to birth) are decreased wool production and higher average fibre diameter.

Secondary follicles, but not primary follicles, are particularly susceptible to the effects of the stress hormone cortisol, indicating that fine wool sheep with a high S:P ratio may be more susceptible to environmental stresses and therefore, more prone to low staple strengths (Hynd, 1995), a major determinant of wool clip value.

1.2.2.3 Secondary to Primary Ratio (S/P ratio)

It can often be difficult to quantify the number of follicles and their density in a skin sample due to collection problems, such as skin stretching during excision of biopsies, sample shrinkage during histological processing and changes in surface area of the sheep. For these reasons, the S/P ratio is routinely used to describe the secondary follicle population in a sheep. It has been reported that foetal skin autographs taken after day 85 consist of only secondary follicle populations and have therefore lost the ability to initiate primary follicles (Schinckel and Ferguson, 1953). This strongly supports the concept of a constant primary follicle population thus supporting the validity of the S/P ratio as a measure of secondary follicle development. S:P follicle ratios provide a reliable index of variation in the secondary follicle population, because: (1) it is unlikely that the preceding maturation of the reference primary follicle can have been seriously damaged (Corbett, 1979) and (2) the primary follicle population is fixed and will not change.

1.2.3 Molecular Basis of Primary Follicle Neogenesis

Several extensive studies conducted in the past decade have provided insight into the molecular control of hair follicle induction and early morphogenesis (differentiation and growth of an initiated hair/wool follicle). More than one hundred individual regulatory and structural proteins have been localised to both the epithelial (epidermal) and mesenchymal (dermal) compartments of the hair follicle (Botchkarev et al., 1999; Stenn and Paus, 2001). There are approximately 20 different cell types in the hair follicle and its associated structures (Rogers and Hynd, 2001). The mechanisms of hair follicle morphogenesis are much better understood than the signals involved in hair follicle cycling. This may be because the complexity of the regulation of hair follicle cycling is far greater than that of follicle initiation (Paus, 1998). Follicle cycling involves three main stages which include: (1) anagen (active growth), (2) catagen (regression of the dermal papilla and follicle), (3) telogen (resting phase). Due to decades of selection for long staple length, the Australian Merino does not actively

cycle through anagen→catagen→telogen but experience extremely long anagen periods. While it is expected that the same regulatory molecules may be used in follicle initiation and cycling, the physiology and molecular biology of the cycling hair follicle will not be discussed in any further detail.

1.2.3.1 First Dermal Signal: Formation of the Epidermal Placode

The epidermal placode, the first histological marker of follicle initiation, is an aggregation of epidermal cells that forms at the site of follicle initiation, beginning approximately days 50-60 of gestation (Hardy and Lyne, 1956; Adelson et al., 1997). It appears that the initial signals arising in the dermis (the “first dermal signal”) cause the formation of these regularly spaced thickenings or placodes (Hardy, 1992; Moore et al., 1998; Millar, 2002). Mouse dermis has been shown to initiate feather buds from chick foot epidermis or scale placodes from lizard epidermis. Therefore, the signal to “make appendages here” arises in the dermis and the epidermis responds by forming a structure that is appropriate to its origin (Hardy, 1992).

WNT signalling is essential in many aspects of development involving epithelial-mesenchymal interactions. Binding of a WNT ligand leads to activation of the WNT receptor (frizzled), followed by cytoplasmic stabilization of β -catenin. β -catenin then translocates to the nucleus forming a transcriptional complex with members of the lymphoid enhancer-binding factor/T-cell factor (LEF/TCF) family of binding proteins. Studies on chicken feather development have shown that the nuclear localization of β -catenin in the dermis occurs 2 days prior to the appearance of placodes (Noramly et al., 1999). Furthermore, it has been shown that *LEF1* is expressed in the mesenchyme of the mouse vibrissae pad and that this expression is required for vibrissae follicle initiation (Kratohwil et al., 1996). Early in development, *Dickkopf 1 (DKK1)* is lowly expressed in the interfollicular dermis but highly upregulated in the dermis surrounding the placode and condensate (Andl et al., 2002). Therefore, it can be speculated that DKK1 is responsible for the concentration of WNT signalling in placodes.

Mice ectopically expressing DKK1, a potent inhibitor of WNT signalling, fail to initiate hair follicles, tooth buds and mammary glands (Andl et al., 2002). These findings demonstrate that WNT signalling plays a role in the first dermal signal of epithelium development in both chicks and mice, suggesting it may also play a crucial role in wool follicle initiation.

In response to the dermal signal, members of several classes of signalling molecules are expressed in the epithelium (including both repressors and enhancers of follicle initiation), resulting in the formation of epidermal placodes. *WNT10b* in chick and *WNT7a* in mouse are expressed evenly throughout the epidermis prior to follicle initiation but become markedly upregulated in placodes (Reddy et al., 2001; Widelitz et al., 2003). Furthermore, similar to *WNT10b* and *WNT7a*, nuclear β -catenin gradually increases in the epidermal regions destined to become placodes. Interestingly, *WNT10b* expression is abolished in *EDA-A1* knockout mice (*Tabby*), indicating that EDA signalling itself stimulates WNT signalling, in turn activating the canonical WNT pathway via β -catenin (Andl et al., 2002). Whether the stimulation is direct or indirect (through a secondary pathway), this demonstrates the complexity of the signalling pathway interaction in follicle initiation. Transgenic mice containing a *TOPGAL* reporter gene responsive to LEF/ β -catenin show expression of the reporter construct in both the dermal condensates and epidermal placodes (DasGupta and Fuchs, 1999), further confirming the importance of WNT signalling in both the dermal and epidermal components of the developing follicle.

Fibroblast growth factors (FGFs) and their receptors (FGFRs) are expressed in initiating follicles, promoting placode formation. Exogenous FGFs have been shown to rescue feather bud formation in the skin of chicks with an ectodermal defect that would otherwise prevent feather bud formation (Chuong et al., 1996).

Transforming growth factor- β 2 (*TGF- β 2*) is also important in follicle initiation as it is expressed in both placodes and condensates. TGF- β 2 soaked beads can induce formation of dermal condensates in chick embryo mesenchyme (Chuong et al., 1996) and induce hair

follicles in mouse embryo explants (Foitzik et al., 1999). Furthermore, mice lacking a functional copy of *TGF- β 2* have reduced numbers of hair follicles.

Members of the tumor necrosis factor (TNF) signalling pathway, including ectodysplasin-A1 (*EDA*), its receptor (*EDAR*) and adapter death domain (*EDARADD*), have been well characterised as important regulators of follicle initiation. Binding of EDA to EDAR recruits EDARADD, which binds selected TRAF proteins and this in turn activates the NF- κ B transcription factor (Botchkarev and Fessing, 2005). Mice knockouts for *EDA* (*Tabby*), *EDAR* (*Downless*) and *EDARADD* (*Crinkled*) present phenotypes similar to that of the human congenital disorder ectodermal dysplasia where patients are born with sparse hair follicles, no sweat glands and malformed teeth (Lyon et al., 1996). The causative mutation for X-linked anhidrotic ectodermal dysplasia lies in the *EDA* gene and in the cases of autosomal recessive and dominant hypohidrotic ectodermal dysplasia, the mutation lies in the *EDAR* and *EDARADD* genes, respectively (Headon et al., 2001; Millar, 2002). *EDA* is expressed ubiquitously in both the epidermis and dermis, prior to and after placode initiation. *EDAR* is expressed ubiquitously prior to follicle initiation but becomes up-regulated only in placodes post-initiation (Mou et al., 2006). EDA is also thought to be cleaved before diffusing to sites of *EDAR* expression (Headon and Overbeek, 1999). Both hair and tooth follicle initiation rely on epithelial:mesenchymal (EM) interactions, highlighting the importance of this signalling pathway in development. The fact that sonic hedgehog (SHH) and BMP signalling only occurs in the presence of EDAR demonstrates that EDAR acts early in initiation (Barsh, 1999), further demonstrating the complexity of the signalling pathway interactions during follicle initiation.

Bone morphogenetic proteins (BMP) act as inhibitors of follicle initiation with ectopic expression of *BMP2* and *BMP4* suppressing feather bud development in chick embryos (Jung et al., 1999). In the mouse, *BMP7* is expressed in placodes and *BMP4* is expressed in the pre-

follicular mesenchyme. In the presence of excess BMPs or in the absence of the BMP inhibitor *Noggin*, follicle initiation is reduced (Botchkarev et al., 1999).

From the literature to date, it is clear that there is not a single gene responsible for placode initiation, nor is this process dependent on one signalling pathway alone (Figure 1-3). Several complex pathway interactions have been identified and evidence also exists to suggest the possibility of rescue mechanisms through other pathways if a deficiency or mutation occurs in the regular signalling molecules. The formation and patterning of placodes results from competition between promoters and inhibitors, acting both within the placode and diffusing into the surrounding epithelium.

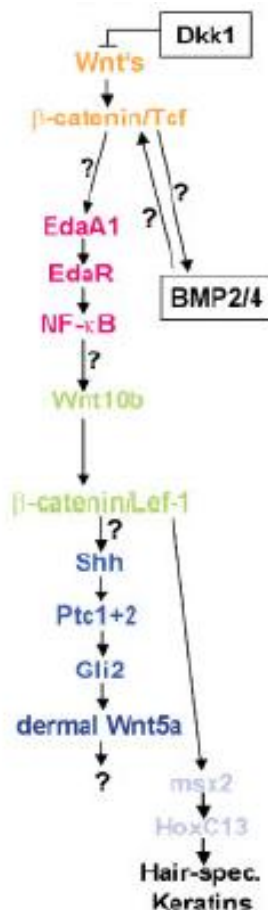


Figure 1-3 Schematic of the complex molecular interactions involved in murine primary follicle initiation (Schmidt-Ullrich and Paus, 2005)

1.2.3.2 First Epidermal Signal: Formation of the Dermal Condensate

Cells of the newly formed epidermal placode signal back to the underlying mesenchyme initiating formation of the dermal condensate, a cluster of “stem-cell like” cells. Tissue recombination experiments have shown that only mouse dermal cells will respond to this signal from mouse epidermal cells (Kollar, 1970; Hardy, 1992). The mechanisms and signalling molecules involved in dermal condensate aggregation (i.e. migration, proliferation and or arrangement amongst placodes) are largely unknown, although mouse and human hair research have indicated the involvement of members of the WNT and SHH signalling pathways (Andl et al., 2002; Michno et al., 2003).

Evidence for the involvement of WNT members in this process was demonstrated by Huelsken et al, (2001) who found that dermal condensates failed to develop in the absence of epithelial β -catenin. These experiments also indicated that SHH signalling is absent from mice follicles lacking β -catenin, indicating that SHH signalling occurs downstream of WNT activation. Although mice lacking the *SHH* gene initiate both placodes and condensates, the follicles fail to mature and the overall number of follicles is decreased (St-Jacques et al., 1998). These experiments show that SHH is not a component of the first epidermal signal but is required for the subsequent epidermal:mesenchymal (EM) signalling that regulates downgrowth of the epidermis and maturation of the dermal condensate (Chiang et al., 1999).

1.2.3.3 Down growth of the epidermal placode

Subsequent to formation of the dermal condensate and SHH signalling discussed above, the plug of cells in the epidermal placode (or primitive ectoderm) overlying the epidermal placode extends down into the dermis (or primitive mesoderm). The leading front of the down-growing follicle (matrix) is highly proliferative and sustains contact with the dermis throughout the process (Stenn and Paus, 2001). The SHH receptor Patched-1 (PTCH1), expressed in mesenchyme adjacent to the placode, is a critical signalling target for SHH. *PTCH1* and *GLII* (a transcription factor activated by SHH) are markedly down-

regulated in *SHH* $-/-$ mice and follicles fail to develop past the hair germ stage in these animals (Chiang et al., 1999). Therefore, the “second dermal signal” is likely to be activated by *SHH* signalling.

1.2.3.4 Formation of the dermal papilla

A molecular signal passing from the epithelial cells of the follicle plug to an adjacent cluster of mesenchymal cells (dermal stem cells or pre-papilla cells) causes the expanding base of the follicle plug to surround the mesenchymal cluster, forming the dermal papilla (Hardy, 1992).

The dermal papilla is essential for follicle formation and dictates the timing and location of the appendage formed; the characteristics of which are determined by the overlying epithelial cells (Alonso and Fuchs, 2003a). The mature dermal papilla of large follicle contains an extensive capillary network that is vital to sustaining the blood flow to the follicle. The dermal papilla of smaller follicles (e.g. wool follicles) do not contain this capillary network. The epidermal cells that surround the dermal papilla form the hair root that produces and is continuous with the hair shaft (Junqueira et al., 1998). Proliferation and differentiation in the mature hair follicle is regulated by complex interactions between specialised epithelial and mesenchymal cells and together with extracellular components effectively control the hair cycle.

1.2.3.5 Formation of the Follicle Bulb

A signal passing from the outer cells of the dermal papilla to the surrounding epithelial cells of the hair plug stimulates them to divide rapidly, in turn forming the hair matrix, also known as the follicle bulb (Hardy and Lyne, 1956; Botchkarev and Paus, 2003, Figure 1-4). Follicle bulb cells, located in a thin layer surrounding the dermal papilla, continue to divide for the life of the follicle, providing daughter cells that differentiate into either inner root sheath (IRS) cells or one of two types of fibre cells, cuticle or cortex (Hardy, 1992). The supply of follicle bulb cells, their distribution as they differentiate into the various layers of

the fibre and inner root sheath and the level of nutrition of the animal, all have a marked effect on wool production rates (Hynd and Masters, 2002).

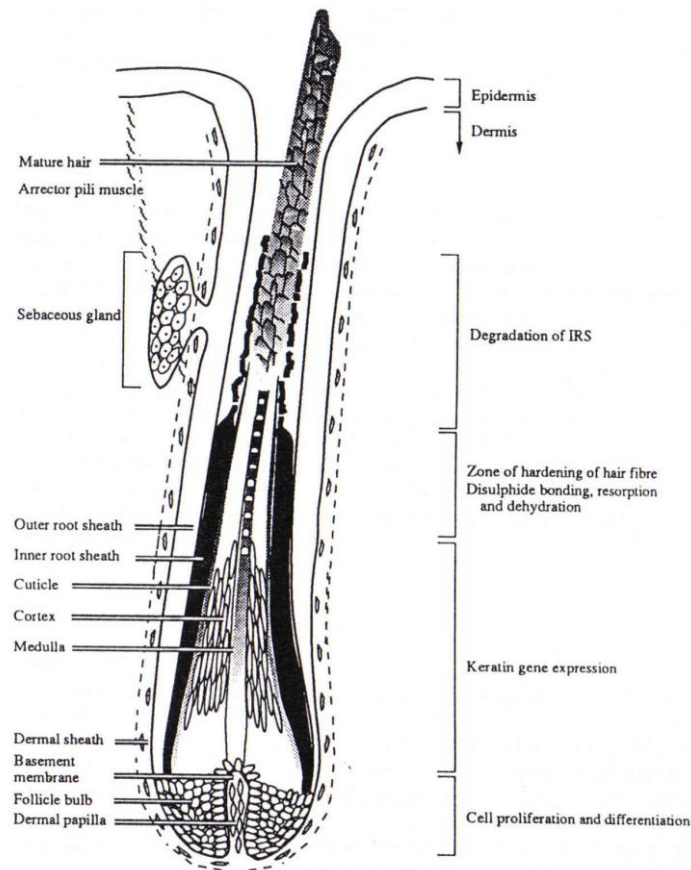


Figure 1-4 *Diagrammatic representation of the different cell types and layered structure of the hair follicle (Powell and Rogers, 1997)*

1.2.3.6 Inner Root Sheath (IRS)

Beneath the skin surface, the hair/wool fibre is surrounded by the inner root sheath which consists of three concentric layers that differentiate from the cells within the follicle bulb: Henle's layer (the outermost layer, adjacent to the outer root sheath); Huxley's layer and the inner root sheath cuticle (Montagna and Parakkal, 1974, Figure 1-4). Inner root sheath cells migrate up the follicle, supporting the maturing fibre until it reaches the level of the sebaceous gland. At this point, the fibre emerges from the skin, and the inner root sheath cells die and are shed from the surface of the epidermis.

Differentiation of the inner root sheath is marked by the production of trichohyalin protein granules, which form a matrix between the keratin filament proteins also

expressed by these cell types. Differences in the rate of inner root sheath cell differentiation and variation in the structure of the trichohyalin molecule produced, distinguishes the three cell types of the inner root sheath from one another (Powell and Rodgers, 1997).

1.2.3.7 Outer Root Sheath (ORS)

The outer root sheath is a layer of cells, continuous with the epidermis, that maintain their own cell population with cellular proliferation along the length of the outer root sheath, providing support to the fibre and follicle (Powell and Rogers, 1994). The outer root sheath consists of basal-like keratinocytes, which can substitute for interfollicular epidermal keratinocytes during wound healing when outer root sheath cells migrate onto the denuded area, thus contributing to epidermal regeneration (Limat et al., 1995; Alibardi, 2004). Histological evidence produced by Bray (1997) suggests that epidermal stem cells are distributed evenly along the upper part of the outer root sheath of the Merino follicle, supplying the follicle with a multipotent stem cell population to maintain the follicle support layers for the life of the follicle.

1.2.3.8 Follicle Accessory Structures

1.2.3.8.1 Sebaceous Gland

Sebaceous glands are holocrine structures that lie in the dermis, containing glands that produce sebum (lanolin in sheep) that flows through small sebaceous ducts into the hair canal and onto the skin surface (Bloom and Fawcett, 1962). The secretory portions of sebaceous glands (alveoli) are rounded sacs formed by a basement membrane supported by a thin layer of fibrous connective tissue. Several adjacent alveoli form a “bunch” that all open into a short duct. A bilobed sebaceous gland forms with both primary and secondary follicles. In the case of primary follicles, the sebaceous gland forms before the dermal papilla, during formation of the follicle plug. However, during secondary follicle morphogenesis, the gland forms in conjunction with the dermal papilla (Hardy and Lyne, 1956), a sequence of events supported by the findings of Carter (1943). The hair canal is produced by two coordinated processes:

keratinisation of the epidermis and disintegration of sebaceous cells that have migrated to the neck of the follicle.

1.2.3.8.2 Sweat Glands (Primary Follicles Only)

Eccrine sweat glands are classified as both secretory and excretory organs, secreting sweat, a dilute electrolyte solution of sodium chloride, potassium and bicarbonate and occasionally employed to quickly excrete orally ingested compounds (Montagna, 1962; Montagna and Parakkal, 1974). Sweat glands are simple, coiled, tubular epithelium consisting of a narrow unbranched excretory duct and a secretory coil. The majority of the secretory portion is located in the dermis and the secretory portion rests on a thick basement membrane. An extensive network of capillaries forms beneath the basement membrane of sweat glands. In sheep apocrine sweat glands (outgrowths of the superior portions of the wool follicles) form in association with the primary wool follicles. The principal role of sweat glands is temperature regulation, which raises the question of the importance of these structures in Merino sheep, since the effectiveness of excreting water below a thick fleece would be low as evaporation rates would be poor. It is also not clear why sweat glands form only with primary follicles.

1.2.3.8.3 Arrector Pili Muscle (Primary Follicles Only)

Connected to the sheath surrounding the follicle and the papillary layer of the dermis are bundles of smooth muscle cells known as arrector pili muscles (Junqueira et al., 1998)(Figure 1-4). The arrector pili muscle forms around the same time that the epidermal down growth is invaginated forming the dermal papilla (Hardy and Lyne, 1956). Disposed in an oblique direction, contraction of these arrector pili muscles results in erection of the primary fibre population, usually in response to stress/fear or cold temperatures.

1.3 Stem Cells in the Skin

Stem cells are generally classified according to the following functions: (1) unlimited or at least high potential of self renewal, (2) multi-lineage differentiation of a single cell, and

(3) *in vivo* functional reconstitution (Verfaillie, 2002). Current literature routinely describes stem cells by their plasticity: (1) totipotent = able to differentiate into any cell type of the species from which it is taken and can be extracted from embryos up to the eight cell stage (Alonso and Fuchs, 2003b), (2) pluripotent = the ability to differentiate into any cell type of the blastocyst from which it is taken, including both the trophectoderm and inner cell mass (Pera et al., 2000), (3) multipotent = a broad range of potency (several cell types) and (4) unipotent = able only to form the cell type of the organ from which it is isolated (Verfaillie, 2002). In the past decade, much has been learned in the area of hair stem cell research; conversely, little is known about the role and fate of ovine skin stem cells.

1.3.1 Embryonic vs Adult Stem Cells

Embryonic stem cells (ESC) are immortal and can be propagated *in vitro*, expanding in numbers indefinitely in a primitive undifferentiated state with each cell retaining the pluripotency of the cell from which it was derived (Pera et al., 2000; Brouard and Barrandon, 2003; Zwaka and Thomson, 2005). Classified as totipotent by some and pluripotent by others, embryonic stem cells were first described using mouse as the benchmark, the first of its type to be isolated (Evans and Kaufmann, 1981). Embryonic stem cells are also known to maintain a stable diploid state with a normal karyotype *in vivo*. It is apparent that significant phenotypic differences exist between murine and primate embryonic stem cells. Molecular markers common to both species provide initial evidence for a universal set of molecular markers, perhaps common to all species. There are no published data available on ovine embryonic stem cells.

Adult stem cells are multipotent, best defined by their ability to self renew and to generate large amounts of tissue, often for a lifetime (Lajtha, 1979; Jensen et al., 1999). The most obvious evidence for the presence of adult stem cells comes from the capacity for wound healing. Furthermore, the production of blood cells occurs successively at defined locations, in the yolk sac of the early foetus, in the liver of the later foetus, and in the bone

marrow of the adult, suggesting that there are reservoirs of progenitors (Domen and Weissman, 1999).

The human epidermis and dermis have proved a fruitful source of adult stem cells employed in research into altering the differentiation lineage of stem cells for use in wound healing and the production of replacement organs (Jahoda et al., 2003).

1.3.2 Epidermal Stem Cells

Adult multipotent stem cells reside at the basal layer of the epidermis, attached to the underlying basement membrane, dividing infrequently to continually renew the outer layer of the skin (Figure 1-5). As adult epidermal stem cells exit the cell cycle, differentiating into transit amplifying cells, they migrate towards the spinous layer of the epidermis. Further cell divisions produce the differentiated cells of the upper spinous and granular layer, which die and are shed from the stratum corneum (Alonso and Fuchs, 2003b).

NOTE:
This figure is included on page 19
of the print copy of the thesis held in
the University of Adelaide Library.

Figure 1-5_A: Structure of skin epithelium and B: Location of the epidermal SC (Alonso and Fuchs, 2003b)

1.3.3 Dermal Stem Cells

Dermal mesenchymal cells possessing multipotent stem cell-like characteristics are thought to be distributed evenly throughout the adult dermis, recruited if required for wound healing, repair of damaged papilla and even to re-populate the haematopoietic and osteogenic systems (Jahoda and Reynolds, 2001; Lako et al., 2002; Gharzi et al., 2003; Jahoda et al., 2003; Reynolds and Jahoda, 2004). Isolated dermal stem cells have been demonstrated to

have transgender hair follicle induction capabilities in the adult skin (Reynolds et al., 1999). Dermal stem cells are also thought to control hair follicle formation in the skin of the embryo (Moore and Moore, 2001). Adult human dermal stem cells have been differentiated *in-vitro* into muscle, neural and haematopoietic cell types and therefore, have a broad range of potency (Lako et al., 2002; Gharzi et al., 2003; Jahoda, 2003; Shi et al., 2004). However, dermal cells are generally classified as multipotent opposed to pluripotent (Reynolds et al., 1999), as there is no evidence suggesting they have the ability to form all cell types of the adult from which they are taken.

1.3.4 Division and Maintenance of Stem Cell Populations

Self renewing tissues, such as blood and skin, must maintain a pool of stem cells throughout life (Bullock et al., 2007). The mechanisms that regulate the proliferation of this pool must be tightly controlled both during embryogenesis and throughout adult life to prevent depletion or amplification of the pool, both of which can lead to a disease state.

In the adult skin, stem cells divide infrequently to generate either two daughter cells that are identical to the founding cells (symmetrical division; Figure 1-6A) or one daughter cell that is identical to the founder and one daughter cell of differing capacity (asymmetrical division; Figure 1-6B) (Brouard and Barrandon, 2003). Embryonic stem cells can be expanded indefinitely, retaining the ability to form every cell type of the body, therefore it has been reported that human embryonic stem cells can differentiate exclusively by symmetrical cell division (Zwaka and Thomson, 2005). Conversely, it is commonly accepted that an efficient way to control the number of cell divisions in order to maintain tissue homeostasis in adult tissue is achieved through asymmetrical cell division (Gambardella and Barrandon, 2003). Asymmetrical cell division results from an unequal segregation of cell fate determinants or from the selective response of each of the two daughter cells to a gradient of signalling molecules in their immediate environment (Le Borgne and Schweisguth, 2003).

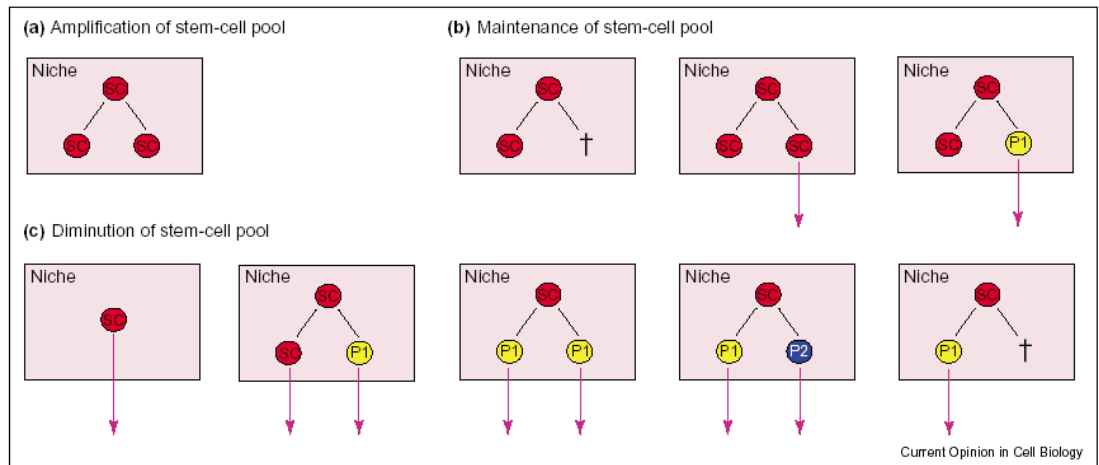


Figure 1-6 *Schematic fate of a dividing stem cell in an epidermal niche (A) Amplification of the stem cell population, (B) Strict maintenance of the population or (C) Diminution of the population (Gambardella and Barrandon, 2003).*

1.3.5 Location of Stem Cells in the Hair/Wool Follicle

The hair follicle is an abundant source of adult stem cells with stem cells being localised to four epidermal-derived parts of the follicle (basal layer of the epidermis, follicle bulge, sweat gland and sebaceous gland) and the dermal-derived papilla (Alonso and Fuchs, 2003b, Figure 1-7). Considering the histological similarity in the structure of hair and wool follicles, one would assume that the basement membrane of the epidermis, sebaceous glands, dermal papillae and the sweat gland of primary follicles would contain stem cell populations, required for maintenance of these cell types. Epidermal stem cells of the follicle bulge migrate down to the follicle bulb where they differentiate into follicle cell lineages of the inner and outer root sheaths, cuticle and cortex, resulting in the production of the wool fibre (Lavker et al., 2003). Merino wool follicles do not possess a bulge region and the exact location of the stem cell compartment has not been extensively researched, although experiments have shown that BrdU label retaining cells reside in the upper part of the outer root sheath (Bray, 1997). Perhaps these cells differentiate upon receipt of the appropriate signal, potentially from the dermal papilla, providing the keratinised cells of the wool fibre for the life time of the animal.

NOTE:
This figure is included on page 22
of the print copy of the thesis held in
the University of Adelaide Library.

Figure 1-7_ Location of stem cells in the mouse hair follicle (Alonso and Fuchs, 2003b)

Dermal sheath cells surround the dermal papilla and are contiguous with the dermis, providing stem cells to the dermal papilla (Reynolds and Jahoda, 2004). Evidence for the existence of stem cells in the dermal sheath was first provided by Jahoda et al (1992); when the hair fibre and base of the follicle were removed experimentally from rat vibrissae follicles, the dermal sheath cells replaced the dermal papilla cells and restored functional hair growth.

1.3.5.1 Mechanisms of Follicle Initiation: Reaction Diffusion Theory vs. Founder Cell Theory

Two theories that attempt to explain wool follicle initiation in terms of stem cells involvement and the subsequent effects on fibre diameter and density have been proposed: the reaction-diffusion theory (Nagorcka and Mooney, 1985) and the founder cell or committed cell theory (Moore et al., 1998). Nagorcka's mathematical reaction-diffusion theory states that a biochemical pattern forming mechanism is responsible for follicle placement, density and size. The mechanism involves diffusing morphogens X and Y across the basement membrane, interacting with a dermal factor Z, and leading to the pre-pattern of primary wool

fibres. It predicts that an inverse relationship between follicle density and fibre diameter is determined by a common factor, $\lambda_e(t)$, described as the “wavelength” of the reaction diffusion system. In this theory, the density and diameter are determined at the same time, with the size of the initiating placode being the determining factor for consequent dermal papilla volume and fibre diameter. The reaction diffusion theory has also been extended to address the formation of both secondary and secondary-derived (branched) follicles as well as several aspects of fibre and follicle structure.

The founder cell theory hypothesised by Moore et al (1998) predicts that a pre-determined pool of dermal papilla stem cells exists in the skin that become committed to follicle initiation forming “pre-papilla cells”. The size of the committed population defines the total amount of fibre producing tissue in the skin. Follicle size, density and fibre dimension are all dependent on the number of committed cells forming each individual follicle with follicle formation ceasing when most or all of the committed cells have been utilised.

Both the reaction diffusion theory and the founder cell theory predict that the follicle density and fibre diameter are determined at initiation, albeit by different mechanisms (Adelson et al., 2002). The founder cell theory fails to account for stem cell division or the recruitment of stem cells from the dermis during follicle development. (Rogers, 2006) The founder cell theory does not attempt to explain other aspects of follicle initiation such as fibre structure and the bilateral structure of the cortex, both of which are addressed by the reaction diffusion theory. Currently, both theories require more experimental evidence. However, evidence from mice as to the potency of promoters and inhibitors of follicle initiation acting both within and in the surrounding epithelium of the developing skin support the reaction diffusion theory more, whilst the relatively short breadth of the founder cell theory leaves more questions unanswered than it attempts to explain.

1.3.5.2 Dermal Condensates: Proliferation, Migration or Both?

The exact cellular mechanisms involved in initiation of the dermal papilla are not yet known. It has been demonstrated that a signal arising in the dermis instructs the epidermis to form a placode, which in turn signals back to the dermis to form the dermal papilla (section 1.2.3.2). Whether these signals are chemotactic in nature, initiating migration of mesenchymal stem cells to the basement membrane, or if they stimulate proliferation of multipotent cells already residing beneath the epidermis, is not clearly understood. It is likely that this dynamic process involves both migration and expansion of the multipotent mesenchymal stem cell population of the dermis.

Fibroblast locomotion or migration is achieved through actin remodelling to form membrane protrusions (lamellipodia), which facilitate cell extension. In mammalian cells, cell proliferation, known as the cell cycle, is under the control of proteins called cyclins, which regulate the transition between two main checkpoints: the G1-S transition, initiating DNA replication, and the G2-M transition, controlling mitosis and cell division. The signalling pathways involved in cell migration and proliferation are discussed in further detail in chapter four.

A cell migration assay using a modified Boyden chamber with 8 μ m pores demonstrated that human epidermal keratinocytes induced significant cell migration in human mesenchymal stem cells. Interestingly, this migration was inhibited by the protein kinase A pathway inhibitor H-89 indicating that this migration could be chemotactic in nature (Akino et al., 2005).

Chick dermal cells marked by injection of a lipophilic dye were dissected and dissociated from the epidermis into single cell layer suspensions. When recombined, a regular array of dermal cells and epidermal placodes was established with the labelled cells distributed randomly among the condensates (Jiang et al., 1999), indicating that the initial position of dermal cells does not determine their ability to induce placodes. These

experiments also demonstrated that at very low cell densities no feather buds are formed. Once a threshold number of cells was achieved, dermal condensation began and as the cell density increased, so did the number of initiated buds. Since the size of the total explant and the size of the primordial condensates remained constant, the extra condensates formed at the expense of the interbud space. Furthermore, both activators and inhibitors of feather bud initiation were expressed within the forming bud. Combined, these results demonstrate that feather bud density and condensate size is modulated by the relative ratios of activators and inhibitors, and further dismisses the idea that condensate density and size is regulated by the number of cells within a pre-determined population of cells as proposed in Moore's founder cell theory.

Chick explant experiments have also shown that the process of dermal condensation *in-vitro* does not appear to involve proliferation since the process occurs within the first 18 hours of culture (Noveen et al., 1995). However, the subsequent outgrowth of the bud, equivalent to down growth of the follicle and maturation of the dermal condensate, entails rapid proliferation of the dermal core, no doubt involving both maintenance of the stem cell pool as well as cell fate commitment and terminal differentiation. These findings also argue against the idea of a periodic dermal signal, complying more with the idea that differences in promoter and repressor levels might account for the regional differences in size and spacing of follicles (Millar, 2002). Also it indicates that mesenchymal cells (pre-papilla cells) have the ability to migrate in response to promoter and inhibitory signals.

1.4 Summary

Primary wool follicles are initiated in the skin of Merino sheep as a result of dynamic interactions between the epidermis and mesenchyme at approximately day 50 of gestation. Although little is known about the exact genes and signalling pathways involved in wool follicle initiation, conservation amongst mammals in the morphology of epithelial appendages (i.e. hair, fur and wool) and their timing during development has meant that data produced in

the mouse, rat and human hair research fields is highly relevant to research into sheep wool follicle initiation. Research focused on mouse and rat follicle initiation have demonstrated the importance of the WNT, BMP, TNF and TGF- β pathways and therefore, the gene candidates selected for the qRT-PCR analysis in this study (chapter 4) lie within these pathways.

For the wool industry, the short-term challenge lies in identifying the specific genes involved in follicle initiation and maturation, characterising the involvement of stem cells in this process, and then transferring this knowledge into DNA-based genetic selection criteria (Adelson et al., 2002). However, experimental data produced during the last decade have shown that no single gene or pathway is solely responsible for this process. Moreover, it appears that “rescue mechanisms” or alternate signalling pathways exist to restore follicle initiation when the primary pathways are mutated or blocked, adding further complication to efforts aimed at manipulating this process for the benefit of Australian wool producers.

1.5 Project Aims and Hypothesis

The primary aim of this research project was to characterise the molecular nature of primary wool follicle initiation, specifically the specification, patterning and formation of the dermal condensate. It was hypothesised that following commitment of the “pre-papilla” stem cell population, dermal condensates are initiated at discrete sites beneath the epidermis as a result of migration and arrangement of these multipotent pre-papilla cells. Furthermore, based on current theories on maintenance of stem cell populations, it was hypothesised that the number of pre-papilla cells in the dermis is not the limiting factor in follicle initiation. A significant mesenchymal stem cell population is retained within the dermis after follicle initiation for wound healing and for the maintenance and repair of papillae.

Chapter Two

General Materials and Methods

Chapter 2 General Materials and Methods

Methods that were utilised in more than one chapter of this thesis are described below.

2.1 Materials

All solutions, buffers and oligonucleotides utilised in this research project are described in appendices I and II.

2.2 Foetal Tissue Collection

Thirty two twin pregnancies were produced via laproscopic artificial insemination of 40 South Australian Merino ewes sourced from a single flock (with similar genetics, average condition score 2, mean fibre diameter (FD)=20 μ M) with the semen from one ram (FD=19 μ M). Ewes were stunned via captive bolt, exsanguinated and the foetuses removed. The foetuses were then exsanguinated and skin samples peeled from the shoulder, midside and rump on days 43, 47, 50, 53, 57, 60, 63, and 68 of gestation, with the day of artificial insemination recorded as day 0. One shoulder sample was fixed in 4% paraformaldehyde (appendix I) for histological analysis. A shoulder, midside and rump sample were frozen in optimal cutting temperature compound (OCT, *ProSciTech*) for laser capture microdissection (chapter 5) and the remaining midside and rump samples were snap frozen in liquid nitrogen for RNA extraction and analysis.

2.3 RNA isolation and purification

Approximately 100-150mg of frozen whole foetal skin were homogenised in 1.1ml of TRIZOL™ reagent (*Ambion*) using an Ultra-Turrax® T-25 basic homogeniser (*Rose Scientific*). A portion of the homogenate (600 μ l) was thoroughly mixed with 120 μ l of chloroform (*SigmaAldridge*) and was phase separated by centrifugation at 12,000g for 15mins at 4°C. The upper aqueous layer (180 μ l) was removed and combined with 180 μ l of RLT buffer from the RNeasy Extraction Kit (*Qiagen*) and 360 μ l of 70% 200-proof AR Ethanol

(Sigma). The RNA was then extracted and purified via the manufacturer's protocol (including DNase treatment) and resuspended in 50µl of nuclease free water (Ambion).

2.4 Estimation of RNA concentration and assessment of RNA integrity

The concentration and purity of the total RNA was estimated using a GeneQuant RNA/DNA calculator (Pharmacia Biotech) with a 70µl quartz cuvette (TE buffer blank). Samples were diluted 1:23 with nuclease free water (Ambion). RNA concentration from the absorbance at 260nm and the 260:280nm ratio were determined. Preparations of total RNA were considered to be of a high quality if the 260:280 ratio was between 1.6 and 2.0. 2µl of RNA was added to 2ul formamide loading buffer (Appendix I) and separated on a 1% agarose (Progen) gel at 100V for 30min and stained with ethidium bromide. The integrity of the 28S and 18S ribosomal bands of the RNA preparation was assessed with UV illumination using a Gel Doc 1000 (Biorad).

2.5 RT-PCR of isolated RNA for cDNA production

cDNA was generated using the OmniScript™ kit (Qiagen) following the manufacturers protocol. Routinely 900-1500ng of RNA in 12µl was combined with 13µl of an OmniScript master mix. The reaction master mix consisted of 1X cDNA Buffer, 500nM deoxynucleotide triphosphates, 10 units of RNase Out (Invitrogen), 1 unit of Omniscript RT (Qiagen), 100nM oligo dTVN primer combination (Appendix II, Table II-1), 100nM gene specific oligonucleotide combination (Appendix II, Table II-2) and 100nM 18S specific primer (Appendix II, Table II-2). The reaction volume was made up to 25µl with nuclease free water. Reactions were incubated at 37°C for 2 hours and heat-inactivated at 65°C for 15mins. cDNA reactions were diluted with nuclease free 10mM TRIS pH 8.0 (Appendix I), aliquoted into single use volumes in 96-well plates, sealed and snap frozen at -80°C.

2.6 Optimisation of PCR conditions for isolation of sheep cDNA sequences

Genomic DNA and cDNA were routinely used to optimise polymerase chain reaction (PCR) and cycling conditions. Reactions were performed in 200µl 8-well PCR strip tubes (*Axygen*). Initially, a standard 25µl PCR Gold reaction consisted of 1X PCR buffer, 400nm deoxynucleotide triphosphates (dNTPs, *Invitrogen*), 400nmol forward and reverse primers (*Proligo*), 2.0-4.0mM MgCl₂, 50-100ng genomic DNA or equivalent cDNA template and 0.5U AmpliTaq Gold (*Applied Biosystems*). The reactions were performed under approximately 25µl mineral oil (*Sigma*) on a Robocycler Gradient Thermocycler (94 version 3.4; *Stratagene*) under the following conditions:

1 cycle: 95°C for 10min (AmpliTaq Gold activation)

35-40 cycles: 95°C for 30sec, T_A for 30sec, 72°C for 30sec (<400 bp) or for 1min (>400 bp)

(T_A= annealing temperature)

An initial temperature gradient of 52-64 and MgCl₂ concentration range of 2.0-4.0mM was trialled and the optimal conditions selected based on these results.

2.7 Analysis of PCR products by agarose gel electrophoresis

Routinely, 4.5µl of PCR products (combined with 0.5µl 10X loading dye, (Appendix I) were separated on a 2-3% low melting point agarose (*Progen*) mini gel in 1xTAE (Appendix I) at 100V for 30 mins in a BioRad mini electrophoresis tank with either 10 or 14 lanes depending upon the number of samples to be analysed. The products were sized against either a pGEM marker ladder (1µg loaded) cut with HinfI, RsaI and SinI (*Promega*) or a pUC marker ladder (0.5ug loaded; *Geneworks*). Gels were stained in 0.5µg/ml ethidium bromide (Appendix I) for 5-10 min, visualised under UV light using a Gel-Documentation 1000 System (*Biorad*), and the images electronically stored.

2.8 Preparation of PCR template and automated sequencing

Double stranded PCR templates were prepared for sequencing by combining 2x25µl optimised PCR for the fragment to be analysed (section 2.6). After confirming successful amplification by gel electrophoresis (section 2.7), the remaining 40µl was purified with QIAquick PCR purification columns (*Qiagen*) following the manufacturer's protocol to remove unincorporated primers and dNTP's. The eluted PCR products were visually assessed via gel electrophoresis and quantified using the GeneQuant RNA/DNA Calculator (*Pharmacia Biotech*). Varied quantities of template, depending on the product size, were combined with 6.4pmol of primer and sent to Australian Genome Research Facility in Brisbane for automated sequencing. The identify of the sequence was confirmed via a blastN search (ANGIS; www.angis.org.au) and ClustalW alignments (ANGIS; www.angis.org.au).

2.9 Optimisation of quantitative RT-PCR reaction conditions

qRT-PCR primers were designed to ovine sequence using Primer 3 (http://biotools.umassmed.edu/bioapps/primer3_www.cgi) and Oligo 6.0 software (*Molecular Biology Insights Inc.*). The primers were designed to span a sizable intron (>500b.p.) so that genomic DNA contamination could not be amplified and the primer pairs had approximate annealing temperatures of 60°C with no dimer formation or hairpin loops. The primer annealing temperature was determined using standard PCR optimisation (sections 2.6 and 2.7) with the addition of 0.03% SYBR green (*Invitrogen*). 1:10, 1:100 and 1:1000 dilutions of the cDNA were then optimised in triplicate in a standard 25ul PCR reaction in 200µl tubes (*Corbett*) using a 36-well rotor RotorGene 3000 (*Corbett Robotics*) and the commercial reagent Power SYBR® Green PCR master mix (*Applied Biosystems*) according to the manufacturers protocol. If the reaction efficiencies were between 0.9-1.1 and there was evidence of only a single product in the melt curve, the reactions were deemed specific and therefore quantitative. Reactions volumes were then scaled to 5µl for the final qRT-PCR

analysis. Final reactions were loaded using an 8-channel liquid handling robot (*Eppendorph*) and the reactions performed in a 384-well LightCycler® (*Roche*).

Chapter Three

Foetal Skin Series and Histology

Chapter 3 Foetal Skin Series and Histology

3.1 Introduction

Hair and wool follicle development occurs once in any mammal's lifetime (Powell et al., 1998). Wool follicles are initiated in the skin of sheep foetuses commencing at approximately day 50 of gestation (Hardy and Lyne, 1956), with the average gestation length of an Australian Merino being 149 days (Cottle, 1991).

In order to study the molecular signals involved in primary wool follicle initiation, a foetal skin series was generated through timed matings and foetal samplings. The aim was to generate a foetal skin series that spanned primary follicle initiation and to conduct a histological characterisation of these samples in order to confirm the timing of follicle initiation.

3.2 Specific Methods

3.2.1 Matings

100 Merino ewes with an average condition score of 3 and a mean fibre diameter of $20 \pm 1.4 \mu\text{m}$, sourced from a single flock, were synchronised 16 days prior to insemination with EASI-BREED™ CIDR (controlled internal releasing device) sheep devices (*Pharmacia Upjohn, Rydalmere NSW*). CIDRs were removed and the ewes super-ovulated 2 days prior to insemination through intramuscular injection of 2mls (800 IU) of pregnant mare serum gonadotrophin (*Intervet; Bendigo East, Vic*). Ewes were fertilized through laparoscopic artificial insemination with fresh semen from a single Merino ram (fibre diameter = $17 \mu\text{m}$) with the day of insemination designated as day 0 of gestation. Ten ewes suspected of being twin-bearing were chosen for the trial after ultrasound pregnancy scanning at day 42 and a further 8 twin-bearing ewes were chosen after a repeated scanning at day 50.

3.2.2 Generation of Foetal Skin Series

On the day of sampling, the pregnant twin-bearing ewes were stunned via captive bolt and exsanguinated. The uterus was exteriorised, the foetuses carefully removed and the litter

size noted. In the case of triplet pregnancies, one randomly-selected foetus was washed in phosphate buffered saline (PBS; Appendix I) and placed in a kidney dish on ice for sampling after the other two foetuses were dissected. The foetuses were washed in PBS (Appendix I), photographed using an Olympus 5.0 mega pixel camera, weighed and exsanguinated. The sex of the foetuses was recorded from day 50 onwards as it was not possible to sex them visually prior to this time point. Skin strips from the shoulder, midside and rump were first scored with a size 10 scalpel and the skin then peeled from the underlying muscle with a blunt ended seca. The midside and rump skin strips from one side of the foetus were placed in cryovials (*ProSciTech, Kirwan Qld*) and snap frozen in liquid nitrogen for RNA extraction. The shoulder strip from the same side was placed on Whatman paper (*Crown Scientific, Minto NSW*) and submerged in 5% buffered formalin for histological characterisation. The shoulder, midside and rump strips from the opposite side of the foetuses were also placed on Whatman paper and frozen in OCT compound (*ProSciTech, Kirwan Qld*) for laser capture microdissection.

3.2.3 Crown Rump Length Measurements

Crown rump length (CRL) measurements were made using the image analysis software analySIS® (*Olympus, North Ryde, NSW*) from the still digital images taken at the time of sampling. Three horizontal scale measurements were made at the far left, centre and far right of the images to convert pixels to mm. A line was drawn from the coccyx bone (base of tail) to the mid point between the eyes (point B-C Figure 3-1) and the distance measured.

NOTE:
This figure is included on page 36
of the print copy of the thesis held in
the University of Adelaide Library.

Figure 3-1_ Physiological locations of foetal lamb measurements (Joubert, 1956).

3.2.4 Processing, Embedding and Sectioning

Foetal skin samples were dehydrated using an Automatic Tissue Processor SE 400 (*Shandon Scientific*) using the following program:

Table 3-1 Tissue Processing Program

Solution	Time (mins)
70% Ethanol	60
80% Ethanol	60
95% Ethanol	30
95% Ethanol	90
Absolute Ethanol	120
Absolute Ethanol	120
Histolene/ Ethanol (1:1)	60
Histolene	120
Histolene	120
Paraffin wax (<i>Histoplast</i>)	120
Paraffin wax (<i>Histoplast</i>)	120

A Tissue Tek II embedding machine (*Lab-Tek Division, Miles Lab. Inc*) was used to embed the processed foetal skin samples in paraffin wax. 7µm section ribbons were cut using a microtome 1512 (*Leitz, GMI Minnesota*) and the ribbon floated from an RO H₂O water bath at 50°C onto Superfrost+™ (*ProSciTech, Kirwan Qld*) slides. The slides were allowed to dry at room temperature for at least 24 hrs prior to staining.

3.2.5 Haematoxylin and Eosin Staining

Paraffin wax embedded foetal skin sections adhered to Superfrost™ plus slides were stained in haematoxylin and eosin using the following optimised protocol:

1.	60°C	10mins
2.	Histolene (ProSciTech, Kirwan Queensland)	15mins
3.	Absolute Ethanol (<i>Crown Scientific</i>)	2mins
4.	80% Ethanol	2mins
5.	30% Ethanol	2mins
6.	Lillee Mayer's Haematoxylin (Appendix I)	5mins
7.	Tap Water	20sec
8.	Acid Ethanol	10sec
9.	Running Tap Water	10mins
10.	Eosin (Appendix I)	10sec
11.	80% Ethanol	7sec
12.	Absolute Ethanol	2mins
13.	Histolene	5mins

Stained slides were then cover slipped directly from the histolene step with Depex (*Sigma, South Croydon Victoria*).

3.2.6 SacPic Staining

Paraffin wax embedded foetal skin sections adhered to Superfrost™ plus slides were stained using the SacPic method according to the following optimised protocol:

1.	60°C	10mins
2.	Histolene	15mins
3.	Absolute Ethanol	2mins
4.	80% Ethanol	2mins
5.	30% Ethanol	2mins
6.	RO Water	2mins
7.	Lillee Mayer's Haematoxylin (Appendix I)	10mins
8.	Tap Water	5dips
9.	70% Ethanol	5dips
10.	Winiwater's Safranin (Appendix I)	12mins
11.	70% Ethanol	2dips
12.	Absolute Ethanol	5dips
13.	Saturated Picric Acid in Ethanol (Appendix I)	5secs
14.	Tap Water	5dips
15.	RO Water	5dips
16.	Picro-Indigo Carmine (Appendix I)	2mins
17.	70% Ethanol	2dips
18.	80% Ethanol	2mins
19.	Absolute Ethanol	2mins
20.	Histolene	5mins

Stained slides were then cover slipped directly from the histolene with Depex.

3.2.7 Histology Images

All images were taken with an Olympus Camedia 8 MegaPixel digital camera through an Olympus Infinity corrected microscope. Images were taken at 10, 20 and 40X through air only.

3.2.8 Statistical Analysis

Microsoft Excel™ was used to perform simple linear regressions between foetal weight and day of gestation, and crown rump length and day of gestation. Regression analysis of foetal weight and crown rump between twins and triplets, and amongst siblings, accounting for day of gestation, was performed in GenStat (*Ceanet, Sydney, NSW*).

3.3 Results

3.3.1 Foetal Measurements

Four foetuses from two twin pregnancies were sampled on days 43, 47, 50, 53, 57, 60, 63 and 68 of gestation. Twin pregnancies were used to reduce the number of pregnant ewes required for the study. At day 43 of gestation, the foetuses were approximately 5cm in length (Figure 3-2), had a mean weight (\pm SEM) of 7.2 ± 0.2 g and a mean crown rump length (\pm SEM) of 79.6 ± 0.7 mm (Table 3-2). At the completion of the sample series (day 68), the foetuses had an approximate length of 13cm (Figure 3-2), a mean weight (\pm SEM) of 120.5 ± 4.7 g, and a mean crown rump length (\pm SEM) of 194.5 ± 3.5 mm (Table 3-2). Variation in the foetal weight data was greater than the crown rump length measurements. As the gestational length increased, so did the extent of variation in both measurements (Table 3-2).

Table 3-2 Summary of foetal data.

Day of gestation	Sample size	Mean Foetal Weight (g \pm SEM)	CoV (%)	Mean CRL (mm \pm SEM)	CoV (%)
43	4	7.2 ± 0.2	5.6	79.6 ± 0.7	1.8
47	4	11.7 ± 0.5	9.0	89.8 ± 1.3	2.8
50	4	17.6 ± 0.8	8.6	105.1 ± 2.9	5.5
53	4	25.2 ± 0.8	6.5	114.1 ± 1.1	2.0
57	5	39.5 ± 1.1	6.3	129.0 ± 1.1	1.9
60	4	55.3 ± 1.3	4.8	145.6 ± 3.4	4.7
63	4	82.0 ± 2.7	6.6	169.4 ± 2.2	2.6
68	5	120.5 ± 4.7	8.6	194.5 ± 3.5	4.0

CRL = crown rump length

CoV = coefficient of variation

SEM = standard error of the mean



Figure 3-2 Digital images of the foetuses sample at: **A** (day 43), **B** (day 47), **C** (day 50), **D** (day 53), **E** (day 57), **F** (day 60), **G** (day 63) and **H** (day 68).

An exponential regression performed between foetal weight and day of gestation demonstrated the two measurements were highly correlated (Figure 3-3; Equation 1).

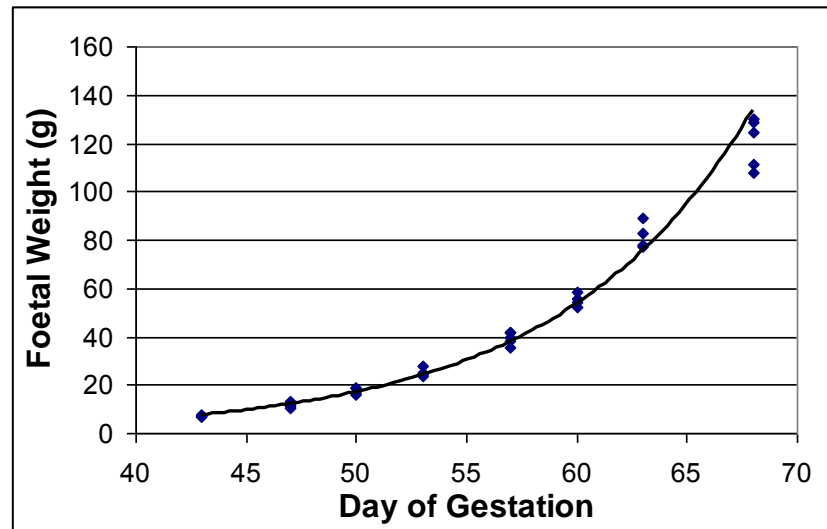


Figure 3-3_ Graph of foetal weight as a function of day of gestation.

$$FW = 0.0552e^{0.1146t} \quad (r^2=0.9907)$$

(FW=foetal weight (g); t= day of gestation)

Equation 1

The regression between crown rump length and day of gestation was also exponential and the two measurements were also highly correlated (Figure 3-4; Equation 2).

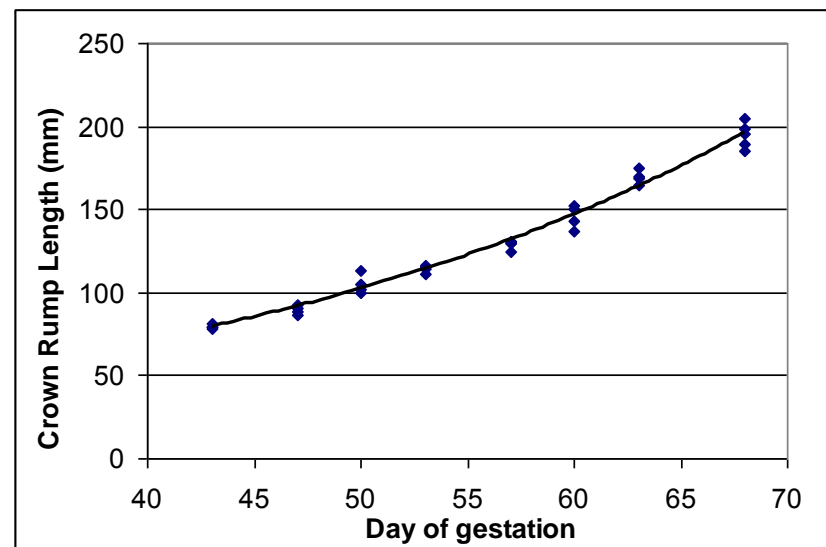


Figure 3-4_ Crown rump length as a function of day of gestation.

$$CRL = 16.568e^{0.0364t} \quad (r^2=0.9791)$$

(CRL=crown rump length (mm); t= day of gestation)

Equation 2

Linear regression analysis of natural log transformed foetal weight and crown rump length showed these two parameters were also highly correlated (Figure 3-5; Equation 3).

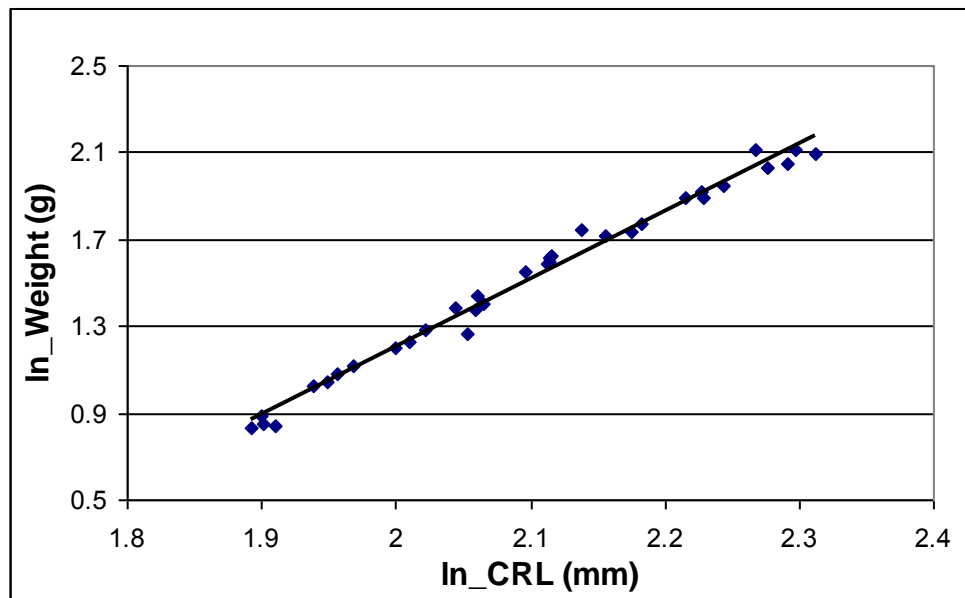


Figure 3-5 *Natural log transformed crown rump length (CRL) vs natural log transformed weight*

$$\ln_Weight = 3.1332 \ln_CRL - 5.0625 \quad (r^2=0.9871)$$

(where CRL = crown rump length)

Equation 3

Regression analysis showed there were no significant differences in weight ($P=0.278$) or crown rump length ($P=0.797$) between twins and triplets. There was also no significant differences in weight ($P=0.834$) or crown rump length ($P=0.884$) between siblings for either twins or triplets.

3.3.1.1 Foetal Data Comparison with a Previous Study

The study by Joubert (1956) is one of the most comprehensive studies of prenatal growth conducted. Therefore, the foetal dimension data obtained herein were compared to the relationships reported by Joubert (1956). The equations for crown rump length as a function of the day of gestation reported in Joubert (1956) were used to calculate: (1) gestational age (calculated gestational age; Table 3-3) using the measured crown rump length, and (2) the

expected crown rump lengths (calculated mean crown rump length; Table 3-3) based on the sample day herein. The difference between the estimated foetal age and the calculated foetal age was greatest at the earliest time point (9 days; Table 3-3). However, at the final time point of day 68, there was no difference between the estimated and calculated foetal ages. Regression analysis of the calculated crown rump lengths (using the equation reported in Joubert (1956), $CRL=0.47155e^{0.05447t}$ where t=day of gestation post artificial insemination) and the actual mean crown rump length (Table 3-3, Figure 3-6, Equation 4) demonstrated that although the relationships were significantly different to each other ($p>0.001$), they were highly correlated ($r^2=0.989$). Since the relationships are correlated but not equal, they cannot be substituted between the studies to estimate foetal age.

Table 3-3 Comparison of measured and calculated (Joubert (1956)) ages and crown rump lengths

NOTE:

This table is included on page 44 of the print copy of the thesis held in the University of Adelaide Library.

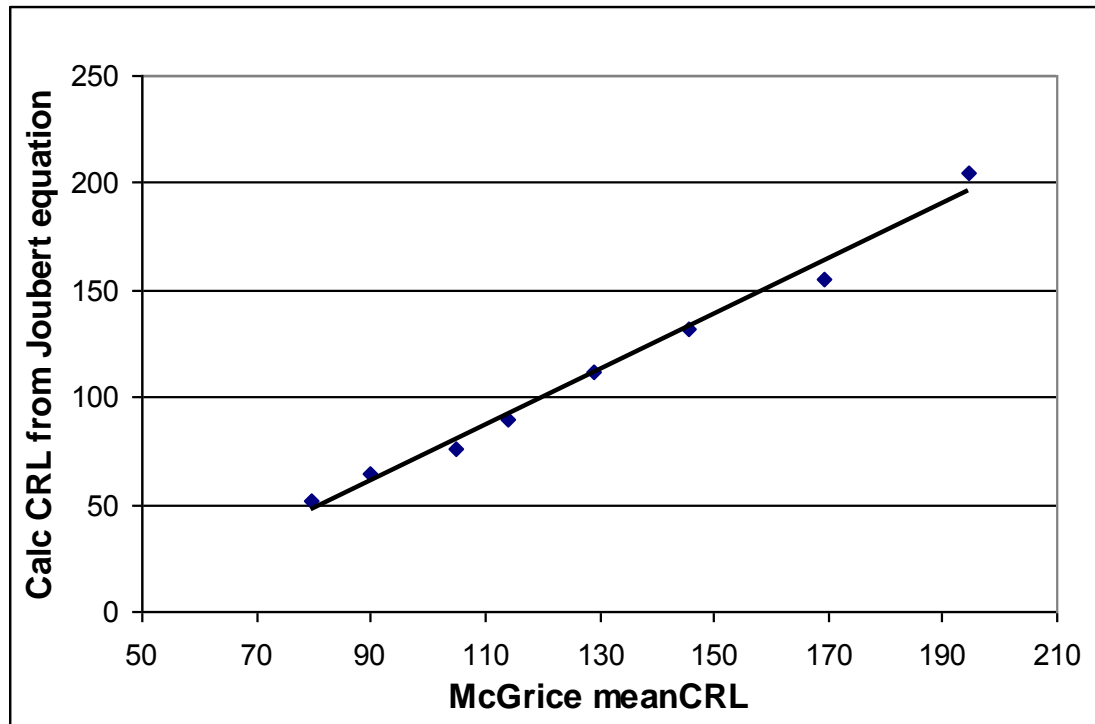


Figure 3-6 Correlations between the calculated crown rump length (equation from Joubert (1956)) and the actual mean CRLs of this study.

$$\text{Calculated CRL} = 1.3003 (\text{mean_CRL}) - 56.57 \quad (r^2 = 0.9891)$$

(where CRL = crown rump length)

Equation 4

3.3.2 Histological Characterisation

At day 43, 47 and 53 of gestation, none of the foetuses sampled showed any signs of follicle initiation (Figure 3-7A-C and Figure 3-8A-C). The epidermis was 1-2 cell layers thick. Although not quantified, the mesenchyme appeared to have a lower cell density than at later time points. At day 57, all 4 samples showed evidence of primary follicle epidermal placodes, with 2 of the 4 samples showing signs of dermal condensation (Figure 3-7E; d57 and Figure 3-8E; d57). Furthermore, although not quantified, there appeared to be an increase in the cell density of the mesenchyme (dermis) at day 57. By day 60, a condensation of mesenchymal cells below the placodes was evident in all samples (Table 3-4). At day 68, all foetal skin samples showed clear evidence of a hair germ, characterised by the initial down

growth of the epidermal placode into the underlying mesenchyme and this down growth was enveloped by the dermal condensate (Figure 3-7G; d68).

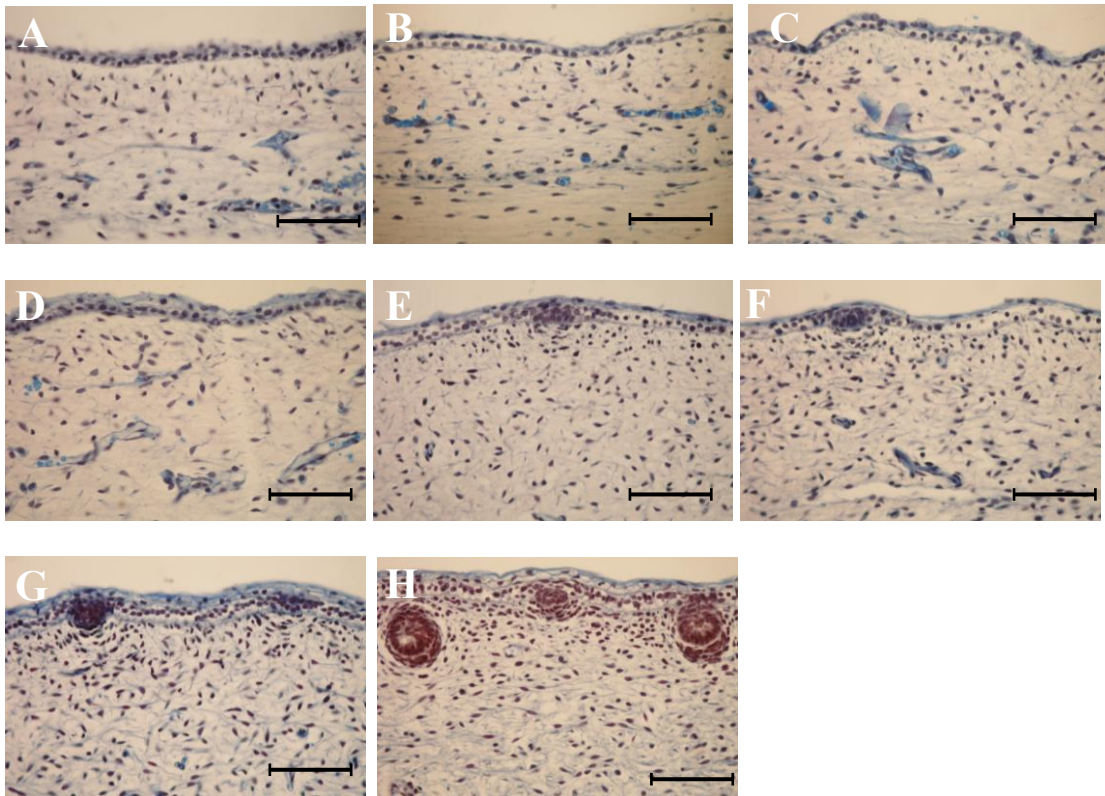


Figure 3-7_SacPic stained 10µM skin sections for histological characterisation of the foetal skin samples; A (day 43), B (day 47), C (day 50), D (day 53), E (day 57), F (day 60), G (day 63) and, H (day 68).

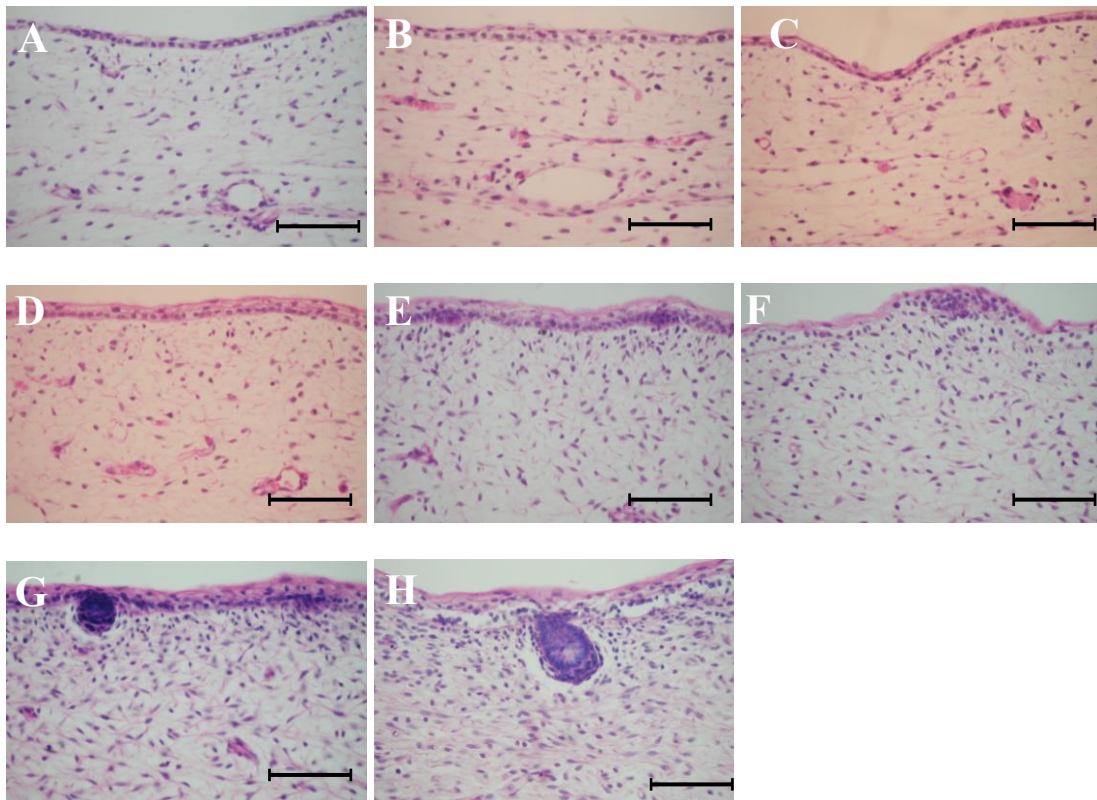


Figure 3-8_ Haematoxylin stained 10µM skin sections for histological characterisation of the foetal skin samples; A (day 43), B (day 47), C (day 50), D (day 53), E (day 57), F (day 60), G (day 63) and, H (day 68).

Table 3-4_ Summary of Histological Characterisation

Day of Gestation	Epidermal Placodes	Dermal Condensates	Hair Germ
43	-	-	-
47	-	-	-
50	-	-	-
53	-	-	-
57	+	-	-
60	+	+	-
63	+	+	-
68	+	+	+

3.4 Discussion

3.4.1 Foetal Sample Series

In order to study the dynamics of wool follicle initiation, foetal samples were generated by timed matings and serial sampling of foetuses from day 43 to day 68, which spans the timing of primary follicle initiation. Whilst generating the foetal time series, an overdose of barbiturates was not used when sacrificing the ewes as this may have affected subsequent gene expression within the foetus and therefore, could have adverse effects on the subsequent expression studies. Twin pregnancies were selected to reduce the number of ewes required for the experiment. This was possible because divergence in the development of twin foetuses due to better nutritional support of one foetus over another is not thought to occur until late in the second and during the third trimesters (Kelly and Newnham, 1989). Due to the inaccuracy of pregnancy scanning at day 50, two sets of triplets were sampled at days 57 and 68.

Artificial insemination was performed 48 hrs after CIDR removal as it has been reported that fertilization rates are higher when insemination occurs at 48 hrs rather than 24 hrs after CIDR removal (Cognie, 1990). The sperm used in the laparoscopic artificial insemination was collected on the day of insemination using teaser ewes and an artificial vagina. Fresh semen was used as fertilization rates are usually 20-30% higher using fresh semen as opposed to frozen semen (Maxwell et al., 1990). The day of insemination was recorded as day 0 of gestation. This day may not be entirely accurate as the exact day of conception can vary due to the time taken for spermatozoan capacitation and survival in the uterine tract. The spermatozoan must undergo capacitation before they can engage in fertilization. Capacitation is reported to take approximately 1.5 hrs in the sheep, and sperm are reported to survive and remain fertile in the reproductive tract for 24 hrs in most mammals (Austin, 1972) and 24-48 hrs in humans (Gwatkin, 1977). Therefore, the age of the foetuses based on the day of insemination was only a predicted foetal age and may vary by 24-48 hrs.

The exponential relationship between foetal weight and day of gestation showed a strong correlation ($r^2=0.9907$) as did the exponential relationship between crown rump length and day of gestation ($r^2=0.9791$). Therefore, a linear regression between the natural log of foetal weight and the natural log of the crown rump length was performed, and verified that the correlation between these two parameters was high ($r^2=0.9871$). The natural log transformation and regression were performed to determine the power of the allometric relationship between weight and crown rump length. The slope of the linear regression was 3.1332, and therefore, weight is proportional to crown rump length raised to the power of 3.1. The strong correlation between these two parameters gives confidence that the crown rump length measurements provide an accurate representation of foetal age and growth across the sample time series.

The foetuses sampled in this experiment were generated through artificial insemination so only their approximate age (post day of insemination) was known. However, where retrospective assessment of gestational age is required, various foetal measurements of skeletal size at the time of slaughter, such as crown rump length (CRL), can be used to estimate the day of pregnancy based on previously published data (Joubert, 1956; Kelly and Newnham, 1989). Therefore, in order to assess the accuracy of the estimated foetal age herein, crown rump length measurements were made using the image analysis program *analySIS*® on photographic digital images taken at the time of sampling. The scale bar (30cm ruler) in some of the images demonstrated that the digital camera was not exactly horizontal to the foetuses, creating potential for error in the measurements made on these images. The positioning of some of the foetuses (i.e. head slightly tilted and tail tucked beneath the foetus, etc.) also made it difficult to determine where to start and finish the measurement. Therefore, the subjective nature of these measurements created a degree of error in these data. In future samplings of this nature, the image should be taken from a retort stand with precise positioning of the foetus, such that the head and the tail are well separated from the animal

and the foetus is laying flat on the surface. This should increase the accuracy of measurements made on the photographic images.

As in previous studies, crown rump lengths were plotted against foetal weight to demonstrate foetal age as a function of weight (Joubert, 1956; Bryden et al., 1972; Sivachelvan et al., 1996). Regression analysis of the calculated crown rump lengths (using the equation reported in Joubert (1956): $CRL=0.47155e^{0.05447t}$ where t=day of gestation post artificial insemination;) and the actual mean crown rump length (Table 3-3, Figure 3-6, Equation 4) demonstrated that although the relationships were significantly different to each other ($p>0.001$), they were highly correlated ($R^2=0.989$). The strong correlation between these two studies further demonstrated that the crown rump length measurements made herein were accurate. The fact that the relationships are not equal demonstrates that Joubert's equations are not accurate for estimating foetal age in Merino foetuses. The equations therefore, cannot be substituted between the studies to estimate foetal age. The data collated in the Joubert study were sourced from many different breeds of sheep, including Merino, Hampshire, Suffolk, Border Leicester, Cheviot and Karakult. Therefore, some of the variation in the data and equations between these two studies can be explained by breed differences. Furthermore, the animals in the study herein were generated through laparoscopic artificial insemination following synchronisation, whereas the foetuses in the previous study were aged according the recorded day of natural mating and did not include oestrous synchronisation. The range in weight and crown rump length data at each time point in Joubert's study was greater than in the current study, and therefore, certain data points placed high leverage on the equations. Therefore, the equations were accurate across the extensive sample series, but not as accurate for estimating weight and crown rump length for specific time points. In addition to this, due to the many breeds included in Joubert's study, the coefficient of variation for crown rump length was 6.23%, whereas the largest coefficient of variation in crown rump length herein was 5.50% at day 50 post insemination (Table 3-2).

Therefore, it can be concluded that the equation for crown rump length (CRL) as a function of day gestation (t) generated herein:

$$\text{CRL} = 16.568e^{0.0364t} \quad (r^2=0.9791)$$

is more accurate for estimating foetal age in Merinos than the equation reported by Joubert (1956) and should therefore, be used in future prenatal studies involving Merinos.

3.4.2 Histological Characterisation

Wool follicles commence initiation in the skin of sheep at approximately day 50 of gestation (Hardy and Lyne, 1956; Hocking Edwards et al., 1996) as a result of dynamic interactions between the primitive epidermis (arising from the ectoderm) and the underlying dermis (arising from the mesoderm) (Powell et al., 1998). Due to morphological conservation amongst mammals, the stages of wool and hair follicle initiation are highly similar. The first sign of epithelial appendage formation is the appearance of epidermal placodes (Paus et al., 1999), which are characterised by epidermal thickenings that appear in an evenly spaced follicle pattern (Moore et al., 1998). Placodes were visible in the histological sections of the foetal samples from day 57 of gestation. The aggregation of mesenchymal cells beneath these placodes began at day 60 and was clearly visible in all animals from day 63 (Figure 3-7 and Figure 3-8).

Primary hair follicles are initiated in the back skin of mice, beginning day 15 of embryonic development (Paus et al., 1999; Rendl et al., 2005) in a process that is morphologically similar to wool follicles. Epidermal placodes are first visible at day 15 of mouse embryonic development, followed by condensation of mesenchymal cells beneath the mouse hair placodes at day 17. Feather placodes are initiated in the skin of chicken embryos at approximately day 6.5, when the epidermal placodes begin to initiate along the back line of the embryo (Sengel, 1975). Feather buds are different to hair follicles in that the buds grow outwards away from the dermis forming the feather tract, whereas hair and wool follicles grow down into the dermis forming the hair or wool canal.

The size, spacing and distribution of primary follicle primordial (the placode and condensate) is referred to as the primary follicle pattern. This pattern is thought to dictate the density, distribution and size of secondary follicles (Mou et al., 2006). In sheep, the secondary follicles are initiated in groups associated with 3 primary follicles at around day 80 of gestation. These secondary follicles then branch at day 100, forming secondary derived follicles. The 3 primary follicles and associated secondary and secondary derived follicles are referred to as a follicle group (Nixon, 1993). The foetal skin series generated herein ended at day 68 of gestation. Therefore, morphological signs of secondary wool follicle initiation were not observed in the histological sections. Since only primary wool follicle initiation was observed in these samples, it can be assumed that the molecular signals arising from them will reflect only the signals involved in primary wool follicle initiation.

3.5 Conclusion

Comparison of crown rump length and foetal weight data with that of previous studies demonstrated that the crown rump length measurements made herein were accurate and that the estimated day of gestation was a reasonable representation of foetal age. Furthermore, the equations formulated herein are more accurate than previously reported equations for estimating foetal age from crown rump length in Merino foetuses and should therefore be used in future prenatal studies involving Merinos.

The histological characterisation of the shoulder skin samples demonstrated that the initiating wool follicles within these foetal skin samples followed the previously described timing and morphology of primary wool follicle initiation. The morphology was also similar to that seen in mouse and rat. Therefore, it can be concluded that the foetal skin series generated herein is appropriate for subsequent molecular analysis of primary wool follicle initiation.

Chapter Four

Quantitative PCR of Whole Skin

Chapter 4 : Quantitative PCR Analysis of Whole Skin

4.1 Introduction

As the link between DNA and protein, the mRNA molecule is of central importance in both biomedical and agricultural research (Randonic et al., 2004). Gene-expression analysis has become increasingly important in many biological research disciplines, as understanding spatial and temporal expression provides an insight into complex regulatory networks and has led to the identification of genes implicated in disease or genes relevant to novel biological processes (Vandesompele et al., 2002; Peirson et al., 2003). Real-time PCR, first described in 1993 as kinetic PCR using ethidium bromide as the fluorescent reporter (Higuchi et al., 1993), is now an established technique for quantifying messenger RNA (mRNA) levels in biological samples. Quantitative Reverse Transcriptase PCR (qRT-PCR) is a real-time PCR technique that involves extracting total RNA from a biological sample (ribosomal RNA and mRNA) and converting it into cDNA prior to PCR quantitation. The synthesis of cDNA is performed by combining RNA with a reverse transcriptase enzyme and oligonucleotide primers that are either random hexamers, oligodT or gene-specific. Generally, qRT-PCR is conducted with either probe-based assays (e.g. Taqman) or the incorporation of fluorescent dyes (such as SYBR green and SYTO9) into double stranded PCR products. qRT-PCR has advantages over traditional mRNA quantification techniques, such as Northern blots and RNase protection assays, that in many cases are unsuitable as their low sensitivity necessitates high concentrations of starting template (Bustin, 2000). Many key proteins (e.g. cytokines and transcription factors) are in such low abundance that qRT-PCR represents the only technique sensitive enough to reliably measure their gene expression *in vivo* (Nolan et al., 2006).

The accuracy and quality of the data produced using qRT-PCR are highly dependent upon RNA integrity, quality, purity and concentration. Low quality RNA may strongly compromise the results of the qRT-PCR analysis (Fleige et al., 2006). Particular attention

must be paid not only to the sample collection strategy and RNA extraction procedure but also to the reaction conditions and normalisation strategy.

4.1.1 Normalisation of qRT-PCR data: geNorm

The relative quantification of gene expression differences between two or more samples is based on normalisation of the target gene expression to stably expressed internal reference gene(s), also known as a “housekeeping” genes (Jung et al., 2007). The purpose of qRT-PCR normalisation is to correct for non-specific variation, such as any differences in RNA quantity and quality and in reverse transcription efficiency, both of which can have an effect on the efficiency of qPCR (Brunner et al., 2004). Careful consideration must be paid when choosing the reference gene(s) for a particular sample series, as not all reference genes are stably expressed in various tissue types. Ideally, the reference gene(s) should not be regulated or influenced by the experimental procedure (Randonic et al., 2004). The accurate quantification of a non-regulated, stably expressed reference genes allows normalisation of any differences in the amount of input RNA and amplifiable cDNA generated by: (1) variation in the quantity of the starting material, (2) the quality of the starting material, (3) slight discrepancies in RNA preparation, and (4) inconsistencies in cDNA synthesis efficiency (Randonic et al., 2004; Huggett et al., 2005).

A recent study has reported that normalising for the amount of input cDNA, through cDNA quantification using Picogreen®, can remove the need for normalisation genes (Libus and Storchova, 2006). However, it can be argued that this approach does not account for variation in transcription rates within and across samples both *in vivo* and during cDNA production. Furthermore, majority of cDNA is produced from ribosomal RNA, so this method would simply be quantifying the 18S and 28S cDNA in each sample.

4.1.2 Candidate Genes for qPCR Analysis of Wool Follicle Initiation

4.1.2.1 Actin-based Fibroblast Migration

Fibroblast locomotion or migration requires regulated actin re-modelling to form membrane protrusions, or lamellipodia, that facilitate cell extension (Pantaloni et al., 2001). Small GTP-binding proteins from the Rho family (e.g. RAC1, RHOa and CDC42), closely regulate the assembly of actin filament structures, such as spikes emanating from the leading plasma membrane of the migratory cells (Hall, 1998). The canonical pathways through which RHOa and RAC1 regulate actin remodelling are best characterised in fibroblasts, a typical migratory cell (Ridley and Hall, 1992). During fibroblast migration, the actin filament barbed ends at the leading edge of the lamellipodia grow rapidly through the polymerisation of actin, while the pointed ends of the filaments depolymerise at the rear in a treadmilling process (Wang, 1985). CDC42 causes formation of filopodia, thin finger-like extensions that contain tight actin bundles, which have been proposed to be involved in extracellular environment recognition (Wennerberg and Der, 2004). Considering the importance of RAC1 and RHOa in assembly and polymerisation of the actin cytoskeleton, these two genes were selected as candidate markers of cell migration for the purpose of this study.

4.1.2.2 Skin Stem Cell Markers

The human epidermis and dermis have proved a fruitful source of adult stem cells for identifying stem cell markers and for altering the differentiation lineage for utilisation in wound healing and production of replacement organs (Jahoda et al., 2003). One such set of potential stem cell markers are the integrin receptors, a family of transmembrane glycoproteins that interact with a variety of ligands. The extracellular domain of integrins interacts with extracellular matrix glycoproteins and the intracellular domain interacts with the cell cytoskeleton (Hynes, 1987). The α and β subfamilies of integrins include receptors for laminin, fibronectin and collagen, important components in the structure of skin. Epidermal stem cells express high levels of $\beta 1$ and $\alpha 6$ integrins (Brouard and Barrandon, 2003), and

therefore, these are routinely used as cell surface markers, in combination with other epidermal stem cell markers (such as p63) when isolating epidermal stem cells. Mice lacking a functional copy of *p63* lack all stratified epithelia (Mills et al., 1999; Yang et al., 1999). However, *p63* expression alone is not sufficient to identify epidermal stem cells because it is expressed by all basal cells and suprabasal cells of the epidermis and outer root sheath (Gambardella and Barrandon, 2003). Hence, a combination of cell surface markers are often used to enrich epidermal stem cells populations (e.g. Integrin bright, CD71 dim) (Webb et al., 2004). Not all $\beta 1$ -integrin-bright cells are stem cells as approximately 40% of basal cells are integrin bright, while the percentage of stem cells in the basal layer is closer to 10%. However, integrin levels can and have been used to reveal the distribution of stem cells in the epidermis (Jones et al., 1995; Jensen et al., 1999). Therefore, although no definitive epidermal stem cell marker has yet been identified, for the purposes of this study, *$\beta 1$ -integrin* was selected as the candidate epidermal stem cell marker gene.

Alkaline phosphatase (ALP) has been previously established as a reliable marker of mesenchymal stem cells, as stromal cells (non-haematopoietic cells of the mesenchyme), thought to be destined to form osteoblasts, express high levels of *ALP* and are closely associated with haematopoietic stem cells (Bianco and Boyde, 1993; Deans and Moseley, 2000). The multipotent cells of the follicular papilla are of a mesenchymal origin and have been shown to have bone marrow forming capacity (Lako et al., 2002). Therefore, these cells express similar mesenchymal stem cell markers, such as *ALP* and *CD34*. Interestingly, *CD34* also highlights cells of the follicle “bulge” (Cotsarelis, 2006a). Live epidermal *CD34*⁺ cells isolated with *CD34* antibodies also express *K15* (follicle bulge cell marker) and overlap with DNA label-retaining cells (Trempeus et al., 2003). *CD34*, therefore, does not discriminate between dermal and epidermal stem cells. Cultured dermal papilla cells have high *ALP* activity (McElwee et al., 2003) and *ALP* is one of the first histological markers of the dermal

papilla (Handjiski et al., 1994). Therefore, for the purposes of this study, *ALP* was selected as the candidate dermal stem cell marker.

4.1.2.3 Cell Proliferation

In mammalian cells, proliferation is under the control of cyclins that regulate the transition between cell stages at two main checkpoints; the G1-S transition, which initiates DNA replication, and the G2-M transition, which controls mitosis and cell division (Xu et al., 2003). Cyclins are chemical modulators of the cell cycle, which function through the activation and association with kinase subunits (Murray, 2004). Cyclin A and E were the first to be discovered in sea urchin eggs (Evans et al., 1983). However, the cyclin family has since expanded to include multiple cyclins and cyclin-dependent kinases involved in the cell cycle, transcription and differentiation. Throughout the cell cycle, there are cyclins associated with G1 phase (cyclin D), S phase (cyclins E and A) and mitosis (cyclins B and A). Cyclins E and D support DNA replication and chromosome duplication (G1-S transition), cyclin A supports these functions and mitosis, whereas cyclin B supports mitosis alone (G2-M transition) (Kakino et al., 1996; Strausfeld et al., 1996).

Modulation of cyclin B1, the regulatory subunit of serine/threonine kinases, is essential for entry into mitosis (Johnson and Walker, 1999); furthermore, over-expression of *cyclin B1* is observed in several cancers (Soria et al., 2000; Yasuda et al., 2002). Depletion of *cyclin B1* levels through the use of small interfering RNAs arrests tumour cells in the G2/M phase of the cell cycle (Yuan et al., 2004), demonstrating that an increase in cellular cyclin B1 is essential for cell proliferation.

Proliferative Cell Nuclear Antigen (PCNA) is a protein clamp involved in DNA replication at the G1/S transition in proliferating cells (Takahashi and Caviness, 1993). PCNA has been used in combination with Ki-67 as a proliferative marker in benign and malignant epithelial lesions of the human parotid gland (Zhu et al., 1999), as a proliferative

marker during embryonic and adult zebrafish hematopoiesis (Leung et al., 2005) and has been well documented as one a many classic cell cycle regulators (Korgun et al., 2006).

Therefore, for the purposes of this study, *CYC B1* and *PCNA* were selected as candidate proliferation markers.

4.1.2.4 Tumor Necrosis Factor Signalling in Hair Follicle Development

The ectodysplasin family of ligands comprise trimeric type II transmembrane proteins, which are produced through the alternate splicing of the ectodysplasin gene. Two splice variants of the *ectodysplasin* gene, *EDA-A1* and *EDA-A2*, differ by only 2 amino acids (Figure 4-1). The differentially-spliced exon 8 comprises the tumor necrosis factor (TNF) binding domain of the protein. Altering this domain by 2 amino acids changes the TNF receptor binding of these ligands (Botchkarev and Fessing, 2005, Figure 4-1). Namely, EDA-A1 is known to bind to the ectodysplasin receptor (EDAR) and the EDA-A2 variant binds to the X-linked ectodysplasin receptor (XEDAR) (Hashimoto et al., 2006, Figure 4-1).

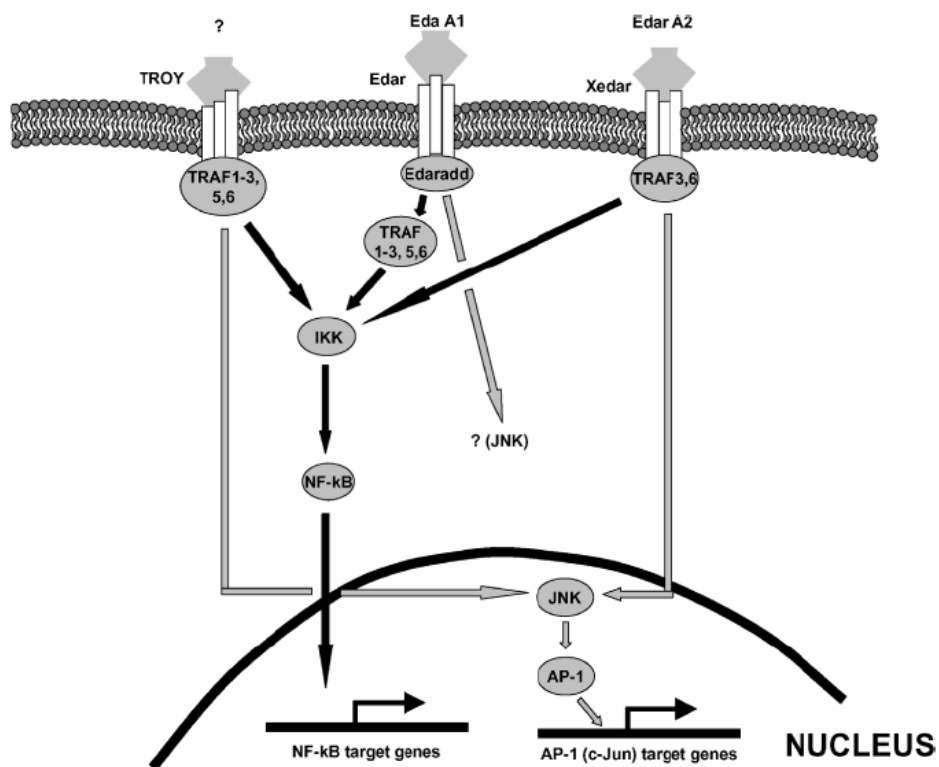


Figure 4-1 The Tumor Necrosis Factor Signalling Pathway, (Botchkarev and Fessing, 2005)

Binding of EDA-A1 to EDAR recruits the cytoplasmic adaptor ectodysplasin receptor adapter death domain (EDARADD), which in turn, induces signalling through the TNF-receptor-associated factor (TRAF). This leads to activation of the I κ B kinase complex (IKK) necessary for translocation of NF- κ B transcription factor to the nucleus (Headon and Overbeek, 1999; Headon et al., 2001; Newton et al., 2004). Binding of EDA-A2 to XEDAR allows direct signalling to the TRAF proteins because XEDAR contains its own adapter death domain (Figure 4-1). Mutations in *EDA*, *EDAR* and *EDARADD* result in the human congenital condition hypohidrotic ectodermal dysplasia, characterised by sparse hair, missing and malformed teeth, and the absence of sweat glands. The causative genes were confirmed by the mouse gene mutant homologs of *Tabby*, *Downless* and *Crinkled* (Ferguson et al., 1997; Headon and Overbeek, 1999; Headon et al., 2001). These mice lack guard, zig-zag and, in most cases, awl hairs. Their teeth are malformed and they have bald patches behind their ears. Null-mutations in *TRAF-6* produce a similar phenotype to *Tabby* and *Downless* without the bald patches behind the ears, with the addition of hypoplastic sebaceous glands (Botchkarev and Fessing, 2005). Interestingly, null-mutations in the *EDA-A2* variant, *TROY* and *XEDAR* result in normal hair development.

Considering the importance of EDA, EDAR, EDARADD and TRAF-6 in hair follicle development and the unknown involvement of XEDAR and TROY in this morphological process, these 6 genes were selected as candidates to study the involvement of TNF signalling in primary wool follicle initiation.

4.1.2.5 Sonic Hedgehog Signalling in Hair Follicle Development

The hedgehog signalling pathway is fundamental in regulating the development of many tissues. Originally described in *Drosophila*, three human homologues have been described to date (Sonic, Desert and Indian), of which, Sonic Hedgehog (SHH) is the most well characterised. Sonic hedgehog (SHH) is a secreted signalling molecule that provides developmental signal that can act at a distance and has different effects depending on its

concentration (Bumcrot and McMahon, 1996; Iseki et al., 1996). SHH is an important morphogen in vertebrate embryonic development (Marigo et al., 1996; Weed et al., 1997; Chuong et al., 2000; Pons and Marti, 2000). Binding of SHH to its receptor Patched-1 (PTCH1), a tumour repressor gene, releases its inhibitory effects on the transmembrane protein Smoothed (Michno et al., 2003), which in turn, activates the transcription factors Gli1,2,3 (Figure 4-2).

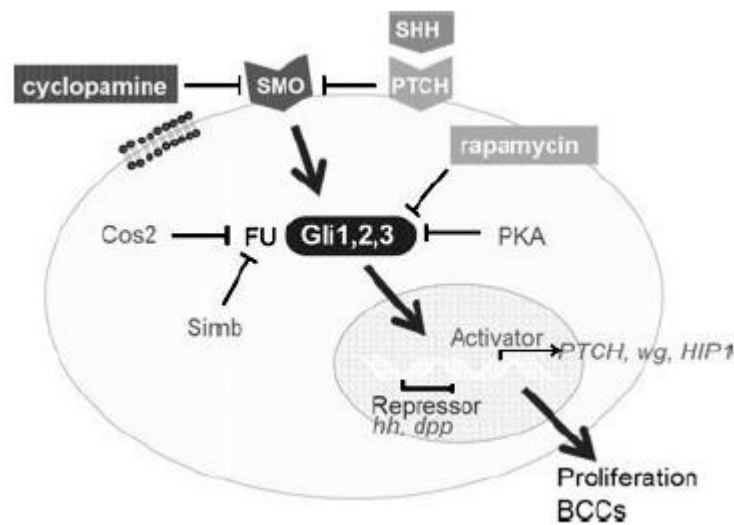


Figure 4-2_Sonic hedgehog signalling leading to proliferation in the skin (Athar et al., 2006)

In epithelial embryology, it has been well characterised that *SHH*, normally expressed in the basal cells of the skin, promotes epidermal differentiation (Adolphe et al., 2004), and in the case of hair and feather follicle initiation, it is required for progression past the hair germ stage. Furthermore, inappropriate activation of the *SHH* signal transduction cascade in human epidermis can cause basal cell carcinoma (Morgan et al., 1998). *SHH* knockout mice develop normal hair germs comprising epidermal placodes and associated dermal condensates but progression through subsequent stages of follicle development is blocked in the skin of mutant animals (St-Jacques et al., 1998; Chiang et al., 1999; Adolphe et al., 2004). Therefore, it is likely that the second dermal signal regulating proliferation and downgrowth of the hair germ is activated by SHH signalling (Ellis et al., 2003) and regulated through PCTH1 and

Smoothened. Since SHH is required for progression past the hair germ stage, it is also commonly used as an *in-situ* marker for hair follicle organogenesis (Iseki et al., 1996). Due to its importance in tumour suppression, the *PTCH1* mouse knockout is embryonic lethal (Nieuwenhuis et al., 1997), and therefore, its specific role in primary follicle initiation is unclear.

Considering the importance of *SHH* signalling in epithelial proliferation and subsequent downgrowth of the hair follicle, this morphogen and its receptor *PTCH1* were selected as candidate genes for the epithelial/mesenchymal interaction in the developing wool follicle that precedes follicle downgrowth.

4.2 Aim

The aim of the qRT-PCR experiments was to ascertain the importance of stem cell migration and proliferation in primary follicle initiation. Furthermore, by measuring the mRNA levels of key signalling molecules from the TNF pathway, the involvement of ectodysplasin signalling in primary wool follicle initiation could be determined.

4.3 Specific Methods

4.3.1 qRT-PCR

Complementary DNA (cDNA) from midside and rump skin samples from 30 foetuses were analysed in triplicate by qRT-PCR. A total of 60 cDNA samples were generated from one midside and one rump skin sample from two foetuses sampled on day 43 and each of four foetuses sampled on days 47, 50, 53, 57, 60, 64, 68. Using the Power SYBR reagent according to the manufacturer's instructions (Applied Biosystems), two genes were measured per 384-well plate with 10 μ l reaction volumes in a 384 well real-time PCR machine (7900, Applied Biosystems). For each gene, a 4 point standard curve was generated using 1:5, 1:25, 1:125 and 1:625 dilutions of a foetal sheep skin cDNA pool covering the gestational time series. The qRT-PCR data produced from a complete run were deemed accurate if the reaction

efficiency was between 0.80 and 1.0 and the melt curve showed evidence of only one specific product, as verified by gel electrophoresis.

4.3.2 geNorm Analysis and Normalisation of qPCR data

A commercially-available normalisation kit, called geNorm (*Primer Design, UK*), containing 12 pre-optimised qPCR assays targeting genes previously reported to be stably expressed in a variety of ovine tissue types, was employed to analyse each foetal skin sample in the series. During a preliminary assessment, only 7 of these assays amplified a single amplicon and/or produced standard curves with reaction efficiencies between the desired 0.8 – 1.0 range. Three assays (18SrRNA, beta-actin and RPLP19) that have previously been used in our laboratory to normalise ovine and bovine qRT-PCR data were also included in the geNorm analysis.

The primer sets supplied by Primer Design (Table 4-1) and the existing primer sets (Table 4-2B, primer sequences in Appendix II) included in the geNorm analysis targeted the following genes:

Table 4-1 Reference gene primer sets supplied by Primer Design

Accession Number	Sequence Definition
AY970970	Ovis aries tyrosine 3-monooxygenase (YWHAZ) mRNA
AY563024	Ovis aries ribosomal protein S26 (RPS26) mRNA
NM_001009284	Ovis aries beta-2 microglobulin (B2M), mRNA
AF233351	Ovis aries malate dehydrogenase (MDH1) mRNA
DQ520732	Ovis aries ribosomal protein S2 (RPS2) mRNA
NM_001009468	Ovis aries H(+)-transporting ATP synthase (ATPsynth), mRNA
AF035421	Ovis aries glyceraldehyde 3-phosphate dehydrogenase (GAPDH) mRNA
DQ239617.1	Ovis aries actin-related protein (ARP) mRNA

Table 4-2 *In house reference gene primer sets (primers in Appendix II)*

Accession Number	Sequence Definition
DQ013885	Ovis aries 18S Ribosomal (18SrRNA) rRNA
NM_001009784	Ovis aries beta actin (bActin), mRNA
AY158223	Bos taurus Ribosomal protein large 19 (RPLP19), mRNA

The relative expression values, as determined from their Ct, were analysed using the geNorm software and pairwise comparisons made between the combinations of reference genes to determine the number of reference genes required to obtain accurate normalisation.

Each foetal skin sample was normalised to the geometric mean of the three most stably expressed reference genes assayed using a SAS mixed model statistical analysis. The normalised expression of each sample was expressed relative to the midside skin sample from day 43 foetus 1 (labelled the relative normalised expression value herein).

4.3.3 Statistical Analysis of Relative Expression Patterns

Statistical analysis of qRT-PCR data was performed in SAS (SAS v9.1, SAS Institute Inc., Cary, NC). The relative normalised expression was analysed using a mixed model with site (midside or rump) and day of gestation as fixed effects and the animal ID as a random term.

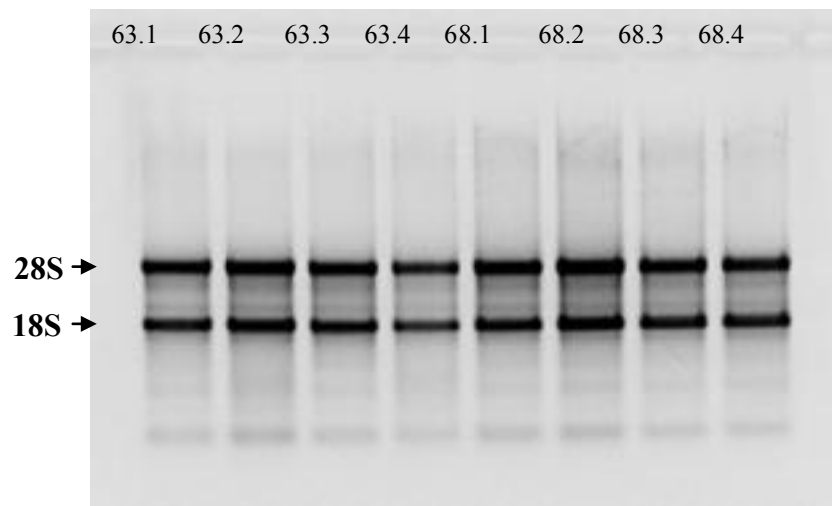
4.4 Results

4.4.1 RNA extractions

Spectrophotometric and gel electrophoresis analysis of RNA quality (Table 4-3) and integrity (Figure 4-3) demonstrated that the extracted RNA was of excellent quality and suitable for the qRT-PCR experiments.

Table 4-3 *Example of RNA extraction quality analysis*

Sample Number	Amount of Tissue Homogenised (mg)	260:280 ratio	RNA concentration (ng/ μ l)	Total RNA eluted from the column (μ g)
63.1	132	1.693	400.4	12.012
63.2	164	1.657	494.7	14.84
63.3	153	1.751	389.2	11.676
63.4	105	1.684	273.5	8.204
68.1	132	1.649	465.7	13.972
68.2	150	1.683	566.5	16.996
68.3	130	1.678	435.9	13.076
68.4	130	1.722	410.7	12.32

**Figure 4-3** *Typical 1% agarose gel showing integrity of the 28S and 18S ribosomal bands (arrows) in midside RNA preparations from day 63 and 68.*

The amount of RNA extracted from the tissue samples increased as the time series progressed presumably due to an increase in complexity and cellularity of the more mature foetal skin samples (Figure 4-4).

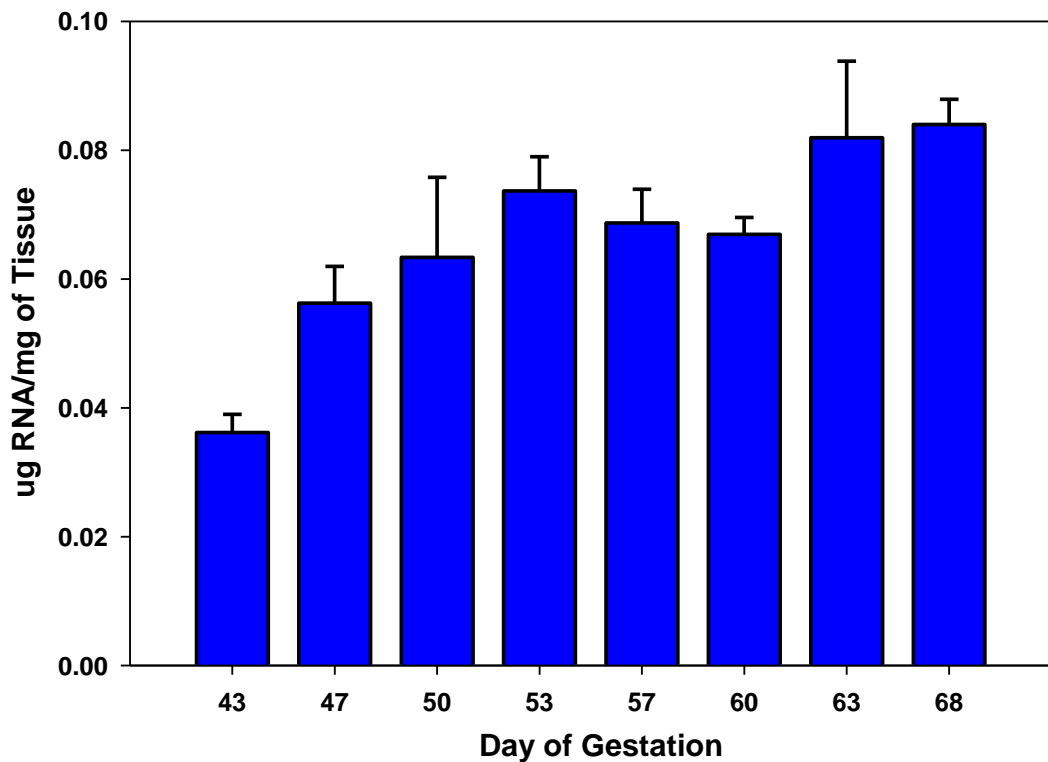


Figure 4-4_ Graph of total RNA extracted per mg of tissue (mean \pm SEM).

4.4.2 geNorm Analysis

Eight sheep geNorm kit gene assays, three existing reference gene assays from our laboratory and 2 target gene assays were included in the geNorm analysis. *RAC1* and *RHOa*, followed by *GAPDH*, were the three most stably expressed genes across the sample series (Figure 4-5). β 2-Microglobulin followed by *β -actin* and *ribosomal 18S* were the least stable reference genes assayed. Pairwise variation analysis (Figure 4-6) of the reference gene combinations demonstrated that by including any additional reference genes other than the three most stably-expressed genes (*RAC1*, *RHOa* and *GAPDH*) would not improve the effectiveness of qRT-PCR data normalisation.

RAC1 and *RHOa* were selected as markers of migration. Therefore, in order to statistically assess these two genes, they were normalised against the geometric mean of *GAPDH*, *YWHAZ* and *ATPsynthase*, the next three most stably-expressed genes (Figure 4-5).

All other target genes were normalised against the geometric mean of the three most stably expressed genes *RAC1*, *RHOa* and *GAPDH*.

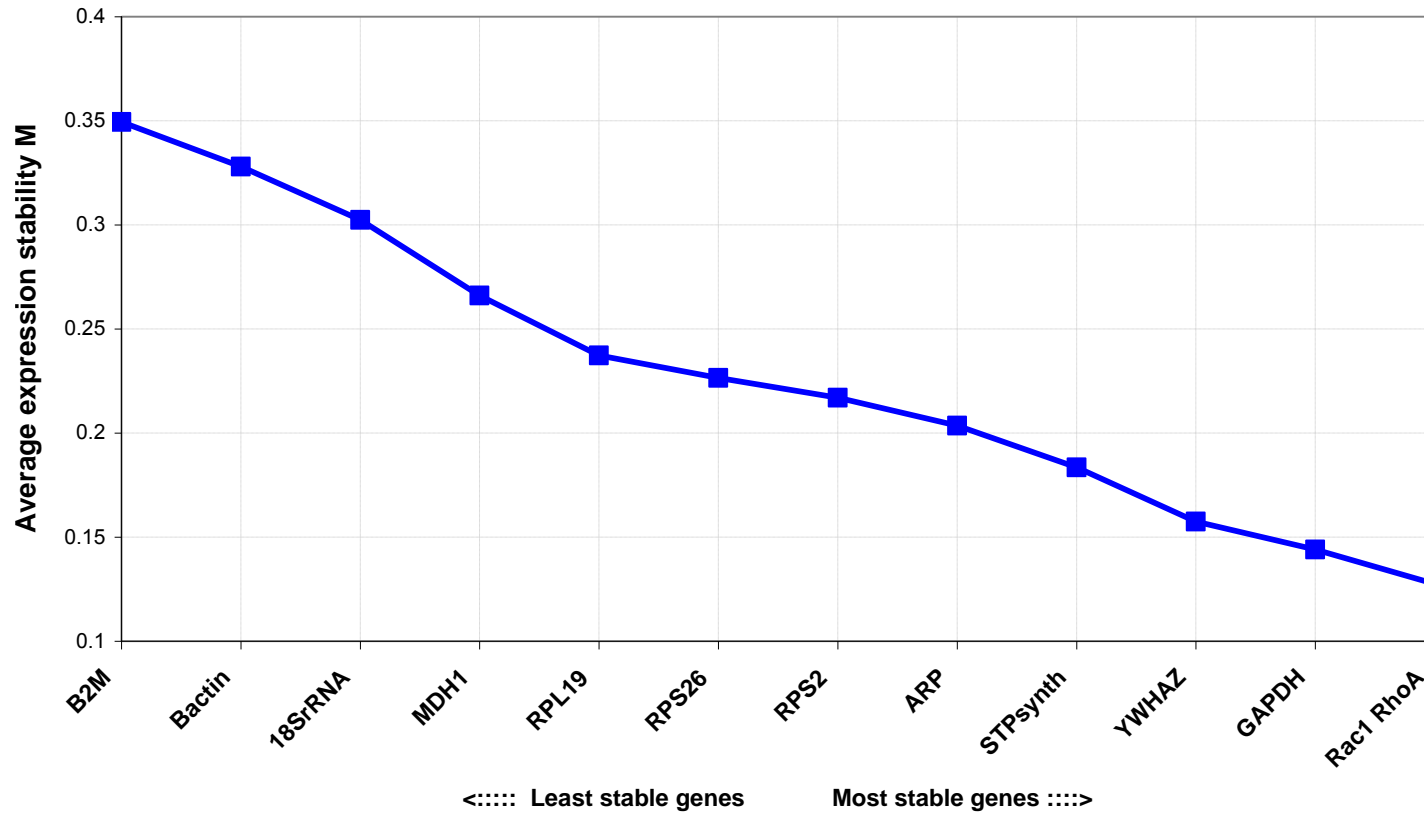


Figure 4-5 Graph representing the average expression stability values (M) of the reference genes assayed at each step during stepwise exclusion of the least stable expressed reference gene (geNorm output).

Starting from the least stable gene at the left, the genes are ranked according to increasing expression stability, ending with the two most stable genes on the right.

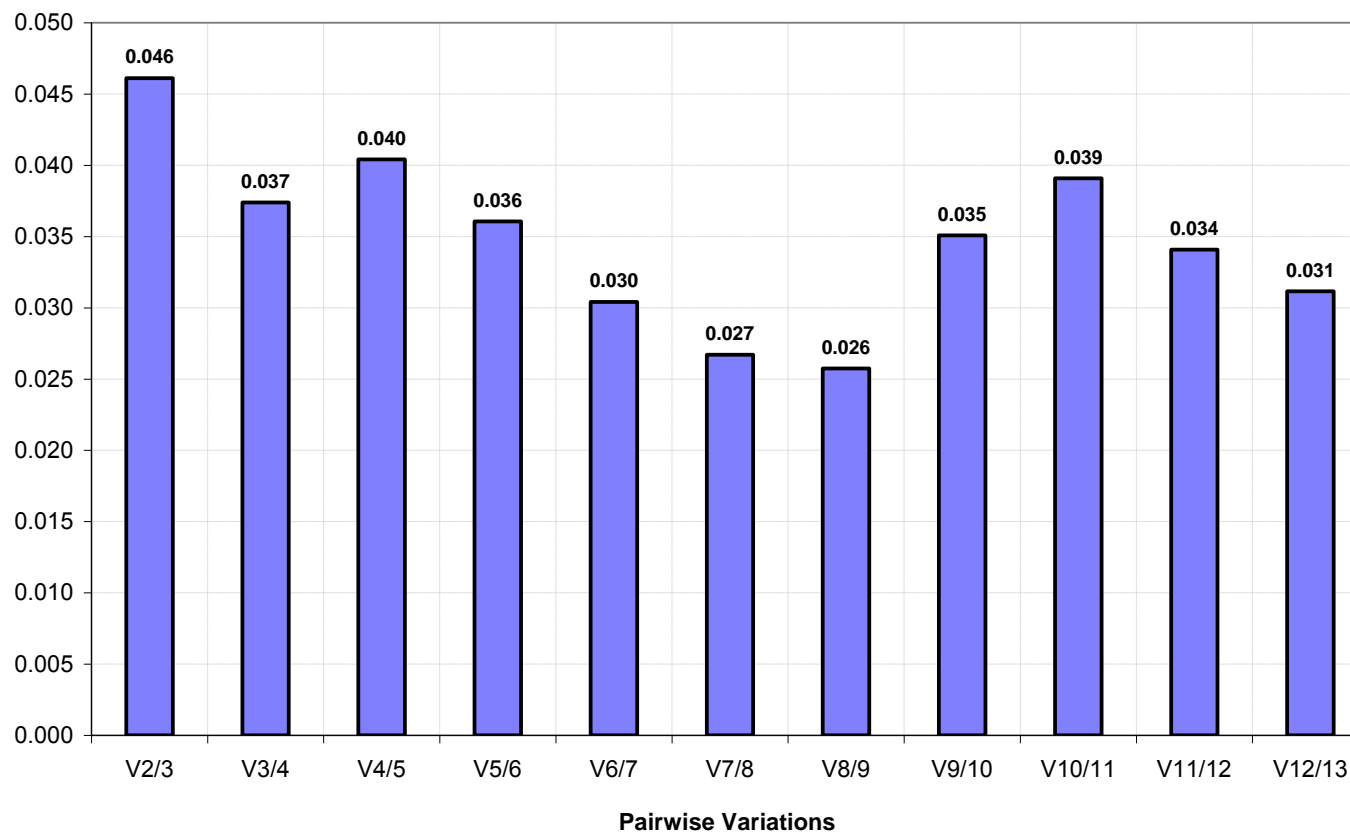


Figure 4-6_ Graph representing the pairwise variation analysis (V) for the reference genes assayed (geNorm output).

This graph demonstrates the levels of variation in average reference gene stability with the sequential addition of each reference gene. The analysis begins with the two most stably expressed genes on the left with the sequential inclusion of a 3rd, 4th 5th gene etc. most stable reference gene, moving to the right. This measure is known as the "pairwise variation V".

4.4.3 Gene Expression Analysis

4.4.3.1 Migration Markers

Analysis of the relative normalised expression showed that day of gestation was not significant for either of the migration markers, *RAC1* ($p=0.051$) and *RHOa* ($p=0.065$) across the time series (Figure 4-7). There was little variation detected amongst the four animals at each time point, and hence, small standard errors. *RAC1* was the most stably expressed gene across this sample series (Figure 4-5).

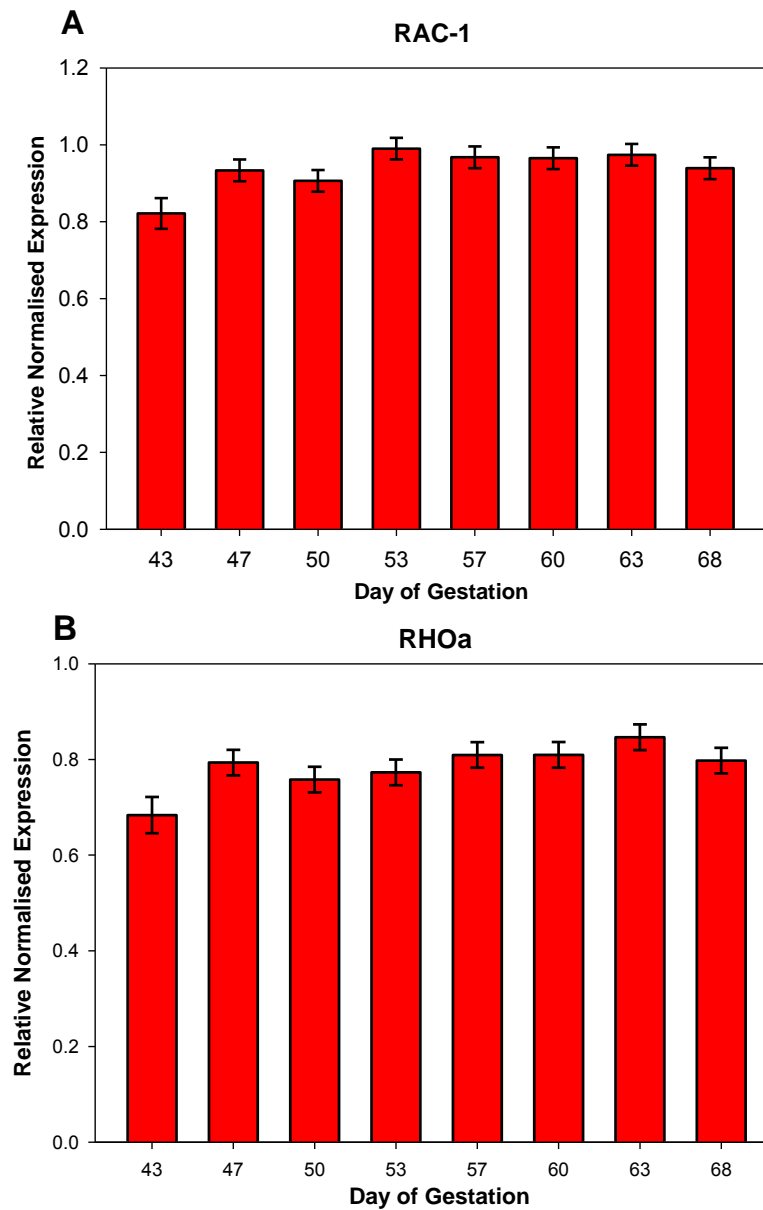


Figure 4-7 Relative expression of (A) *RAC-1* and (B) *RHOa* normalised to *GAPDH*, *YWHAZ* and *ATPsynthase* (mean \pm SEM; day 43 $n=4$, day 47-68 $n=8$)

Although day of gestation had no significant effect in the model, there was a significant site (midside or rump) effect detected for both *RAC1* ($p=0.04$; Figure 4-8A) and *RHOa* ($p=0.0001$; Figure 4-8B), with both markers showing higher expression in the midside compared to the rump. *RAC1* were expressed 1.03x (3%) higher in the midside and *RHOa* was expressed 1.09x (9%) higher in the midside. There was no significant site by day interaction for either of the migration markers.

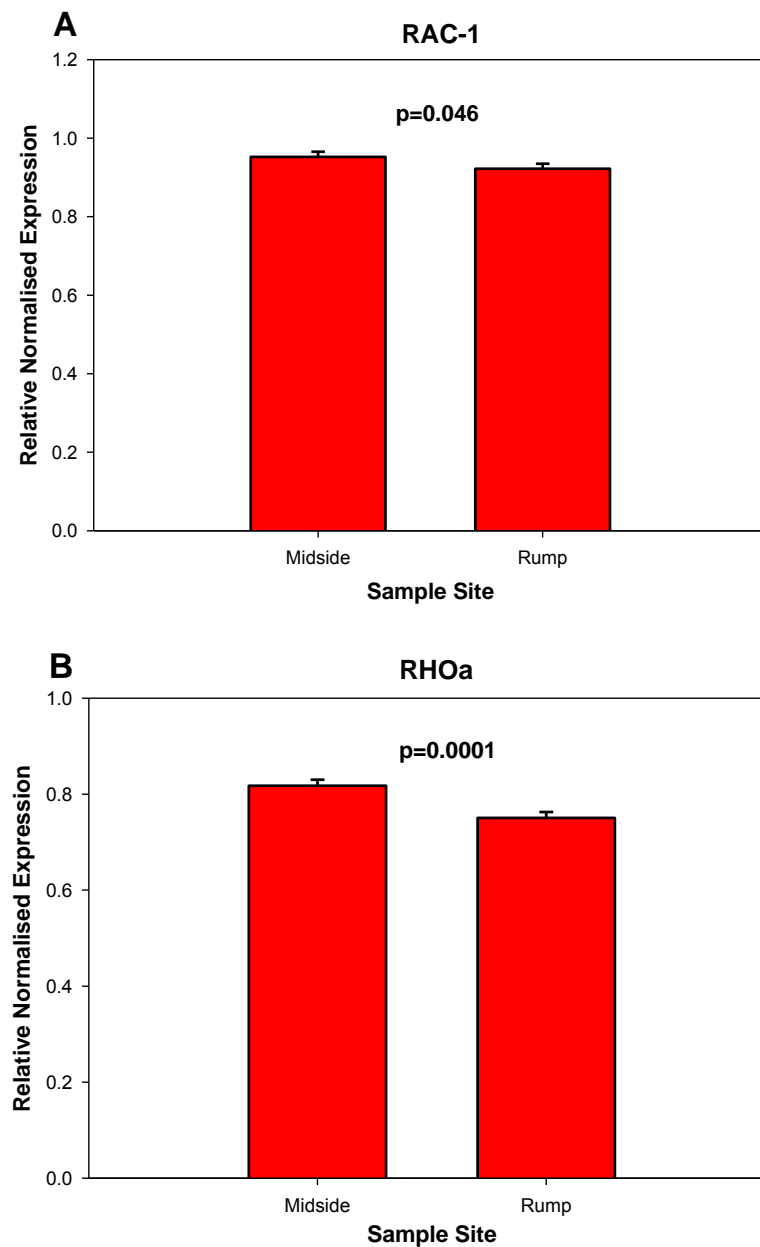


Figure 4-8 Site differences in relative normalised expression of (A) *RAC1* and (B) *RHOa* (mean \pm SEM; $n=30$)

4.4.3.2 Stem Cell Markers

Analysis of the relative normalised expression of stem cell markers *β 1-integrin* and *alkaline phosphatase* (ALP) demonstrated that day of gestation was significant for both markers *β 1-integrin* ($p=0.0005$; Figure 4-9A) and *ALP* ($p=0.0007$; Figure 4-9B). There was an 18% and 134% increase in expression from days 53 to 68 for *β 1-integrin* and *ALP*, respectively. Both stem cell markers had their lowest expression at day 53 and their highest at day 68. Variation in expression of these markers amongst the four animals at each time point was lower for *β 1-integrin* than *ALP*, resulting in smaller standard errors.

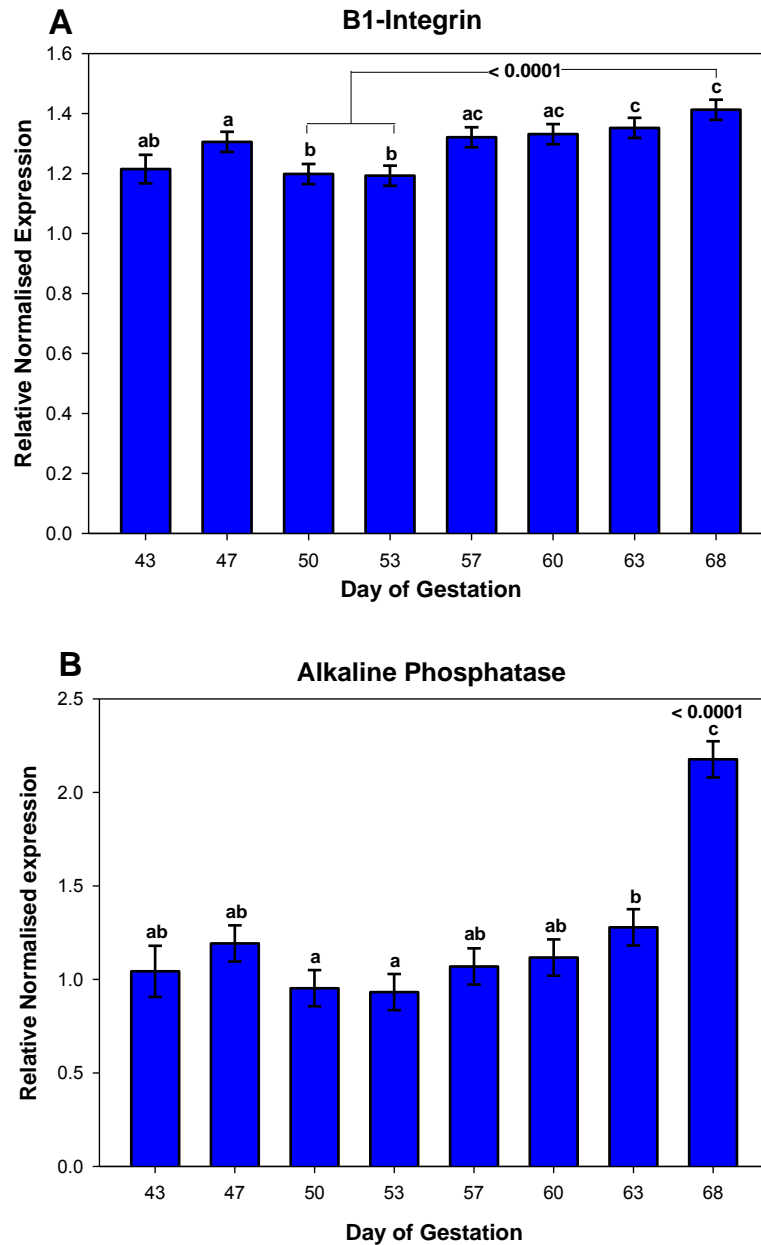


Figure 4-9 Relative expression of (A) $\beta 1$ -Integrin and (B) Alkaline Phosphatase, normalised to *RAC1*, *RHOa* and *GAPDH* (mean \pm SEM; day 43 n=4, day 47-68 n=8)

Significant differences were also detected between samples from the midside and rump for the stem cell markers with $\beta 1$ -integrin ($p < 0.0001$) and ALP ($p < 0.0001$) with both showing higher expression in the rump compared to the midside. There was no significant site by day interaction for either of the stem cells markers.

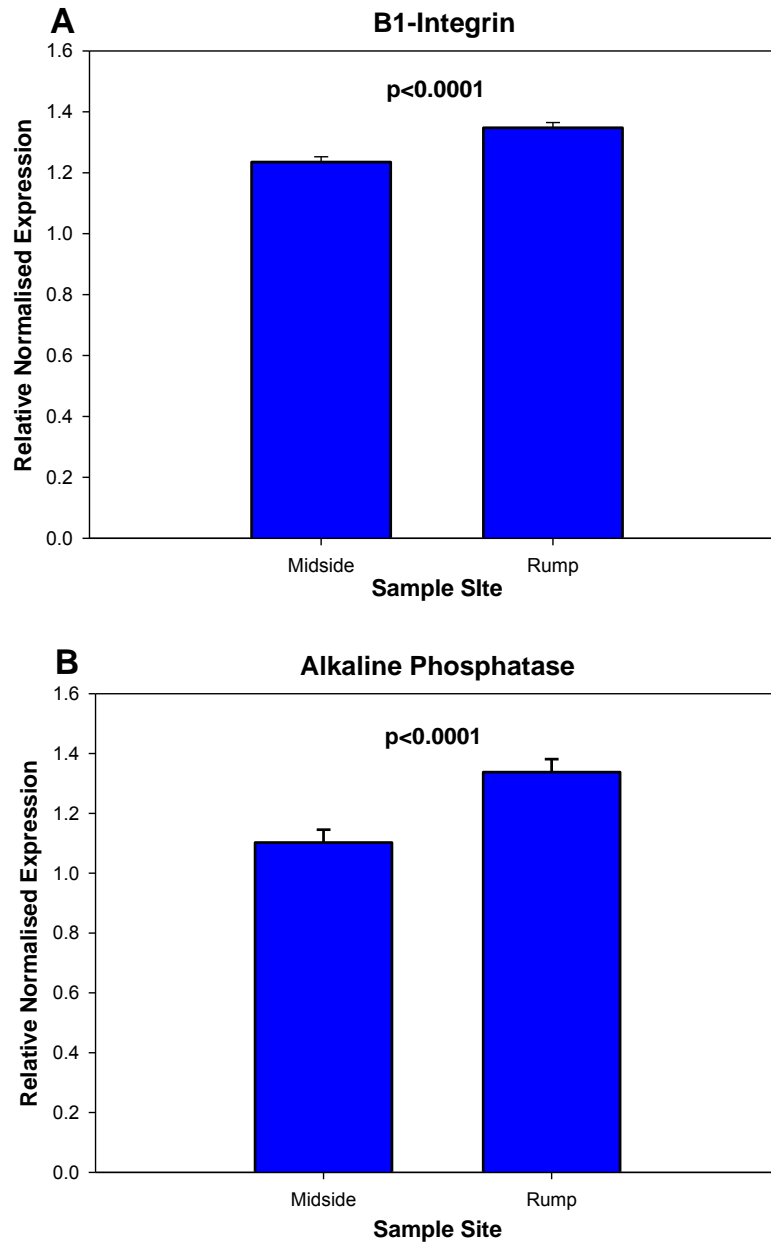


Figure 4-10 Site differences in relative normalised expression of (A) $\beta 1$ -Integrin and (B) Alkaline Phosphatase (mean \pm SEM; n=30)

4.4.3.3 Proliferation Markers

Analysis of the relative normalised expression of the candidate proliferation markers demonstrated that day of gestation was not significant for *cyclin B1* (*CYCBI*; $p=0.58$; Figure 4-11A), but was significant for *proliferative cell nuclear antigen* (*PCNA*; $p=0.009$; Figure 4-11B). There was a significant 15% decrease in expression of *PCNA* between days 50 and 53. *PCNA* expression was lowest at day 63, where mRNA levels were 20% lower than at day

53. At each time point, variation in the mRNA levels amongst the four animals was lower for *PCNA* than *CYCBI*.

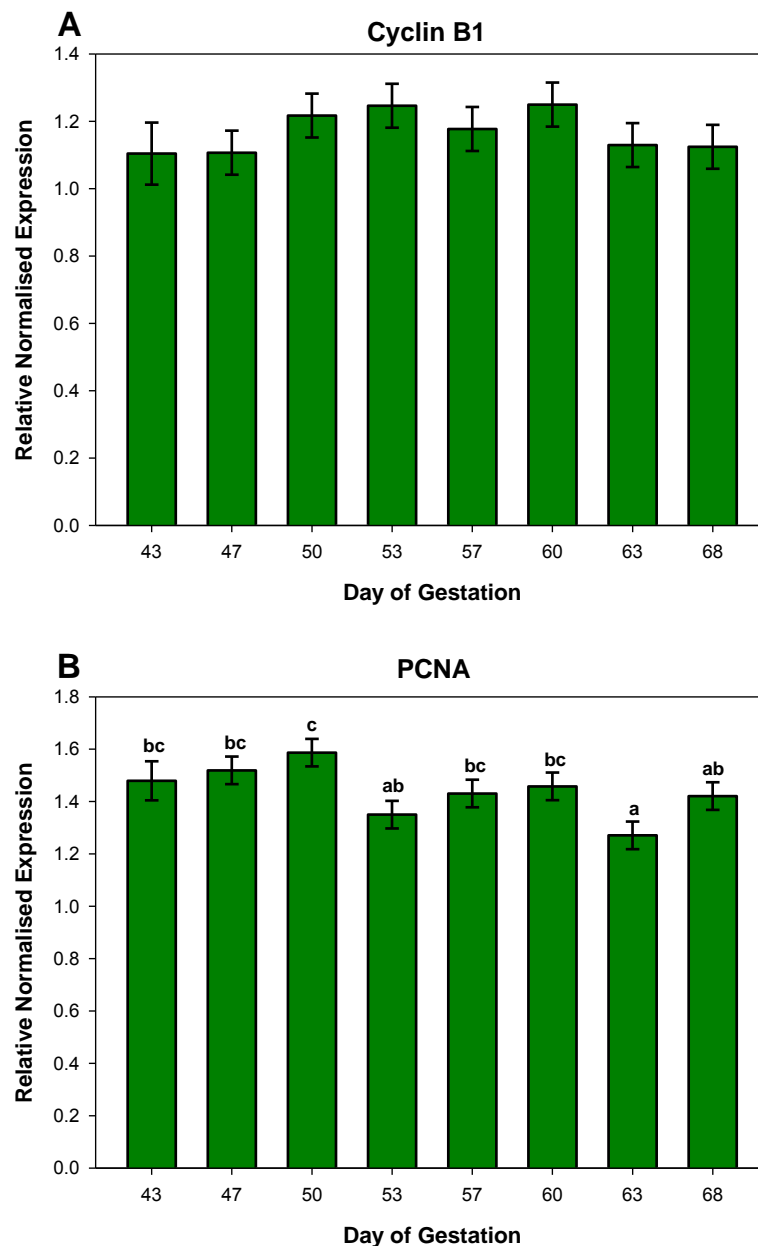


Figure 4-11 Relative expression of (A) *Cyclin B1* and (B) *PCNA*, normalised to *RAC-1*, *RHOa* and *GAPDH* (mean \pm SEM; day 43 n=4, day 47-68 n=8)

There was no significant difference detected between the midside and rump samples for *CYCBI*. However, *PCNA* was expressed significantly higher in rump skin compared to midside skin ($p=0.005$). There was no significant site by day interaction for either of the proliferation markers.

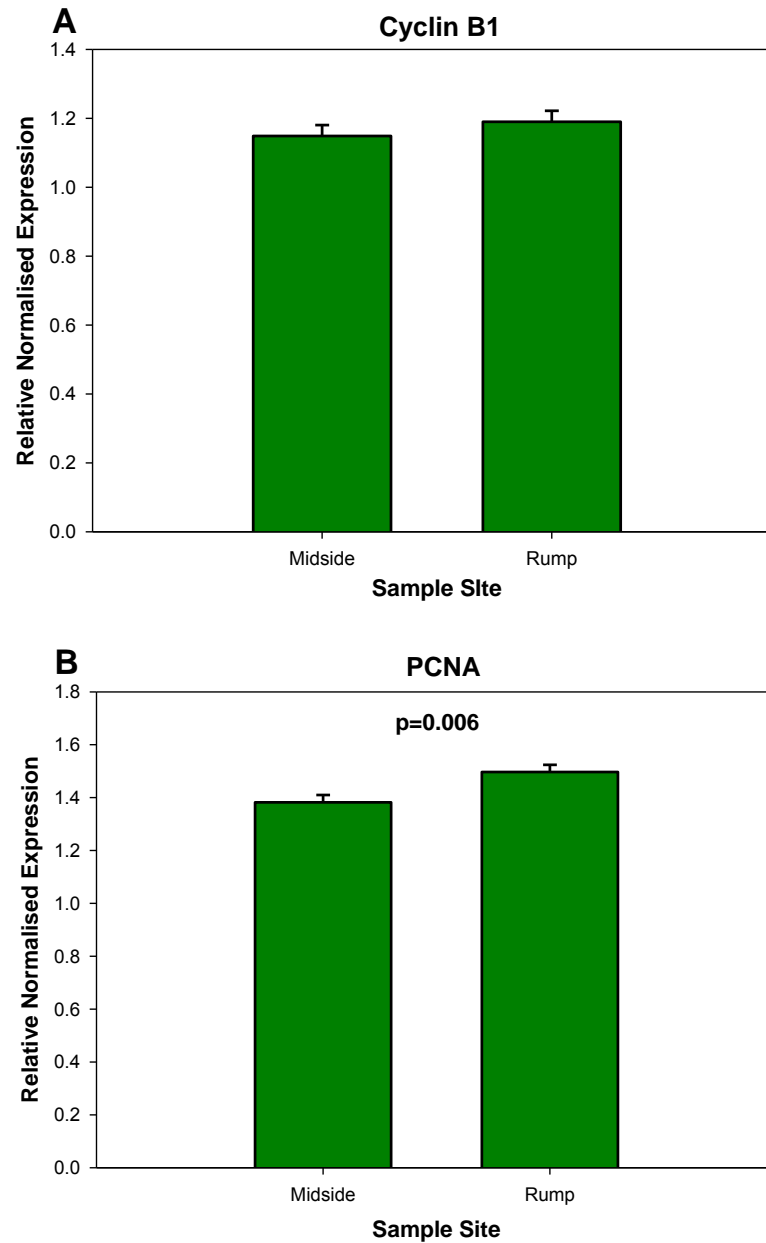


Figure 4-12 Site differences in relative normalised expression of (A) Cyclin B1 and (B) PCNA (mean \pm SEM; $n=30$)

4.4.3.4 Tumor Necrosis Factor Signalling Pathway Members

Analysis of the relative normalised expression showed that day of gestation was significant for *ectodysplasin* (*EDA*; $p=0.03$; Figure 4-13A) and its receptor (*EDAR*; $p<0.0001$; Figure 4-13B). *EDA* showed a significant 36% increase in expression from days 43 to 53 and expression was at its highest on day 60. *EDAR* mRNA levels increased 6.5-fold (650%) from day 50 to 68, and at day 68 were significantly higher than at all other time points.

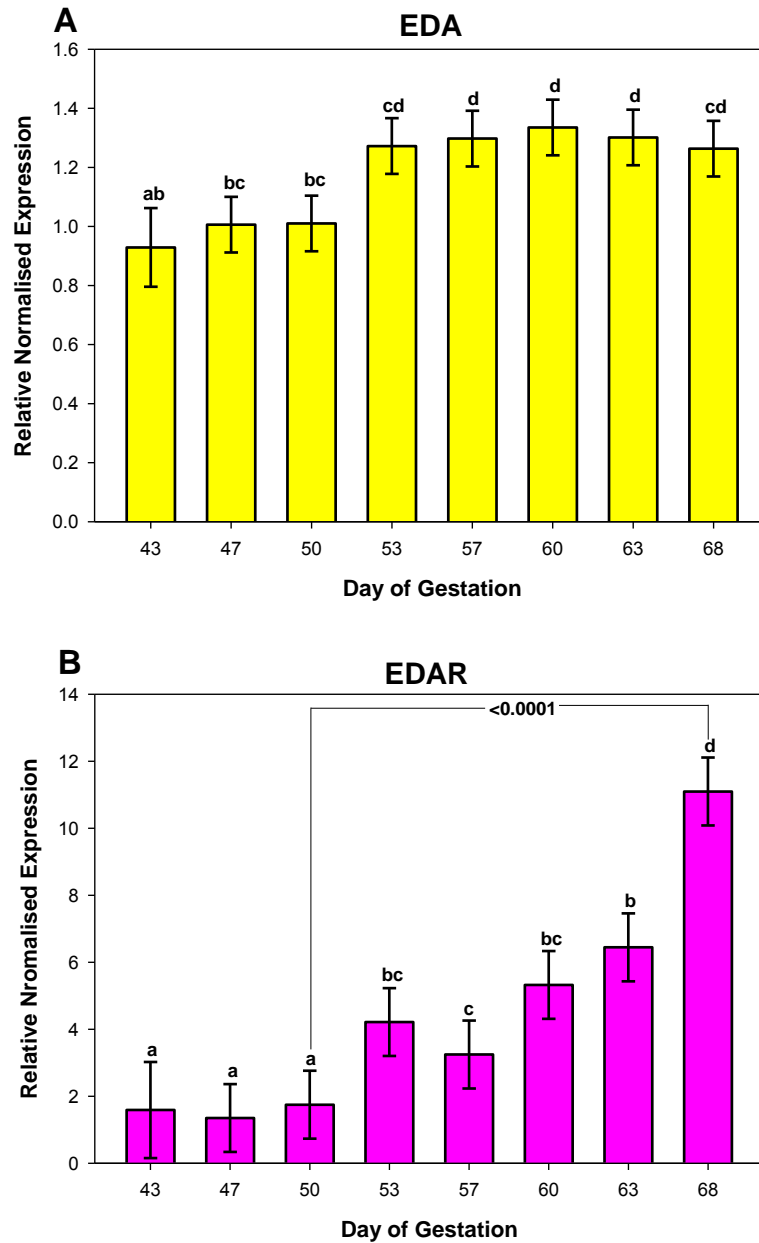


Figure 4-13 Relative expression of (A) Ectodysplasin (EDA) and its receptor (B) EDAR, normalised to RAC1, RHOa and GAPDH (mean \pm SEM; day 43 n=4, day 47-68 n=8)

EDA and EDAR mRNA levels were significantly higher in the midside compared to the rump, $p < 0.0001$ and $p = 0.01$, respectively. There was no significant site by day interaction for either EDA or EDAR.

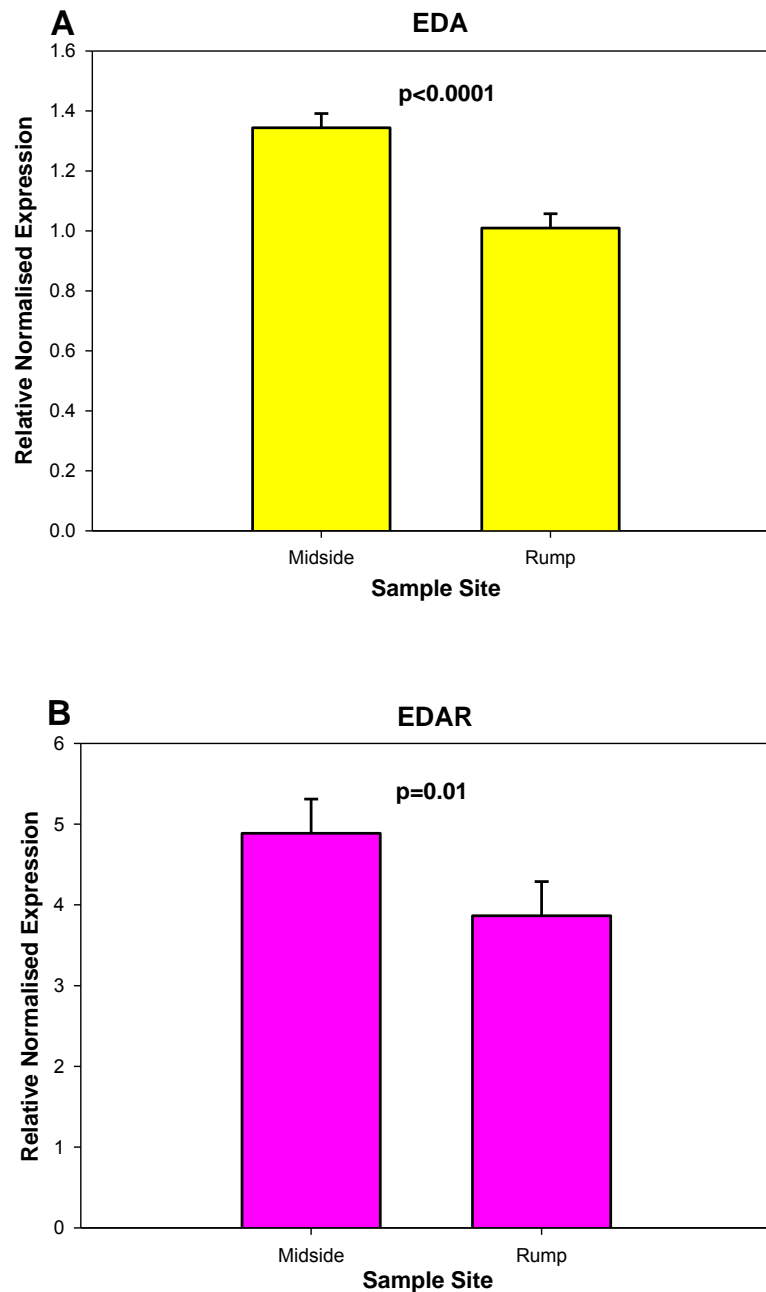


Figure 4-14 Site differences in relative normalised expression of (A) EDA and its receptor (B) EDAR (mean \pm SEM; $n=30$)

Analysis of the relative normalised expression for the *tumor necrosis factor receptor superfamily member 19 (TROY)* and ectodysplasin A2 receptor (*XEDAR*) showed that day of gestation was significant for *TROY* ($p=0.04$; Figure 4-15A) but not for *XEDAR* ($p=0.56$; Figure 4-15B). There was a significant 46% increase in *TROY* mRNA levels from day 50 to 53, followed by a 35% decrease at the following time point on day 57.

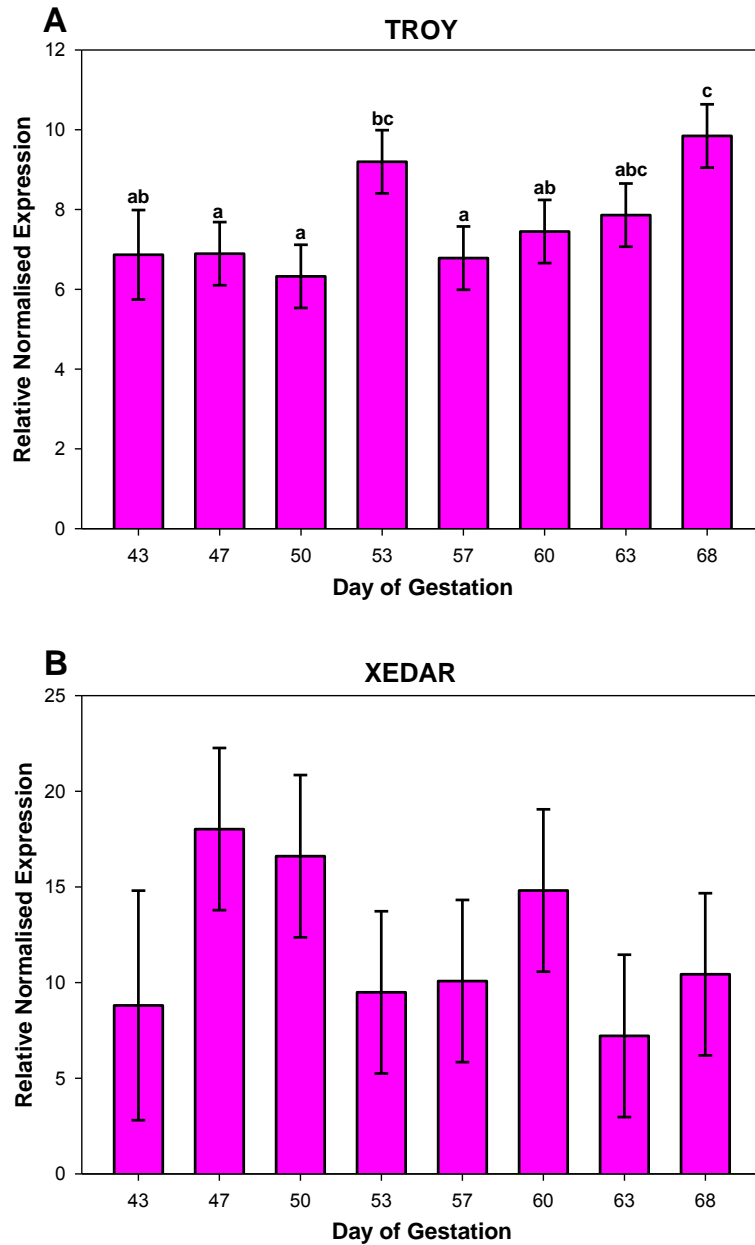


Figure 4-15 Relative expression of TNF receptors (A) *TROY* and (B) *XEDAR*, normalised to *RAC1*, *RHOa* and *GAPDH* (mean ± SEM; day 43 n=4, day 47-68 n=8)

TROY mRNA levels were significantly higher in the midside compared to the rump ($p=0.0002$). The opposite trend was observed for *XEDAR* with the rump samples showing significantly higher expression levels compared to the midside ($p=0.01$). There was no significant site by day interaction for *TROY* or *XEDAR*.

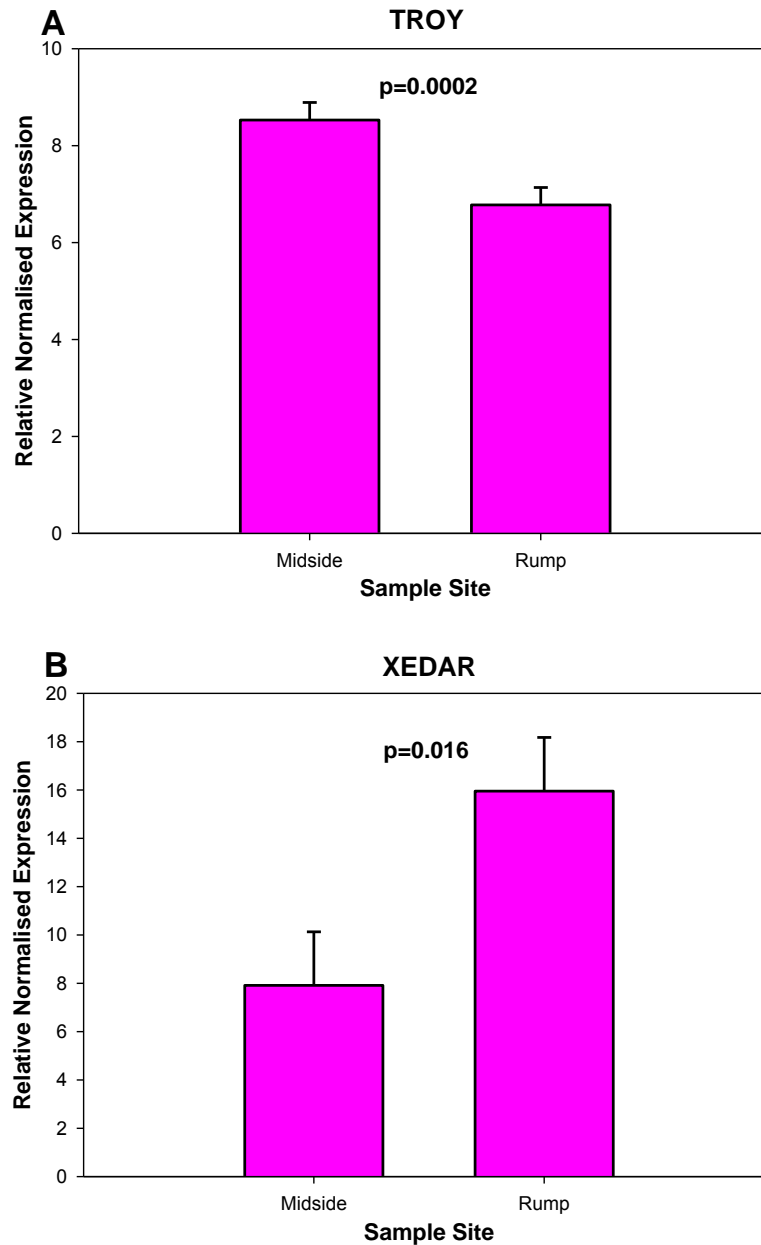


Figure 4-16 Site differences in relative normalised expression of TNF receptors (A) TROY and (B) XEDAR (mean \pm SEM; $n=30$)

Analysis of the relative normalised expression for *ectodysplasin receptor adaptor death domain (EDARADD)* and *tumor necrosis factor receptor-associated factor 6 (TRAF-6)* showed that day of gestation was significant for *TRAF-6* ($p=0.0004$; Figure 4-17B) but not for *EDARADD*. *TRAF-6* expression was relatively stable from days 43 to 60. The only significant change in expression of *TRAF-6* occurred from days 60 to 63 where mRNA levels increased by 17%. There was a large amount of variation in expression of *EDARADD* amongst animals of similar ages.

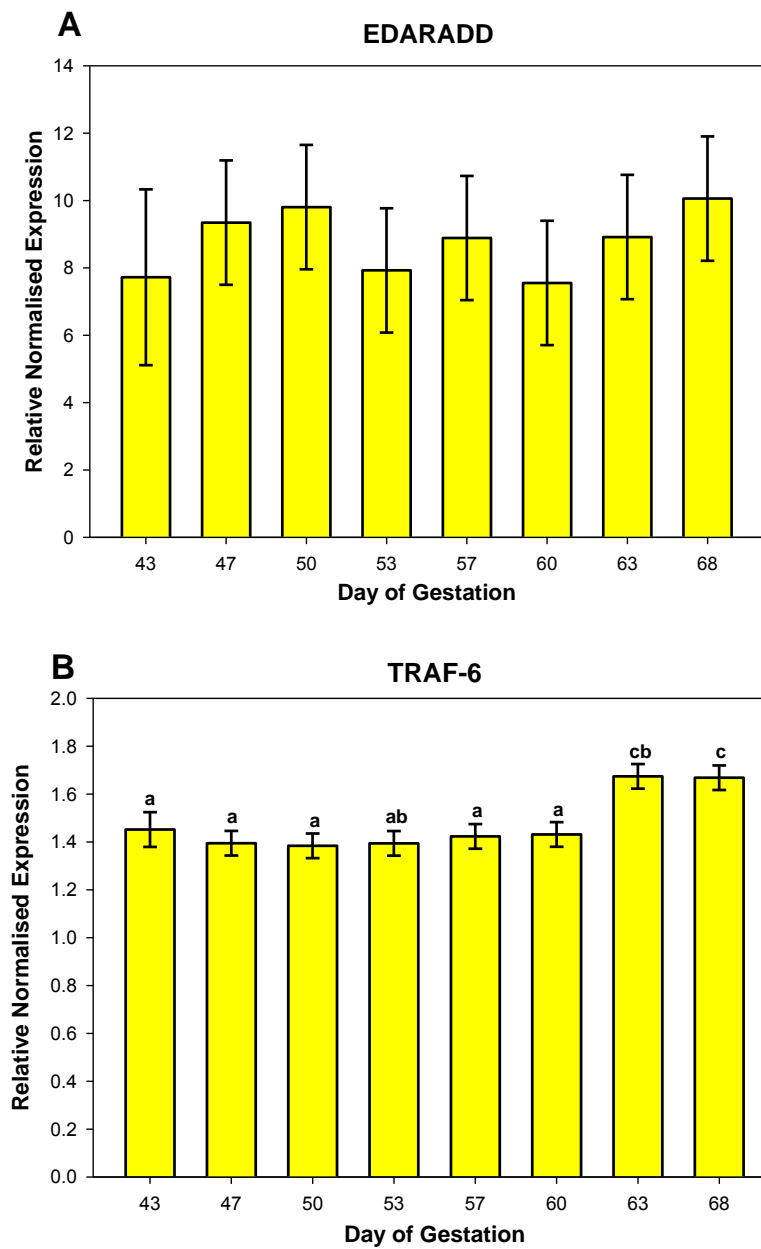


Figure 4-17 Relative expression of intracellular signalling molecules (A) EDARADD and (B) TRAF-6, normalised to RAC1, RHOa and GAPDH (mean ± SEM; day 43 n=4, day 47-68 n=8)

Both ligands showed significantly higher mRNA levels in the rump compared to the midside (*EDARADD* p=0.03, *TRAF-6* p=0.01). There was no significant site by day interaction observed for either ligand.

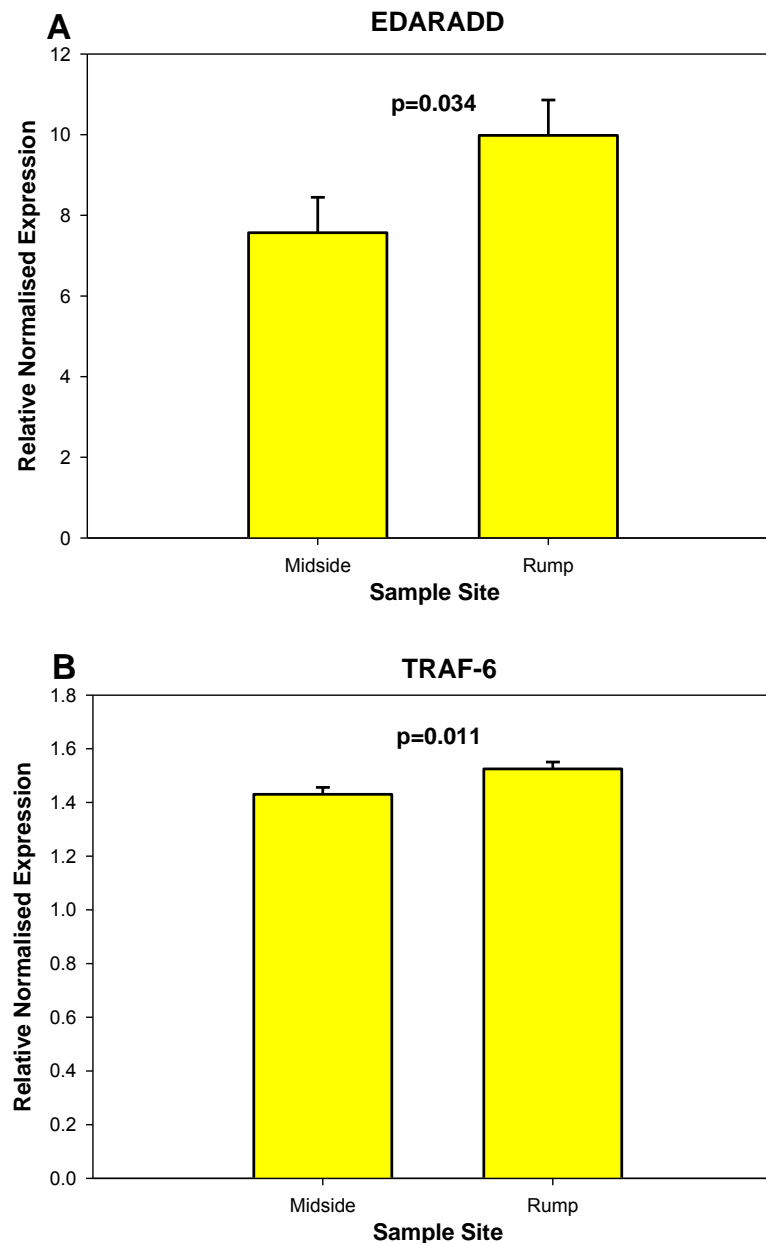


Figure 4-18 Site differences in relative normalised expression of TNF ligands (A) EDARADD and (B) TRAF-6 (mean \pm SEM; n=30)

4.4.3.5 Sonic Hedgehog Signalling Pathway

Due to very low mRNA levels, a reproducible quantitative PCR assay for the *sonic hedgehog* gene could not be optimised. Although several primer pairs were trialled, the amplicons produced reaction Cts greater than 30 and the triplicate measures had large standard deviations. Therefore, the results from this assay are not reported herein. Although the *sonic hedgehog* ligand was not detectable at a quantitative level in this time series, the mRNA level appeared to increase in the last set of foetal skin samples collected (day 68). Day

of gestation for the SHH receptor *PTCH1* was significant with a large increase in mRNA levels observed towards the end of the time series (Figure 4-19). *PTCH1* expression increased gradually from day 47 to 57 and then increased by 57% by day 60, a further 36% by day 63 and finally increased by 87% from days 63 to 68.

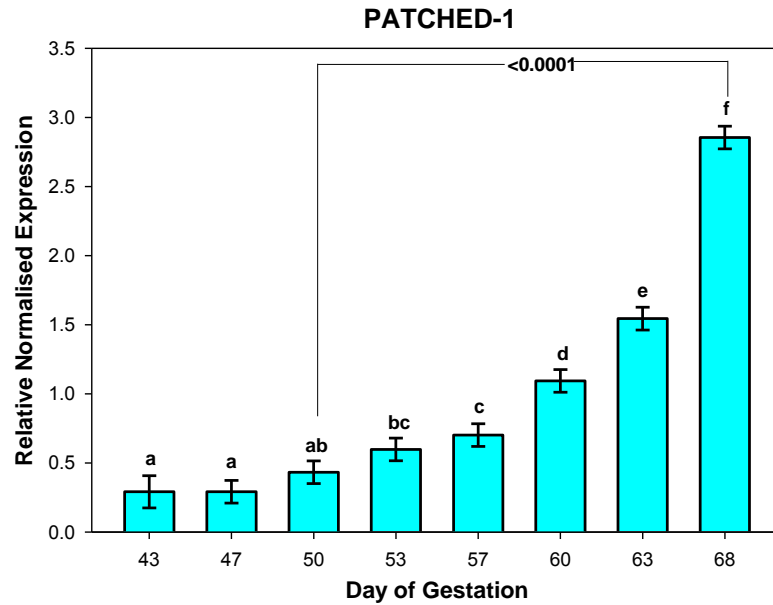


Figure 4-19 Relative expression of the sonic hedgehog receptor patched-1(*PTCH1*), normalised to *RAC1*, *RHOa* and *GAPDH* (mean \pm SEM; day 43 n=4, day 47-68 n=8)

There was no significant difference in the expression of patched-1 between the midside and rump samples (Figure 4-20; $p=0.267$).

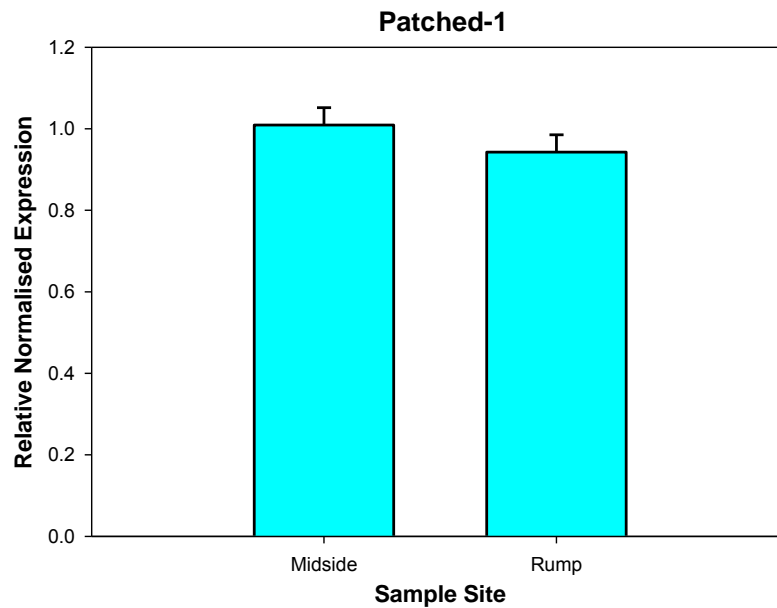


Figure 4-20 Site differences in relative normalised expression of the sonic hedgehog receptor *patched-1* (mean ± SEM; n=30)

4.4.3.6 Gene Expression Correlations

The gene expression analysis software tool GenEx (MultiD Analyses, Sweden) was used to perform cluster analysis on the normalised expression values (Figure 4-21). Cluster analysis revealed correlations between the expression patterns of: (1) the TNF family members *EDAR* and *EDARADD* and *PTCHI*, (2) the stem cells markers *ALP* and *β1-integrin*, (3) the TNF ligand *EDA* and receptor *XEDAR*, and (4) the proliferation markers *PCNA* and *CYCBI* (Figure 4-21).

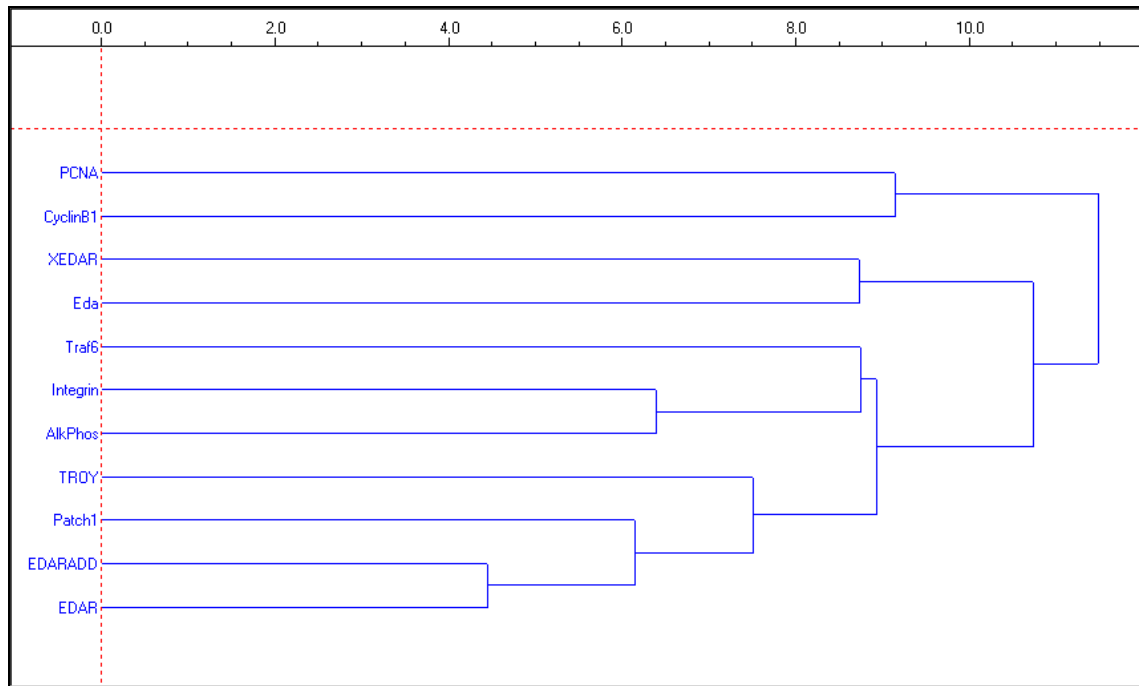


Figure 4-21 Cluster analysis of the relative normalised expression of all target genes.

4.5 Discussion

Quantitative reverse transcriptase PCR (qRT-PCR) was employed to measure the mRNA levels of 13 target genes and 11 normalisation or “house-keeping” genes. Particular attention was paid during the RNA extraction and purification processes to ensure all aqueous contaminants and aromatic extraction compounds (e.g. phenol) were removed prior to reverse transcription, thereby providing optimal RNA purity and integrity (Table 4-3, Figure 4-3). It is known that RNA degradation can occur during the sampling procedure, extraction and storage if the RNA is not kept at the correct temperature (Huggett et al., 2005). Samples were therefore snap frozen in liquid nitrogen and stored at -80°C prior to extraction to maintain RNA quality.

When performing qRT-PCR analysis, two experimental protocols can be followed: (1) relative quantification, using cDNA or cloned DNA dilutions to construct standard curves that account for amplification efficiency differences between qRT-PCR assays (with arbitrary units), or (2) absolute quantification, where known concentrations of *in vitro* transcribed RNA transcripts that correspond to each target gene are included in the reverse transcription step so

that the efficiency of this procedure can be determined for each gene along with the amplification efficiency of each PCR amplicon. Absolute quantitation of transcripts allows the precise determination of copy number per cell, total RNA concentration, or unit cell mass (Bustin, 2000). Relative quantification can account for the influence of any unavoidable artefacts of sample preparation and reverse transcription (Garcia-Crespo et al., 2005). Relative quantification was the chosen method herein for this reason and because it is also the most appropriate option for investigating the expression of many target genes. Furthermore, qRT-PCR only quantifies steady state mRNA levels with accurate quantitation revealing nothing more about transcription levels or mRNA stability (Bustin, 2002). It may be misleading to report qRT-PCR data per cell or mg of tissue (as in absolute quantitation) as the mRNA levels may not actually reflect the levels of protein produced by the cells in the tissue sample. Absolute quantification also does not account for differences in PCR efficiency between pure populations of *in vitro* transcribed RNA standards and the heterogeneous mix of whole tissue cDNA in unknown samples, potentially creating errors in quantification from the standard curve. However, relative quantitation can be more demanding in that it requires accurate quantitation and normalisation to total RNA and the selection of multiple highly stable reference genes. A six point standard curve of 1:5, 1:25, 1:125 and 1:10, 1:50, 1:250 cDNA transcribed from a pool of RNA from day 50 to day 68 was used for the purpose of relative quantitation in this study.

Although previous studies on ovine gene expression have been reported using only one reference gene for normalisation (Laud et al., 2001; Grubor et al., 2004; Hein et al., 2004), the use of at least three stably expressed normalisation genes is recommended for accurate normalisation of qRT-PCR data (Vandesompele et al., 2002). The common normalisation genes employed in most studies include *18S ribosomal RNA (r18S)*, *glyceraldehyde 3-phosphate dehydrogenase (GAPDH)* and *β -actin (ACTB)*. Unless inter-sample variation is assessed for in the “traditional” normalisation genes, sample-to-sample

variation can introduce significant bias in gene expression profiles when only one normalisation gene is used (Garcia-Crespo et al., 2005). Therefore, the use of more than one normalisation gene in a robust method described by Vandesompele *et al* (2002) was utilised herein. The expression of 11 normalisation genes was assessed across the sample series and their expression stability (i.e. how stable their mRNA levels were across the sample series) analysed using geNorm v3.5 (Excel-based macro package designed by Vandesompele *et al*, 2002). The method involves selecting the three most stably expressed genes and normalising the target gene expression to the geometric mean of the three most stably expressed “housekeeping” genes. Interestingly, geNorm analysis of 11 normalisation genes along with the 13 target genes revealed that the migration markers *RAC1* and *RHOa* were the two most stably expressed genes across the samples series.

Consideration was also given to standardising the quantity of RNA included in each reverse transcription reaction in order to initially normalise for input total RNA content.

4.5.1 Gene Expression Analysis of Candidate Migration Markers

The Rho-GTPases play crucial roles in cellular processes such as polarisation, cell-cell and cell-matrix adhesion, membrane trafficking and transcriptional regulation (Hall, 1998; Jiang et al., 2006). The ordered assembly and disassembly of the actin cytoskeleton mediated through Rho-GTPase signalling represents a major component of cellular homeostasis, particularly in dynamic tissue remodelling as represented by the foetal skin series herein. The large number of cellular processes the Rho-GTPases *RAC1* and *RHOa* are involved in may explain why these selected migration markers were the most stably expressed genes.

Although no significant differences in gene expression were observed across the skin sample series for either of these two Rho-GTPases assayed (when normalised against the next three most stably expressed normalisation genes), this class of genes has been implicated in the mediation of hair cell development and stereocilia morphogenesis in the inner ear and they may also modulate outer ear hair motility (Kollmar, 1999). Furthermore, the conditional

deletion of the *RAC1* gene in the mouse skin, including the potential follicular and epidermal stem cell compartments, results in alopecia because of defective hair development. Surprisingly, mice lacking this Rho GTPase do not display major alterations in the interfollicular skin (Castilho et al., 2007)

With this in mind, *RAC1* and *RHOa* may very well be involved in establishment of the primary follicle pattern, particularly the migration of mesenchymal pre-papilla cell (stem cells) and/or basal layer epidermal stem cells. However, due to the complexity of the tissue remodelling occurring in both the follicular and inter-follicular regions, these specific migrations may not have been detected in whole skin qRT-PCR.

4.5.2 Gene Expression Analysis of Candidate Stem Cell Markers

Both *alkaline phosphatase* and *$\beta 1$ -integrin* showed significant changes in mRNA levels across the foetal gestational ages assayed. *$\beta 1$ -integrin* mRNA levels were significantly higher at day 57 (compared to day 53), which coincided with the formation of epidermal placodes. *$\beta 1$ -integrin* levels peaked at day 68, 1.16-fold higher than at day 53 ($p < 0.0001$). *ALP* mRNA was significantly higher at day 63 compared to day 53; the time point when the histology showed clear dermal condensate formation. The trend in *alkaline phosphatase* expression showed a gradual increase from day 53, with mRNA levels peaking at day 68.

The integrin receptors are a family of heterodimer transmembrane glycoproteins that interact with a variety of ligands and participate in cell-matrix adhesion and cell-cell adhesion (Hynes, 1987). *$\beta 1$ -integrin* knockout mice exhibit severe skin blistering, hair defects accompanied by massive failure of the basement membrane assembly and a failure of hair follicle keratinocytes to invaginate into the dermis (Raghavan et al., 2000). With this in mind, the peak in *$\beta 1$ -integrin* mRNA levels at day 68 may reflect an expansion in the epidermal stem cell population at the base of the hair germ as it grows down into the dermis forming the primary wool fibre canal.

ALP activity has been detected in restricted mesenchymal regions of mouse vibrissae follicles with its potency and localization changing dramatically during the hair cycle. It was postulated that these dynamic changes of *ALP* expression might be related to the role of the dermal papilla in hair induction (Iida et al., 2007). *ALP* expression has also been previously utilized as a simple marker to identify hair follicle mesenchyme derived cells with hair follicle inductive abilities (McElwee et al., 2003). Most importantly, ALP is well known to be a marker of dermal papilla cells, particularly in cell culture. The spike in *ALP* expression at day 68 (1.8-fold increase) is either a reflection of the expanding dermal stem cell population as the condensate expands and matures into the dermal papilla or a reflection that as the dermal condensates differentiate into dermal papilla cells, they begin to express higher levels of *ALP*. Based on the reported higher expression levels of *ALP* from dermal papilla cells in culture, it can be hypothesized that the later explanation is the more likely reason behind the observed peak at day 68.

4.5.3 Gene Expression Analysis of Candidate Cell Proliferation Markers

PCNA, a nuclear homotrimer protein, has long been regarded as a proliferation marker because it is expressed late in G1 phase and early in S phase (Takahashi and Caviness, 1993). However, recent evidence indicates that PCNA can bind to a variety of factors, such as p21, that are required for cell cycle progression, replication and DNA repair (Korgun et al., 2006). This perhaps explains why the significant changes in *PCNA* mRNA levels determined across the sample series did not coincide with the morphological changes observed in the histological characterisation. In previous studies, PCNA has been employed in a variety of applications including:

- (1) to determine the proliferative status of lesions around ill-fitting dentures (Coelho and Zucoloto, 1999),
- (2) in conjunction with MIB-1 indices as a reliable marker for discriminating between benign and malignant tumours of the parotid gland (Zhu et al., 1999),

- (3) to mark cell proliferation in embryonic and adult zebra fish hematopoietic tissues in order to identify populations of progenitor cells (Leung et al., 2005), and
- (4) as an internal reference gene for PCR analysis of formalin fixed tissues in veterinary medicine (Schiller et al., 2003).

CYCB1 is the regulatory subunit of the “M-phase promoting factor”. Correct CYCB1 regulation is essential for the initiation of mitosis as it accumulates in the cytosol during late S phase and G2 and enters the nucleus at the onset of mitosis (Bailly et al., 1992). Inhibiting cyclin B1 in tumour cells results in an increase in apoptosis by 40-50% and suppresses proliferation by up to 80% (Yuan et al., 2004). The oscillation of cyclin B1 throughout the cell cycle was first described in the sea urchin oocyte cell cycle (Evans et al., 1983). It has since been shown that cyclin B1 is expressed ubiquitously in all mammalian cells. It is expressed at minimal levels in G1, begins to increase in the cytoplasm during S phase, rises significantly during the G2 phase and localises to the perinuclear region of dividing cells, and peaks during the G2/M phase, particularly in the nucleus, essentially initiating mitosis (Kakino et al., 1996). *CYCB1* mRNA levels increase by over 50-fold in somatic cycling mammalian cells as the cells progress through G1 and S into G2/M (Maity et al., 1995). Although the increase in CYCB1 protein that is required to activate the “maturation promoting factor” is likely to depend on its mRNA level, the activation that triggers the progression into mitosis is dependent on the binding of CDK-1 as well as a series of phosphorylation and dephosphorylation events (Hwang et al., 1995). The complexity and large number of the binding, phosphorylation and dephosphorylation events that CYCB1 is involved in during the transition into mitosis may explain why no significant differences in *CYCB1* mRNA levels were detected in this foetal sample series.

4.5.4 Ectodysplasin Signaling During Primary Wool Follicle Initiation

The crucial role of *EDA* in hair follicle development was first evident in mice with spontaneous mutations in the corresponding gene, *Tabby*, which showed a lack of guard and

zig-zag follicles and replicates the symptoms of the human congenital disorder hypohidrotic ectodermal dysplasia (Ferguson et al., 1997). Over-expression of *EDA* leads to enlarged placodes and exposure of embryonic skin to EDA post-placode initiation can induce placode enlargement, reducing the inter-placode space and leading to fusion of these enlarged placodes (Mustonen et al., 2004). Originally, only the *EDA-A1* and *EDA-A2* variants were well described, but recently, a larger repertoire of mouse *EDA* splice variants has been described including *EDA-A1*, *EDA-A1'*, *EDA-A2*, *EDA-A3*, *EDA-A4*, *EDA-A5*, *EDA-A5'*, *EDA-A6*, *EDA-A6'* (Hashimoto et al., 2006). The position of the qRT-PCR primer used in the qRT-PCR assays herein did not discriminate between any of the *EDA* variants described. The reported *EDA* mRNA levels are, therefore, total *EDA* expression, incorporating many of the variants expressed in skin during primary wool follicle initiation.

qRT-PCR analysis showed *EDA* mRNA levels were significantly different across the sample series, but did not show the same fluctuations as its receptor *EDAR*. *EDA* levels increased at day 53, immediately preceding placode formation and these levels were maintained at slightly higher levels during dermal condensate and hair germ formation.

EDA is widely expressed in the mouse epidermis (Botchkarev et al., 2002), and when provided to cultured cells in a diffusible form, allows follicle pattern formation in culture. In transgenic mice where *EDA* was targeted to the epithelial compartment of developing skin, multiple hair follicles formed where there would otherwise have been interfollicular space (Zhang et al., 2003). This indicated that *EDA* has the capacity to regulate basic developmental decisions, switching cells from interfollicular to follicular fates. Mou et al (2006) raised the possibility that follicle patterning is controlled by restriction of *EDAR* competence to respond to *EDA*, rather than changes in the actual ligand concentration because an accurate follicle pattern could still be generated in the absence of *EDA* through *EDAR* over-expression. This is consistent with the gene expression pattern shown herein, in that *EDA* mRNA expression was moderately increased at placode initiation and maintained.

However, it was the dramatic fluctuations in its receptor, *EDAR* that coincided with important follicle formation events observed in the histological characterisation of the foetal sample series.

The function of *EDAR* was first described in mouse when physical mapping of a family with similar phenotype to the *Tabby* (*EDA*) knockout revealed a 600kb deletion in the *Downless* locus (Headon and Overbeek, 1999). This TNF protein showed similar cytoplasmic “death domain” regions to other TNF receptors, and like *EDA*, localised to the epithelial cells at the base of newly established placodes. Prior to follicle initiation, *EDAR* is uniformly expressed throughout the basement membrane and becomes focally-unregulated immediately prior to the appearance of placodes. *EDAR* is also markedly unregulated in initiating and down-growing placodes and is downregulated in the surrounding epithelium (Headon and Overbeek, 1999; Botchkarev and Fessing, 2005; Mou et al., 2006). This is consistent with the expression pattern described herein in that *EDAR* transcripts increased 2 fold from day 43 to day 53, immediately prior to the appearance of placodes at day 57. Furthermore, by day 68, *EDAR* mRNA levels were 5-fold higher compared to day 50, prior to follicle initiation.

The cytoplasmic adaptor *EDARADD*, like *EDA* and *EDAR*, is critical for normal mouse and human hair follicle development as well as tooth initiation (Headon et al., 2001; Tucker et al., 2004). Mutations in the autosomal *EDARADD* loci causes hypohidrotic ectodermal dysplasia in humans (Munoz et al., 1997) and when the mouse homologue, *Crinkled* is knocked out, the resulting phenotype is identical to the *Tabby* and *Downless* mice described above (Headon et al., 2001). *EDARADD* is also expressed at the same time points and within similar skin structures as *EDAR*. Although in wild type mice embryos *EDAR* is uniformly expressed throughout the basement membrane prior to follicle initiation and becomes focally upregulated in initiating and down-growing placodes and downregulated in the surrounding epithelium, this dynamic *EDAR* expression is not seen in *EDARADD* *-/-* mice embryos. Thus, the *EDARADD* signal transduction from *EDAR* is essential in establishing the

primary follicle pattern (Mou et al., 2006). In contrast to the expression patterns seen in mouse skin, no significant difference in *EDARADD* expression was detected in this study during primary wool follicle initiation in sheep. However, there was a large difference in expression between animals of the same gestational age, producing large standard errors (Figure 4-17). This may have potentially masked any distinct changes in mRNA levels across the sample series.

Unlike *EDAR*, *XEDAR* and *TROY* do not appear to have critical roles in hair follicle formation in mice. *XEDAR* knockout mice display apparently normal hair development (Newton et al., 2004), as do *TROY* knockout mice which exhibited no obvious physical abnormalities or alterations in behaviour, locomotion, or fecundity (Shao et al., 2005). *TROY*, also known as *TAJ*, has been shown to be important in regulating axon regeneration through the activation of RhoA (Shao et al., 2005). *XEDAR*-transduced signals are dispensable for development of ectoderm-derived organs (i.e. hair and teeth), but play an important role in skeletal muscle homeostasis (Newton et al., 2004).

No significant difference in *XEDAR* mRNA levels was detected across the foetal skin series herein, perhaps due to the high degree of variation between animals of similar gestational ages. In contrast to literature in mice, the significant changes in *TROY* mRNA coincided with distinct changes in the skin morphology in that *TROY* expression at day 53 (immediately prior to the appearance of placodes) was significantly higher than at days 50 and 57. Furthermore, at day 68, *TROY* mRNA expression was significantly higher than all other sampled time points (Figure 4-15). Interestingly, the expression pattern of *TROY* was distinctly similar to *EDAR* mRNA expression, although the differences in mRNA levels were not of the same magnitude (Figure 4-13 and Figure 4-1).

Tumor necrosis associated factor 6 (*TRAF6*) is an adapter protein that links the signals from *TROY*, *XEDAR* and *EDAR* (through *EDARADD*) to activation of the transcription factor $\text{NF}\kappa\text{B}$ (Naito et al., 2002). *TRAF6* knockout mice also display the hypohidrotic

ectodermal dysplasia phenotype, identical to *Tabby* and *Downless*. Day of gestation was a significant variable in the mixed model analysis of *TRAF-6* mRNA across the sheep foetal sample series. A significant 20% increase in expression was detected at day 63, which was maintained through to day 68. This coincided with the appearance of dermal condensates and hair germ formation in the histological characterisation, respectively, and also accompanied increases in mRNA expression of *EDAR* and *TROY*.

4.5.5 Gene expression analysis of Sonic Hedgehog and Patched-1 during primary follicle development

Hedgehog signalling is one of the most fundamental signal transduction pathways in embryonic development and is indispensable in both embryogenesis and adulthood (Michno et al., 2003). In skin, the SHH pathway is crucial for maintaining stem cell population and for regulating hair follicle and sebaceous gland development (Athar et al., 2006). The “second dermal signal” regulating proliferation and downgrowth of the follicle epithelium is likely to be activated by SHH, as downgrowth does not occur in *SHH* knockout mice (St-Jacques et al., 1998; Millar, 2002). Similarly, mice knockouts for *GLI-2*, a transcription factor activated by SHH, show an identical phenotype. Although the *PTCH1* knockout is embryonic lethal, mice expressing a *PTCH1* variant with a truncated C-terminal domain display normal hair follicle development (Nieuwenhuis et al., 1997). *PTCH1* mutations in humans have been previously reported in basal cell carcinomas (BCC) (Athar et al., 2006), demonstrating its importance in regulating proliferation at the epidermal basement membrane.

Although numerous PCR assays were trialled, a reproducible quantitative assay could not be optimised for *SHH*. In comparison, a reliable quantitative assay for the receptor *PTCH1* was optimised with relative ease. *PTCH1* mRNA expression showed a gradual increase from day 47 to 57 and then rose by 57% at day 60 and increased by a further 87% from days 63 to 68. The expression pattern observed herein is consistent with this signalling pathway activating the first dermal signal, initiating primary follicle organogenesis,

characterised by the proliferation, maturation and downgrowth of the epidermal placode into the underlying mesenchyme.

Although small amounts of *SHH* mRNA were detected from day 43 through day 60, because the assays produced Cts greater than 30 they were deemed non-quantitative and therefore not reported in this study. *SHH* mRNA copies did appear to increase at day 68 (results not shown), which is consistent with previously reported data indicating that SHH activates the second dermal signal, initiating maturation, proliferation and downgrowth of the epidermal placode (Chiang et al., 1999). In a similar but more extensive study conducted concurrently (Bawden et al; unpublished data), *SHH* mRNA transcript levels were also extremely low from days 35-65 of gestation and then rose progressively before peaking around day 80. During primary follicle downgrowth, the number of epidermal cells expressing *SHH* is small in comparison to the total number of cells in the whole embryonic skin sample. Furthermore, *SHH* is restricted to the epidermal components of the downgrowing hair germ, whereas *PTCH1* expression has been detected in both the outer root sheath of the epidermis and within the dermal papilla (Michno et al., 2003; Rendl et al., 2005). Therefore, the total number of *PTCH-1* mRNA molecules would be greater than the number of *SHH* mRNA molecules. Another explanation for the vast difference in the levels of *SHH* and *PTCH1* mRNA could be that the proliferation of the hairgerm is mediated through responsiveness to SHH rather than through regulation of the total *SHH* transcript level.

4.5.6 Differences in Gene Expression between the Midside and Rump

Distinct differences in the mRNA levels of particular transcripts between the midside and rump was an unexpected result. Significant site differences in mRNA levels was observed for *RAC1* (p=0.046), *RHOa* (p=0.0001), *β 1-integrin* (p<0.0001), *ALP* (p<0.0001), *PCNA* (p=0.006), *EDA* (p<0.0001), *EDAR* (p=0.01), *TROY* (p=0.0002), *EDARADD* (p=0.034) and *TRAF-6* (p=0.011). However, *CYCB1*, *XEDAR* and *PTCH1* showed no significant

differences between the midside and rump. The shoulder samples collected during the foetal sample series were fixed in paraformaldehyde and subsequently used for histological characterisation, and therefore, could not be included in the qRT-PCR analysis.

Initially, it was thought that the significant differences in gene expression between the midside and rump skin samples may be attributed to differences in the input RNA concentrations. However, re-analysis of the RNA concentration in the diluted RNA samples used in the reverse transcription reactions demonstrated there was no significant difference in the mean RNA input between midside and rump samples. In addition to this, some target genes showed a higher expression in the midside skin samples whilst others showed higher expression in the rump. Furthermore, even the two most stably expressed genes, *RAC1* and *RHOa*, showed small significant differences in gene expression between the midside and rump, when normalised to the next three most stably expressed genes, *GAPDH*, *YWHAZ* and *ATPsynthase*. Differences in follicle density, and therefore, fibre diameter between the midside and rump may account for some of the differences in gene expression. Typically, the fibres on the rump of a Merino sheep are approximately 1µm wider than the midside (Figure 6-2), which would be associated with a 20% decrease in follicle density (Young and Chapman, 1958).

Another explanation for these results may lie within the establishment of different follicle types that respond differently to changes in environmental conditions. For example, under environmental stress caused by poor nutrition or prolonged stress (e.g. persistent threat from predation), sheep may shed wool fibres, however, usually only from the posterior and ventral regions of the animal. Secondary follicles, but not primary follicles, are particularly susceptible to the effects of the stress hormone cortisol, indicating that fine wool sheep with a high S:P ratio may be more susceptible to environmental stresses (Hynd, 1995). It could be hypothesized that differences in gene expression or the signalling pathways (or more specifically the receptors within these pathways) utilised during follicle initiation may be

responsible for establishing follicles that respond differently to environmental factors. Therefore, the differences in mRNA levels observed between the midside and rump may reflect the dynamic follicle patterning across the animal.

In the search for a replacement to mulesing, Australian agricultural researchers have recently described a “bare-breech” phenotype where the sheep have a naturally bare area around the breech that extends down the inside of the legs (Hebart et al., 2006). The severity of the breech bare area seems to have a strong environmental component as the animal’s “bareness score” can vary from year to year, depending on the amount of rainfall, the ewe’s litter size and lactation state. These factors indicate that under nutritional stress, the follicles in the breech area respond differently than the follicles on the midside and rump. Considering that the rump samples in this study were cut from the hind of these foetuses by running the scalpel blade along the hind hip and extending down adjacent to the tail, these rump skin samples could quite possibly have contained follicle inductive cells from the breech area. This provides an alternate explanation for the differences in gene expression observed between the midside and rump foetal skin samples.

4.6 Conclusion

The qRT-PCR experiments have demonstrated that alkaline phosphatase and the TNF signalling pathway are important in the establishment of primary wool follicles and are likely to also be involved in wool follicle patterning. Furthermore, the gene expression analysis has indicated a novel role for RAC-1 and RHOa as potential normalisation genes for qRT-PCR investigations in embryonic skin. The similarities in expression trends between mice and sheep in the TNF signalling pathway and the conservation in histology between mice, sheep and humans during follicle initiation suggests that sheep could be an excellent intermediate model between mice and human hair research because the slow cycling, long anagen wool follicle in sheep is a closer representation of the human scalp follicle than the fast cycling, short anagen of mice hair follicles.

Chapter Five

Laser Capture Microdissection of Foetal Sheep Skin

Chapter 5 : Laser Capture Microdissection of Foetal Sheep Skin

5.1 Introduction

Expression analysis studies using complex heterogeneous whole skin samples can often produce inconclusive results with the signals arising from the non-target tissues confounding the expression levels from the target cell types. Laser capture microdissection (LCM) is a specific micro-isolation technique for procuring specific homogenous or localised cell populations from histological sections of numerous tissue types. The technology is relatively new and was developed through an intensive collaboration between bioengineers and cancer research groups (Emmert-Buck et al., 1996), resulting in the commercial development of the Arcturis CapSure Polymer system (*Molecular Devices, NSW*). Two additional commercial laser capture microdissection systems have since been developed, the Leica Laser Microdissection system (*Leica Microsystems, VIC*) and the PALM Laser Capture Microdissection and Pressure Catapulting system (LMPC[®]; PALM[®], *Carl Zeiss Pty. Ltd, VIC*). The systems differ in the wavelength of the laser as well as the capturing methods and vessels.

Laser capture microdissection has been used in combination with PCR, qRT-PCR and microarrays for research on prostate cancer (Rubin, 2001), breast cancer tissue (Lehmann et al., 2000; King et al., 2005) and analysis of adjacent neural subtypes (Luo et al., 1999). This sophisticated and specific cell isolation technique has been demonstrated to cause little or no diminishment of PCR efficiency from DNA or RNA. Additionally, native enzymes have been recovered using laser capture, which remain active (Emmert-Buck et al., 1996). The PALM laser microdissection pressure catapulting, RNA isolation and qRT-PCR was optimised herein for the microdissection of foetal Merino sheep skin for primary wool follicle initiation research.

5.2 Aim

The aim was to optimise the sectioning, staining, laser capture microdissection, RNA extraction and cDNA production from laser captured microdissected cells of foetal sheep skin, in order to analyse the difference in expression of selected members of the tumour necrosis factor signalling pathway. The source material was regions of follicular and non-follicular skin derived from day 60 foetal sheep skin. Particular emphasis was placed on RNA integrity throughout the process and efficient, reproducible and traceable production of cDNA.

5.3 Specific Methods

5.3.1 Frozen tissue sectioning and fixation

10µm sections were taken from foetal skin frozen in optimal cutting temperature compound using the Microm HM550 cryostat (*Carl Zeiss, NSW*); block temperature of -20°C and chamber temperature of -25°C. Initially, two serial sections were melted onto room temperature SuperFrost+ slides (*ProSciTech, Kirwan Qld*) and immediately air-dried at room temperature for 30sec. Slides were then fixed in ice-cold 70% ethanol for 2mins and allowed to drain and dry within the cryostat chamber for a minimum of 10mins. Other slide types were also trialled, including uncoated glass slides, poly-l-lysine coated slides (*ProSciTech, Kirwan Qld*) and PALM PEN membrane slides (*Carl Zeiss, NSW*). Further optimisation of the protocol showed the air drying and the ethanol fixation steps were unnecessary, and therefore, were excluded from the protocol. Sections were stored at least overnight or for up to 12 weeks at -80°C in slide boxes containing silica beads before staining and LCM.

5.3.2 Haematoxylin and Eosin staining of frozen sections for laser capture microdissection

Slides were removed from -80°C storage and immediately transferred to a container with dry ice and silica beads. Slides were then quickly transferred to the first staining vessel containing 80% ethanol and stained with the following protocol.

1.	80% AR Ethanol	30sec
2.	30% AR Ethanol	30sec
3.	Autoclaved DEPC Treated RO Water	30sec
4.	Lillee Mayer's Haematoxylin (Appendix I)	1dip
5.	Autoclaved DEPC Treated Tap Water	10sec
6.	Autoclaved DEPC Treated Tap Water	30sec
7.	70% AR Ethanol	30sec
8.	0.5% Eosin (Appendix I)	20sec
9.	90% AR Ethanol	30sec
10.	Absolute AR Ethanol	30sec

Slides were then allowed to drain and dry in a slide rack inside a container with dry ice and silica beads for a minimum of 10 mins. Initially, the slides were placed in Lillee Mayer's haematoxylin for 1 min. However, this time was gradually decreased until the desired colour intensity was achieved and to reduce the time the sections were at room temperature in an aqueous based stain. The eosin concentration was also reduced from 1% to 0.5% to reduce the intensity of the stain.

5.3.3 Laser Capture Microdissection Protocol

Prior to LCM, initially slides were placed in an air tight container with silica beads to equilibrate to room temperature (approx 2mins) and then placed on the stage. Later, slides were taken from dry ice and dipped in 100% ice cold absolute AR ethanol. The excess ethanol was then carefully blotted away and the slide placed on the stage. The region(s) to be captured were located and selected with the PALM robotic software (*Carl Zeiss, NSW*) and 30-40µl of the capturing solution was pipetted into the cap of a 0.5µl microfuge tube (*Ambion, NSW*) and fitted into the cap holder of the PALM LCM System. Capturing solutions trialled included RNAlater (*Invitrogen*), TRIZOL (*Invitrogen*), Lysis solution (microRNA extraction kit; *Ambion, NSW*) and RLT buffer (RNeasy micro extraction kit,

Qiagen, VIC). Laser pressure catapulting was performed under the 10x objective during the initial extraction optimisation and under the 20x objective when isolating the whole epidermis, dermis or whole follicle regions (developing hair germs). PALM laser pressure catapulting (LPC) settings were as follows: 10x objective, CUT: energy = 60, focus = 72; LPC: energy = 85, focus = 70. 20x objective, CUT: energy = 60, focus = 72, LPC: energy = 85, LPC = 70. Once the laser pressure catapulting was complete, the microfuge cap was carefully closed and spun briefly in a bench top microfuge (*Adelab, SA*) to collect the contents at the bottom of the tube (RNA later, TRIZOL, lysis solution) and either placed on ice or at room temperature in the case of the RLT buffer (as per the manufacturer's protocol). If several captures were to be performed, the tubes were placed at -80°C until sufficient tissue had been microdissected. The solutions were then rapidly thawed in a metal block at room temperature and combined prior to extraction.

5.3.4 RNA extraction from laser captured tissue

5.3.4.1 TRIZOL and RNAqueous Micro Extraction Protocols

When the laser pressure catapulted material was captured into TRIZOL reagent, a further 70µl of TRIZOL was added and the tube shaken vigorously for 1min. The solution was then phase separated with 20µl of chloroform and centrifuged at 13,000g at 4°C. The aqueous phase was removed, combined with an equal volume of 100% AR ethanol and lysis solution (RNAqueous-Micro extraction kit; *Ambion NSW*), applied to the column and extracted via the manufacturer's protocol, including DNase treatment in solution following elution from the column. When captured into RNAlater™ (*Qiagen, VIC*) or lysis solution (from the RNAqueous-Micro extraction kit; *Ambion NSW*), a further 70ul of lysis solution was added and the sample incubated at 42°C for 20 min. The solution was then applied to the RNAqueous micro column (*Ambion, NSW*) and extracted using the manufacturer's protocol, including DNase1 treatment in solution following elution from the column.

5.3.4.2 Qiagen RNeasy Micro Extraction Kit

The RNeasy micro extraction procedure required the laser pressure catapulted material to be captured into 30-40 μ l of RLT buffer in the cap of a 0.5ml microfuge tube (*Ambion, NSW*). The solution was spun down in a bench top microfuge and then vortexed for 30 secs. The cap was re-spun to collect the contents at the bottom of the tube and stored at room temperature (if the extraction was to be completed on the same day) or snap frozen at -80°C and stored until sufficient material had been captured from numerous laser capture experiments. The frozen captured material was rapidly thawed in a metal block at room temperature and then several RLT preparations combined and the volume was adjusted to 350 μ l (if the combined preparations did not exceed 350 μ l). An exogenous RNA control (0.2pg of luciferase RNA, *Promega, NSW*) was added to each preparation and the total RNA extracted according to the manufacturer's protocol, including the addition of carrier RNA. If the volume of combined RLT buffer preparations exceeded 350 μ l, the protocol was scaled to account for the increased volume, with only the amount of luciferase control and carrier RNA added remaining constant regardless of the volume.

5.3.5 Estimation of RNA quality and quantity

DNase treated RNA (2 μ l) was analysed on a Nanodrop spectrophotometer (*Biolab, VIC, Australia*) for both quantity (260nm) and quality (260:280nm ratio). Routinely, the amount of RNA extracted was below the lower limit of detection for this system. However, when the RNA concentrations were within the detection limits of the Nanodrop, the concentrations were used as a guide for determining the input quantity for reverse transcription. Visualisation of RNA integrity via electrophoresis was attempted but due to the very small amount of RNA present in each LCM sample (less than 5ng total), this was not achievable.

5.3.6 Reverse Transcription of RNA

Gene specific primers (GSP; Appendix II Table II-2), random hexamers (*Invitrogen, VIC, Australia*) and the Oligo dTVN primer (where V = A, C, G and N = A, T, C, G; Appendix II Table II-1) were trialled in the reverse transcription of RNA extracted from LCM tissue. The Sensiscript and Omniscript RT kits (*Qiagen, VIC*) were trialled. It was determined that the Sensiscript kit was the more efficient in producing cDNA from laser captured RNA samples. A standard 20 μ l reaction consisted of 1 μ M GSP combination or 10 μ M oligo dTVN, 5mM dNTPs, 1x reaction buffer (*Qiagen, VIC, Australia*), 10U RNase OUT (*Invitrogen, Vic*), 5U SensiScript Reverse Transcriptase (*Qiagen, Vic*) and the entire column volume of purified RNA (which varied depending on the extraction method used). It was later determined that using GSP combinations not only limited the number of transcripts that could be assayed, but significant interactions between the primers caused a dramatic decrease in the reverse transcription efficiency and random hexamer priming was not as efficient as Oligo dTVN. It was, therefore, determined that Oligo dTVN priming was the best option for this application.

5.3.7 Cells Direct One-Step Kit

Another method trialled was the Cells Direct One-Step RT-PCR Kit (*Invitrogen, Vic*). The laser pressure catapulted material was captured into the lysis solution (supplied with the kit) and then extracted in solution using the manufacturer's protocol, including in solution DNase treatment. The DNAase was inactivated using the high salt inactivation reagent rather than exposing the RNA to extreme heat.

5.4 Results

5.4.1 Optimisation of Sectioning and Staining for Laser Capture Microdissection

In order to assess the quality of the RNA extracted from the cells in the samples frozen into OCT compound, 10 and 20 10 μ M OCT sections were cut and immediately placed in the lysis buffer of the RNAqueous extraction kit (*Ambion, NSW*). The RNA was extracted on

columns and eluted in two volumes: A, the first 12 μ l elution and B, the second 12 μ l elution. The amount of RNA extracted was at the lower limit of spectrophotometric detection; therefore, the quality and integrity of RNA could only be assessed by gel electrophoresis. The integrity of the 28S and 18S bands had been maintained during the sampling, freezing and sectioning process (Figure 5-1).

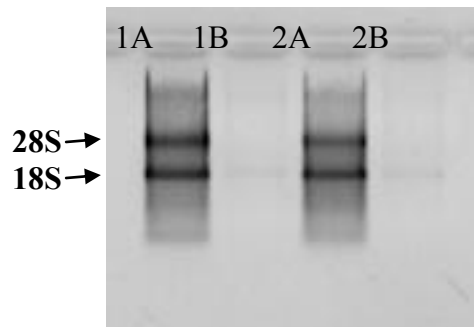


Figure 5-1 Analysis of the integrity of ribosomal 18S and 28S RNA extracted from OCT sections.

Lane 1A and B: 20 x 10 μ m OCT sections, Lane 2A and B: 10 x 10 μ m OCT sections; A=first 12 μ l and B=second 12 μ l elution.

Eight 10 μ m OCT sections were cut onto 4 superfrost + slides and the slides stored at -80°C overnight with silica beads. Eight sections were then adhered to 4 fresh slides and a comparison of air drying time, fixation length and storage conditions conducted (Figure 5-2). The eight sections were then scraped from the slides and the RNA extracted using the RNAqueous extraction kit (*Ambion, NSW*). The results demonstrated that storing the sections overnight at -80°C with silica beads enhanced the quantity and quality of the RNA extracted from the sections (lanes 1-4 versus lanes 5-8 Figure 5-2). Furthermore, the results showed that a longer air drying time degraded the RNA (lanes 2 and 4) and a longer fixation time did not improve RNA yields (lane 1 versus lane 3). It was noted that a longer fixation time essentially hardened the tissue and therefore, could affect staining and laser pressure catapulting. It was, therefore, decided that air drying the sections would be kept to a minimum time and eliminated if possible. Also sections would be stored overnight with silica beads to enhance removal of water from the fresh sections.

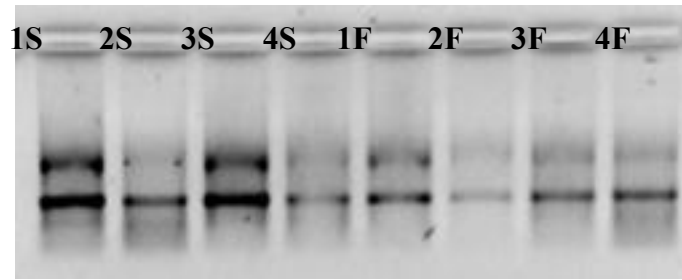


Figure 5-2_ Comparison of the effects of varied air drying time, fixation time and storage of sections on the integrity of ribosomal RNA.

Lane 1_30s air dry, 1min fix; lane 2_1min air dry, 1 min fix; lane 3_30s air dry, 5 min fix; lane 4_1min air dry, 5 min fix. S=sections stored overnight at -80°C with silica beads; F=sections cut fresh.

The RNA extracted from laser capture microdissected samples was of such a low concentration it could not be visualised by gel electrophoresis (Figure 5-3, lane 3). Therefore, in order to demonstrate that the RNA within the laser capture microdissected material was of a high quality, the sections remaining on the slide after LCM was completed (termed “tissue remnants”) were scraped from the slide and the RNA extracted using the RNAqueous extraction kit (*Ambion, NSW*) and eluted in 2x12µl volumes of nuclease free water (NFW; Figure 5-3).

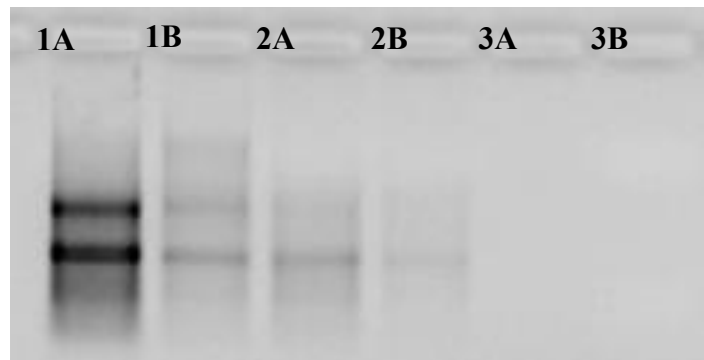


Figure 5-3_ Visualisation of RNA quality after staining and laser capture microdissection.

A=1st 12µl elution, B=2nd 12µl elution. Lane 1_ after H&E staining, lane 2_ tissue remnants post LCM and lane 3_ LCM material. Bands represent 18S and 28S ribosomal RNA. Cycling conditions were: 95°C 10min; 20cycles of 95°C 15sec, 60°C 20sec. Results shown are from a single experiment, similar results were obtained from replicate measures.

A 18S rRNA gene specific oligonucleotide (10µM; Appendix II Table II-1) was then incorporated with the Sensiscript RT kit (*Qiagen, Vic*) to conduct semi-quantitative RT-PCR

on the first 12µl elutions from the RNA extractions (1A, 2A and 3A in Figure 5-3) both with (+RT) and without reverse transcriptase enzyme (-RT). 18S rRNA products (amplified with 18S rRNA primers Appendix II Table II-2) were visible on a 2% agarose gel within 20 cycles of PCR and no products were formed in the -RT or no template control (NTC) reactions. The absence of an 18S product in the negative controls eliminated the possibility of genomic DNA contamination in the RNA preparations and DNA contamination in the PCR reagents (Figure 5-4).

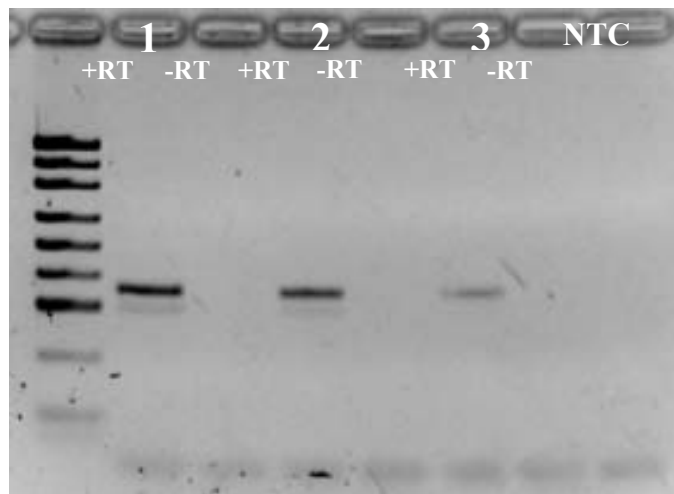


Figure 5-4 18S semi-quantitative RT-PCR on the RNA in figure5-3.

Sample 1_after H&E staining, sample 2_remnant tissue post LCM and sample 3_LCM material. Results shown are from a single experiment, similar results were obtained from replicate measures.

5.4.2 Optimisation of RNA extraction and RT-PCR of Laser Capture Microdissected

Material

The efficiency of the Invitrogen 1-step kit was compared to the RNAqueous micro RNA extraction kit used in combination with the Sensiscript RT kit (*Qiagen*), employing either Oligo dTVN or a gene specific primer combination (GSP). Two or four large squares of tissue (one screen viewed under the 10x objective) were laser pressure catapulted into microfuge tubes. One remaining section post-laser pressure catapulting was scraped from the slide (termed “remnant tissue”) and all samples processed with the 1-step kit (which includes RNA extraction and reverse transcription with random hexamers). The above laser pressure

catapulting experiment was then repeated and the RNA extracted from the samples with the RNAqueous micro kit and cDNA generated with the Sensiscript kit (with either oligo dTVN or GSP). PCR was then performed on all samples with 18S rRNA primers, comparing both extraction and reverse transcription efficiency of the two kits and RT approaches. RNA extraction and/or RT efficiency was significantly lower in the laser pressure catapulted samples when extracted with the 1 step kit compared to the RNAqueous kit, regardless of the RT primers used (1 step kit in lanes 2 and 3, 5 and 6 of Figure 5-5 compared to Sensiscript in lanes 9 and 10). The Sensiscript kit using oligo dTVN primers improved cDNA yield from LCM material in comparison to GSP (RNAqueous combined with Sensiscript in lanes 9 and 10 (using oligo dTVN) vs. lanes 13 and 14 (using GSP) Figure 5-5), as no 18S PCR product was produced when GSP were used. Furthermore, the remnant tissue sample produced a more intense band when oligo dTVN primers were used (Figure 5-5, lane 8) compared to GSP (Figure 5-5, lane11). The RNAqueous micro extraction kit in combination with the Sensiscript RT kit therefore, was used in subsequent optimisation reactions.

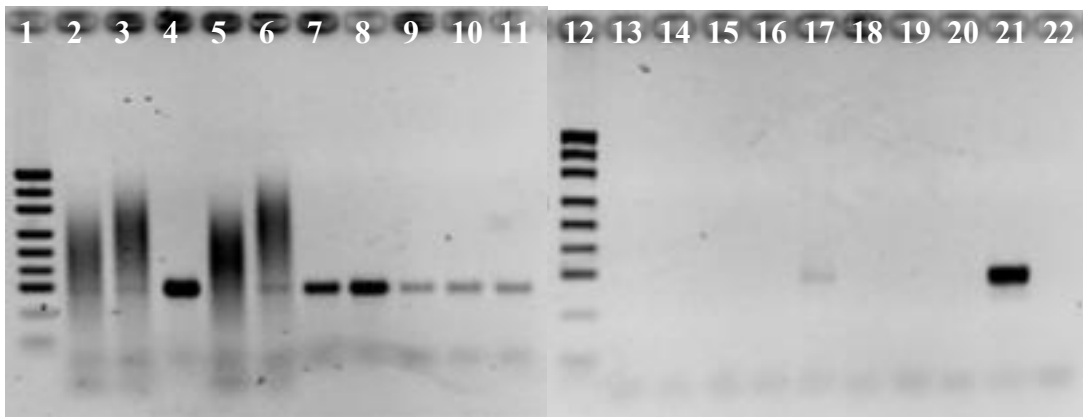


Figure 5-5_ Comparison of extraction and RT efficiency of the 1-step kit and RNAqueous combined with sensiscript.

Lane 1 and 12_pUC DNA markers, Lanes 2-7 Qiagen 1-step kit combined with sensiscript using either oligo dTVN (lane2_2squares, lane3_4squares, lane4_remnant tissue) or a GSP combination (lane5_2squares, lane6_4squares_lane7_remnant tissue), lane 8-11,13,14_Ambion RNAqueous kit combined with sensiscript using either oligo dTVN (lane8_remnant tissue, lane9_2 squares, lane 10_4 squares) or GSP combination (lane11_remnant tissue, lane13_2 squares, lane14_4 squares). Lanes14-20_no RT control repeats of lanes 2-13). Lane21_positive control, lane22_no template control. Results shown are from a single experiment, similar results were obtained from a repeated experiment.

A similar approach was used to compare the efficiency of using dTVN and random hexamers with the Sensiscript RT kit. cDNA samples were assayed for 18SrRNA, keratin-5, collagen and β 1-integrin. These experiments demonstrated that using oligo dTVN was a more efficient approach for producing cDNA for analysis of several gene transcripts (Appendix II Table II-1).

Having shown that Sensiscript was an efficient means of synthesising cDNA from LCM tissue, the efficiency of two RNA extraction kits was compared, RNAqueous (*Ambion*) verses RNeasy (*Qiagen*). One stained OCT skin section was scraped into either lysis solution (RNAqueous) or RLT buffer (RNeasy) in replicated experiments conducted in tandem. The exogenous luciferase RNA (LUC; 0.2pg) was added to all LCM tissue preparations and the total RNA was extracted according to the manufacturer's protocol. The total RNA concentration of each preparation was estimated using the Nanodrop spectrophotometer (*Thermo Scientific, USA*). The results indicated that the RNA concentrations of the samples extracted using the RNeasy column were higher than those extracted with the RNAqueous kit (Table 5-1).

The spectrophotometric measurements were used as a guide for RNA concentration and approximately 50ng of RNA used to generate cDNA with the Sensiscript RT kit. The cDNA samples were assayed for the exogenous control luciferase (Figure 5-6) and 18SrRNA (results not shown) using qRT-PCR. In both quantitative RT-PCR (qRT-PCR) assays, the fluorescence of the RNeasy extracted samples reached the cycle threshold (Ct) 2-3 cycles before the RNAqueous extracted samples indicating that the use of the Qiagen RNeasy kit with the Qiagen Sensiscript RT kit was approximately 8-fold more efficient. Therefore, the Qiagen RNeasy kit was used for the RNA extraction step in all subsequent experiments.

Table 5-1_ Comparison of the Qiagen RNeasy extraction kit and the Ambion RNAqueous extraction kit RNA concentration and quality

Sample	[RNA] ng/ μ l	OD 260:280	Luciferase assay Ct
RNaqueous 1	4.48	1.75	11.2
RNaqueous 2	3.51	1.96	10.8
RNeasy 1	6.45	1.79	8.7
RNeasy 2	5.78	2.00	8.8

[OD 260:280 indicates RNA quality, pure RNA has a 260:280 ratio of 2.0, Ct = cycle threshold which is indicative of cDNA transcript level, higher Ct indicates a lower cDNA transcript level]

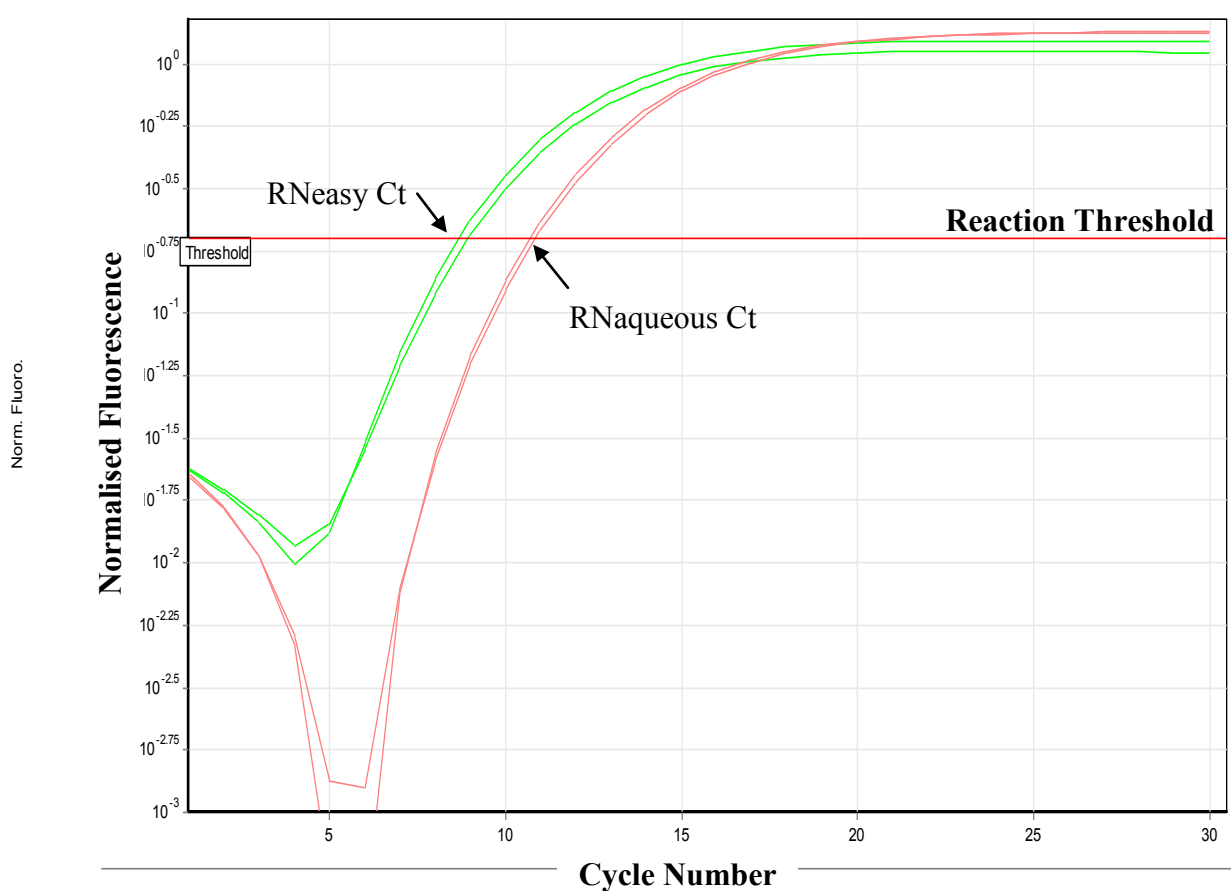


Figure 5-6_ Comparison of the qRT-PCR amplification of an exogenous mRNA control (luciferase, LUC) in samples extracted with the RNeasy and RNAqueous kits.

Fluorescence (from SYBR) increases as the PCR product is produced. Higher Ct (reaction threshold) indicates a lower cDNA transcript level. Reaction threshold is set by the user in the exponential phase of the qPCR reaction. Results shown are from a single set of RNA extraction and qRT-PCR experiments. Similar trends were obtained from repeated experiments (results not shown).

In order to demonstrate the specificity of the LCM and catapulting process, regions of the epidermis and the underlying dermis (Figure 5-7) were catapulted into the caps of separate microfuge tubes. The RNA was then extracted using the RNeasy kit (Qiagen) and reverse

transcribed with the Sensiscript RT kit (*Qiagen*), as described previously. cDNA samples were assayed for *18S ribosomal RNA (18SrRNA)*, the epidermal structural marker *keratin-5 (KRT5)* and the dermal structural marker *collagen (COL3A1)*; Figure 5-8). *18SrRNA* was detected in all captured tissue regions. *KRT5* was only detected in the epidermal and remnant tissue preparations, while *COL3A1* was only detected in the dermal and remnant tissue preparations. Minor amounts of *KRT5* genomic contamination was detected, as seen by the faint band in the –RT control reaction (Figure 5-8B, lane 5). The product is slightly larger than the target product because the primers span the two introns between exons 6 and 8.

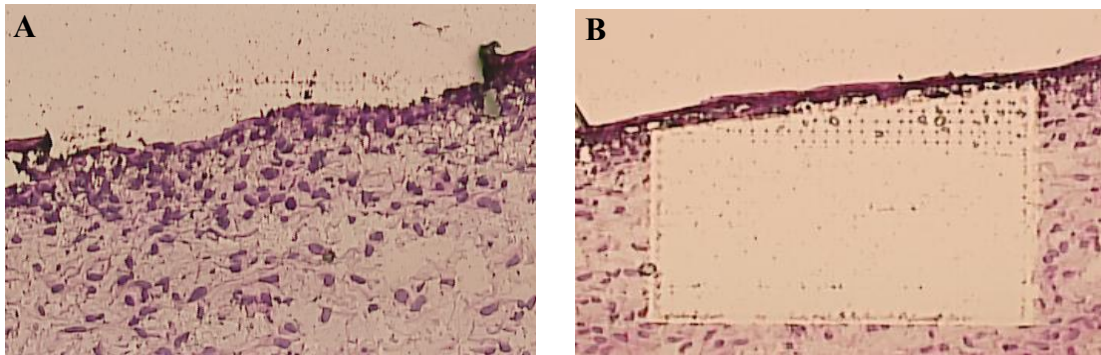


Figure 5-7_ *The regions of (A) epidermis and (B) dermis laser capture microdissected from foetal sheep skin.*

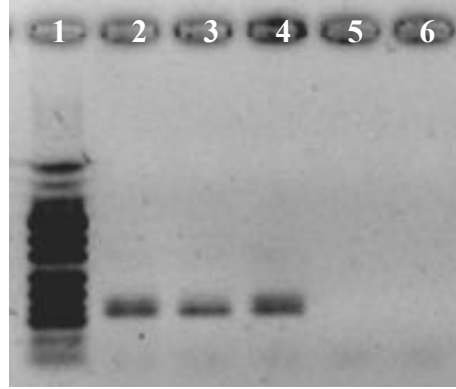
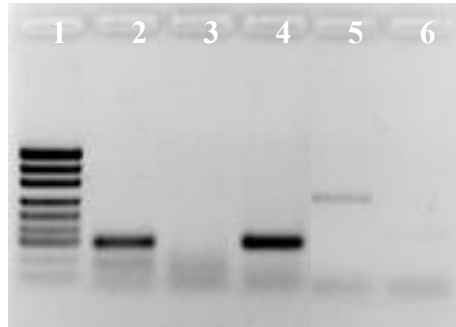
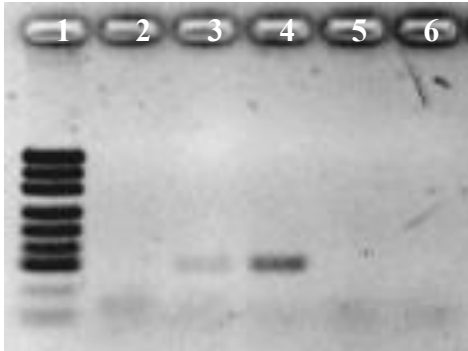
A) *18SrRNA*B) *Keratin-5*C) *Collagen*

Figure 5-8 Laser capture microdissection of the epidermis and dermis: PCR analysis for A) *18SrRNA*, B) *keratin-5* and C) *collagen*.

Lane 1: pUC DNA marker, lane 2: epidermis, lane 3: dermis, lane 4: remnant tissue, lane 5: no RT, lane 6: no template control. Results shown are from a single set of experiments. Similar results were obtained from three separate laser capture microdissection and PCR experiments (results not shown).

5.4.3 Optimisation of Slide Type for Laser Pressure Catapulting

A comparison of the laser pressure catapulting efficiency from PALM membrane, uncoated glass, poly-l-lysine treated slides and superfrost+ slides was conducted. Two 10 μ M OCT sections were adhered to one of each of the slide types. One half of a section was then laser pressure catapulted into 40 μ l of RLT buffer. The remaining half of the section was scraped from the slide and placed into 350 μ l of RLT buffer. From an additional PALM

membrane slide, 6 regions (fields of view at 20x objective) of epidermis and dermis were laser pressure catapulted (LPC) into separate microfuge tubes. The RLT buffer of the laser pressure catapulted samples was adjusted to 350µl and 0.1pg of luciferase (*LUC*) control exogenous RNA added. The RNA was extracted from the LCM material using the RNeasy micro extraction columns according to the manufacturer's protocol, including an "on-column" DNase treatment.

A second exogenous RNA control was added to LCM and remnant tissue samples prior to RNA extraction. A short poly-adenylated RNA transcript, *chloramphenicol transporter CAT*, was included to compare RNA extraction efficiency across the samples. cDNA was synthesized from the entire 12µl RNA elution from each LCM sample (including the addition of the exogenous control, *CAT*). The remnant tissue RNA samples were diluted 1:2, and the sample split equally between the remnant tissue cDNA sample and the -RT control. The cDNA samples were diluted 1:25 prior to qRT-PCR analysis of the exogenous controls *LUC* and *CAT*, and diluted 1:5 for analysis of the reference genes (endogenous controls) *18S rRNA*, *GAPDH*, *RPL19* and the epidermal and dermal marker genes (*KRT5* and *COLL3A1*, respectively). The exogenous controls *LUC* and *CAT* showed that RNA extraction and reverse transcription efficiency was similar between all samples and slide types as the controls are added after the LPC process is complete.

RNA transcript concentration of the endogenous control and epidermal/dermal markers between the LPC half section and the scraped half sections was negligible when PALM membrane slides were used (Figure 5-9A). However, there was a striking difference between the two samples (LPC vs scraped) when poly-l-lysine (Figure 5-9B), superfrost+ slides (Figure 5-9C) or uncoated (Figure 5-9D) were used. Transcripts for the endogenous controls and epidermal/dermal markers were detected approximately 8 cycles later when uncoated, poly-l-lysine or superfrost+ slides were used (Figure 5-9B,C,D), which would be indicative of approximately 256 times difference in RNA transcript levels. These results

demonstrated that the laser pressure catapulting from membrane slides was far more effective than from all other slide types.

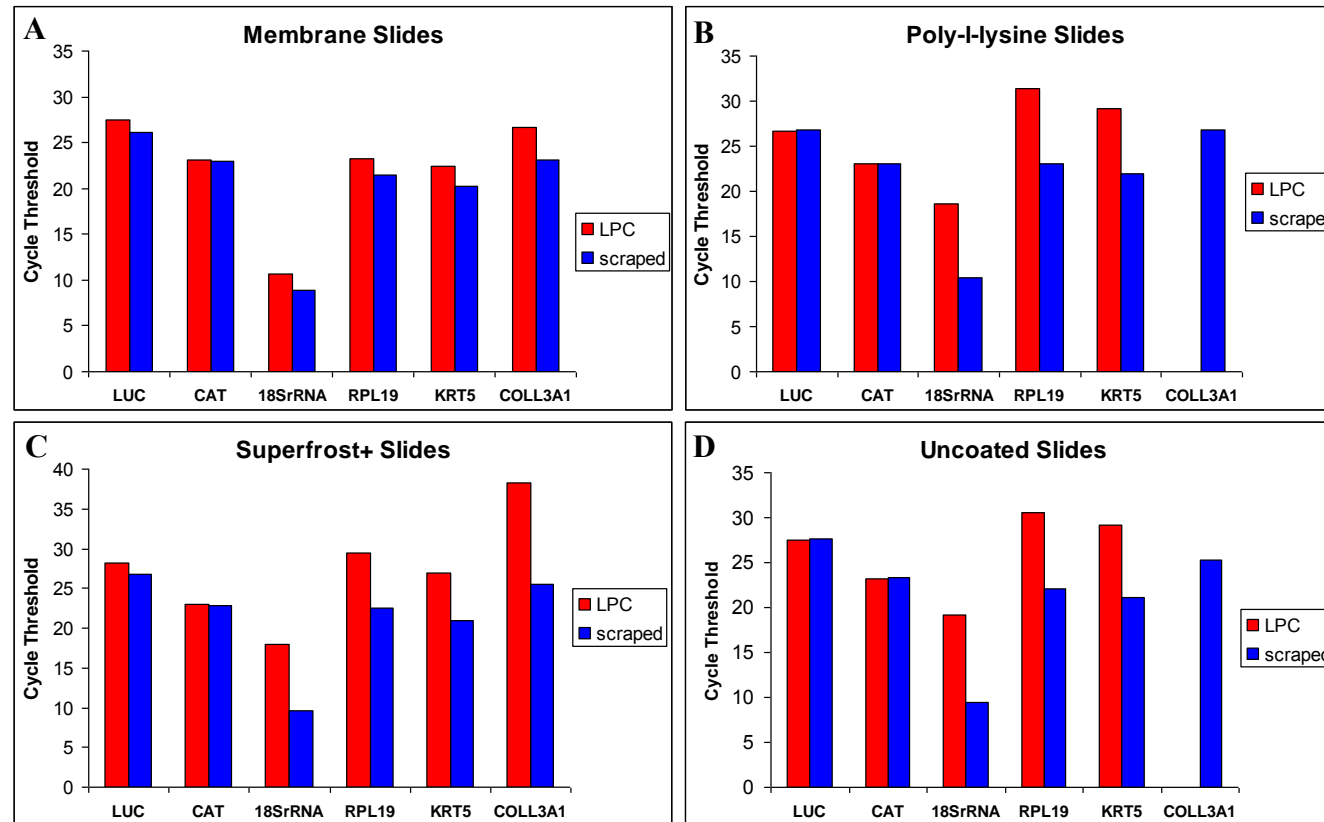


Figure 5-9 Graphical representation of laser capture microdissection slide type comparison.

Cycle thresholds for qRT-PCR analysis of endogenous and exogenous controls and structural markers. Cycle threshold is representative of mRNA transcript level with a higher Ct indicating a lower mRNA concentration of that transcript. Foetal skin tissue was laser pressure catapulted from (A) PALM membrane slides, (B) Poly-l-lysine coated slides, (C) Superfrost+ slides, (D) Uncoated slides. Results shown are from a single set of experiments. Similar results were obtained when the experiment was replicated (results not shown)

5.4.4 Laser capture microdissection and qRT-PCR analysis of follicle regions vs. non-follicle regions of foetal sheep skin.

Having optimised the sectioning, staining, RNA extraction, reverse transcription and the appropriate slide type for LCM and qRT-PCR analysis of foetal sheep skin, these techniques were employed to determine if there are difference in expression of the TNF pathway genes between follicle regions vs. non-follicle regions in day 60 foetal skin. The selected genes were demonstrated to be differentially expressed during wool follicle initiation in whole skin (chapter 4). All initiating follicle structures (placodes and underlying condensates; Figure 5-10), present in 4 OCT sections cut from each of the four animals sampled on day 60, were laser pressure catapulted from PALM membrane slides into RLT solution (termed “follicle regions” herein). An area devoid of initiating follicle structures, but the same size as the follicle region captured, in adjoining tissue was also excised into a separate tube (termed “non-follicle regions” herein). The RNA was extracted and reverse transcribed with the inclusion of the *LUC* exogenous control prior to RNA extraction and *CAT* control prior to reverse transcription in all samples. The RNA extracted from the sections remaining on the final slide after catapulting was split equally into two cDNA preparations, (1) remnant tissue (+RT) and (2) –RT. The cDNA samples were diluted 1:5 and qRT-PCR assays conducted for *LUC*, *CAT*, *18SrRNA*, *RPL19*, *KRT5*, *COLL3A1*, *RAC1*, *RHOA*, *EDA*, *EDAR*, *EDARADD*, *TROY*, *XEDAR*, *TRAF6* and *PTCH1*. All assays included a 3 point cDNA dilution standard curve (pooled cDNA samples at 1:5, 1:50, 1:500) plus no RT and no template control reactions with the Ct produced from the first cDNA standard dilution used as the positive control (Figure 5-11, Figure 5-12 and Table 5-2).

The exogenous controls showed that RNA extraction and reverse transcription was comparable between the follicle and non-follicle regions and expression of the endogenous controls *18SrRNA* and *RPL19* were similar in both regions. As expected, *KRT5* mRNA levels were higher in the follicle regions and *COLL3A1* was higher in the non-follicle regions

(Figure 5-11 and Table 5-2). The TNF ligand *EDA*, intracellular signalling molecule *TRAF6* and receptor *XEDAR* mRNA could not be detected in either preparation. *TROY* and *PTCHI* were detected in the follicle region but not in the non-follicle region. *EDAR* expression was slightly higher (Ct difference of 1.71 = approximately 3.3x higher expression) in the follicle regions. *EDARADD* expression was similar between the follicle and non-follicle regions (Figure 5-12 and Table 5-2).

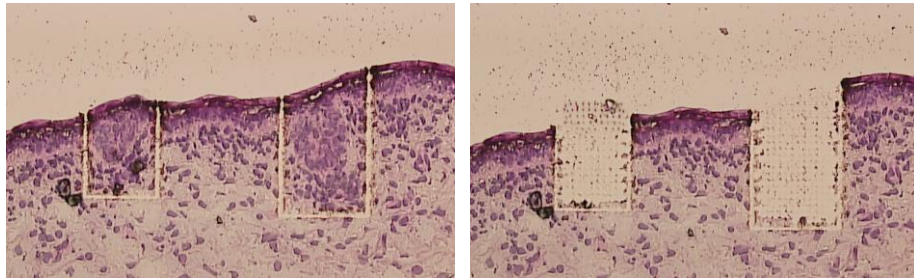


Figure 5-10_ The histological structures captured from day 60 skin for comparison of follicle regions (epidermal placode and dermal condensate) and non-follicle regions (interfollicular space).

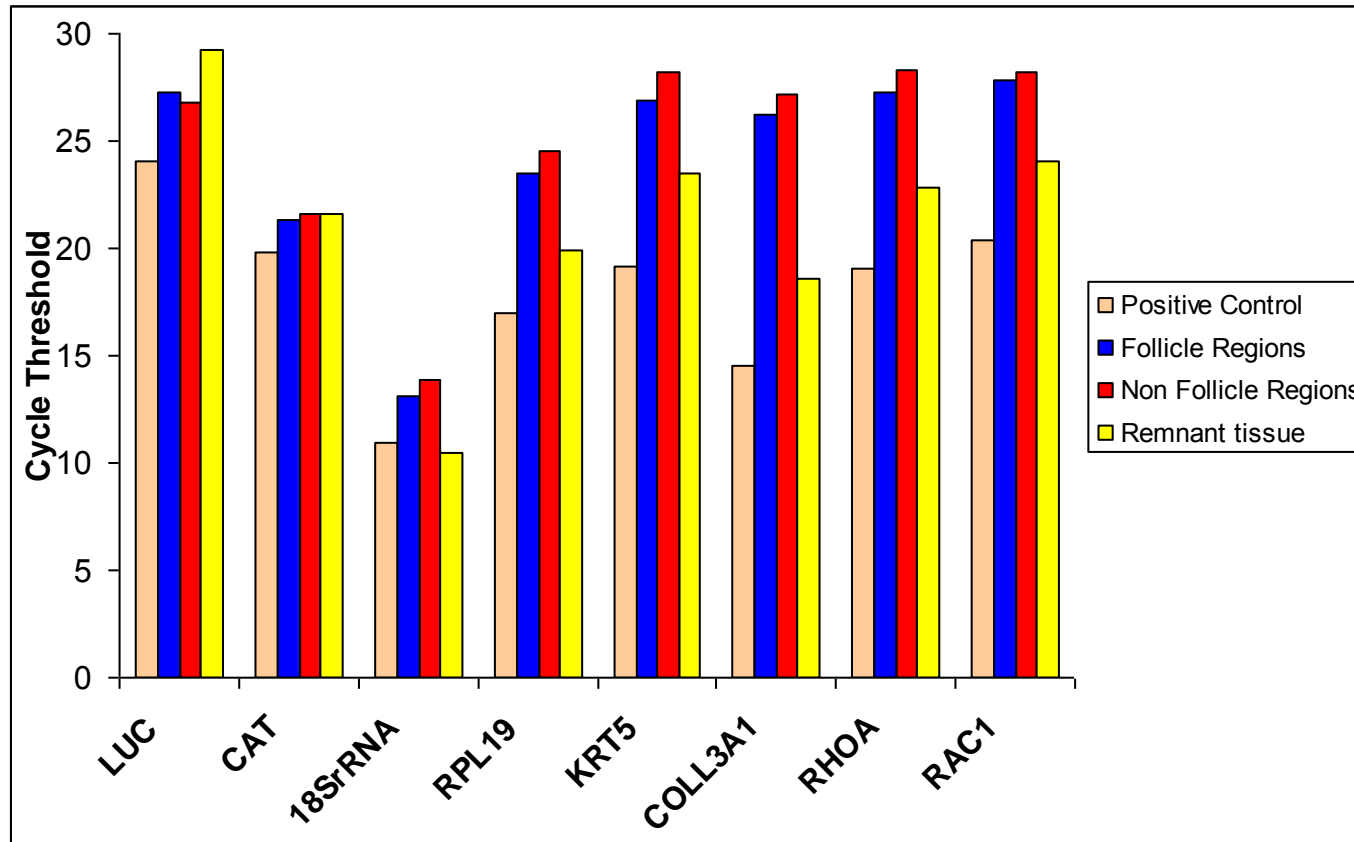


Figure 5-11 Graphical representation of qRT-PCR analysis of exogenous and endogenous control genes in follicle regions vs non-follicle regions.

LUC and *CAT* were exogenous controls, *18SrRNA* and *RPL19* were endogenous controls, *KRT5* and *COLL3A1* were epidermal and dermal structural markers, *RHOA* and *RAC1* were most stably expressed genes in the whole skin analysis. Cycle threshold is representative of mRNA transcript level with a higher Ct indicating a lower expression level of that transcript (from a single measurement). Results shown are from a single set of laser capture microdissection and qRT-PCR experiments.

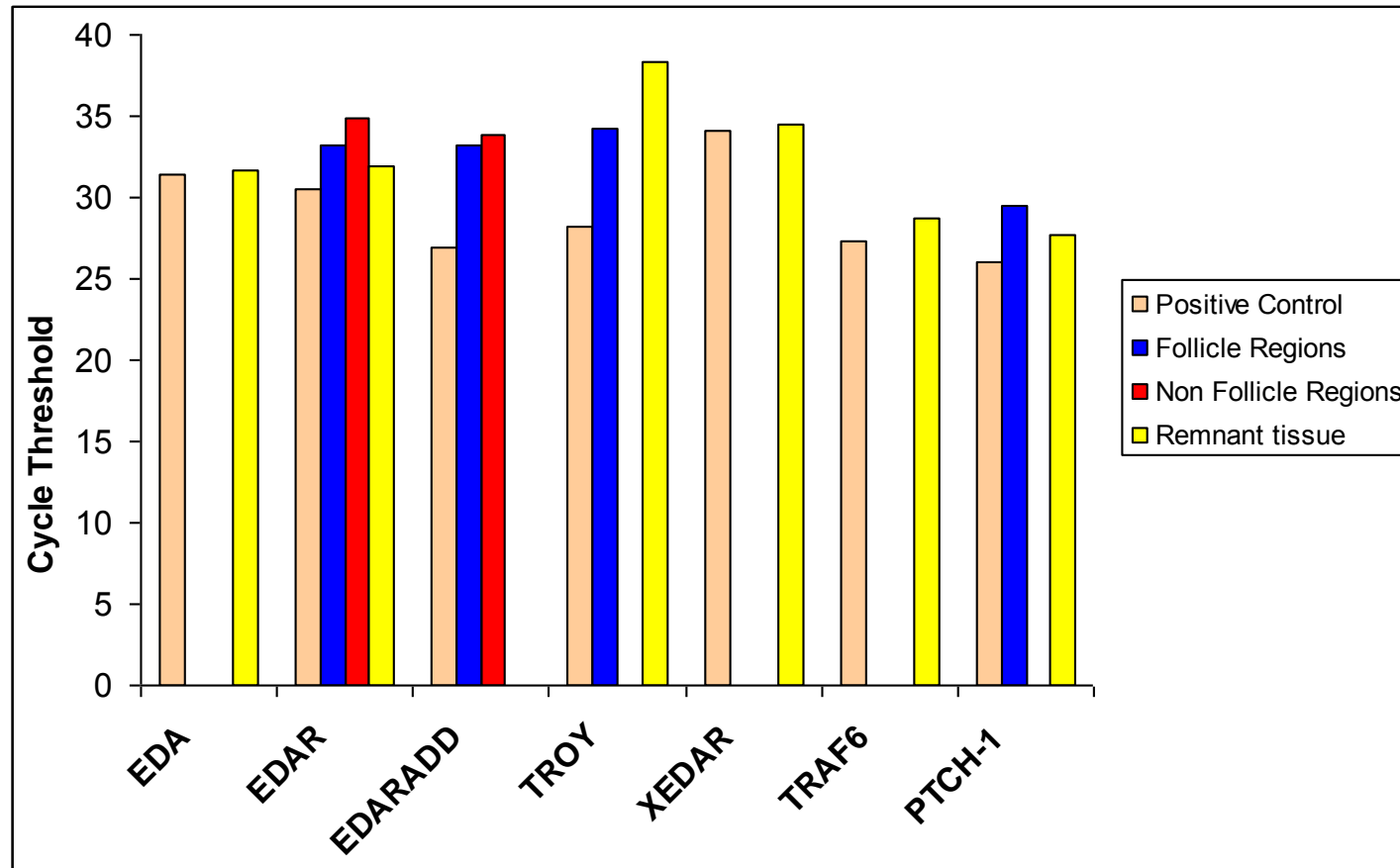


Figure 5-12 Graphical representation of qRT-PCR analysis of selected TNF signalling pathway members and PTCH1 in follicle regions vs non-follicle regions.

Cycle threshold is representative of mRNA transcript level with a higher Ct indicating a lower expression level of that transcript (from a single measurement). Results shown are from a single set of laser capture microdissection and qRT-PCR experiments.

Table 5-2 *Ct values from laser capture microdissection and qRT-PCR analysis of follicle regions vs. non-follicle regions of day 60 foetal sheep skin.*

Numbers are cycle thresholds (Ct) for cDNA samples assayed. Cycle threshold is representative of mRNA transcript level with a higher Ct indicating a lower expression level of that transcript (from a single measurement). Day 60 foetal sheep skin was laser captured from PALM membrane slides. Results shown are from a single set of laser capture microdissection and qRT-PCR experiments

Sample	Exogenous Controls		Endogenous Controls		Structural Markers		Migration Markers		Tumor Necrosis Factor Pathway Member						<i>SHH</i> receptor <i>PTCH1</i>
	<i>LUC</i>	<i>CAT</i>	<i>18SrRNA</i>	<i>RPL19</i>	<i>KRT5</i>	<i>COLL3A1</i>	<i>RHOA</i>	<i>RAC1</i>	<i>EDA</i>	<i>EDAR</i>	<i>EDARADD</i>	<i>TROY</i>	<i>XEDAR</i>	<i>TRAF6</i>	
Positive Control	24.0	19.8	10.9	17.0	19.2	14.5	19.0	20.3	31.4	30.5	27.0	28.2	34.1	27.3	26.0
Follicle Regions	27.2	21.3	13.1	23.5	26.9	26.3	27.2	27.9	-	33.2	33.2	34.2	-	-	29.5
Non Follicle Regions	26.8	21.7	13.8	24.6	28.2	27.1	28.3	28.2	-	34.9	33.9	-	-	-	-
Remnant tissue	29.2	21.6	10.5	19.9	23.5	18.6	22.8	24.1	31.7	31.9	-	38.3	34.5	28.7	27.7
No RT	-	-	29.8	36.8	-	-	36.2	37.4	-	-	-	-	-	-	-
No Template Control	-	-	-	-	-	-	-	-	-	-	-	-	-	-	-

5.5 Discussion

Techniques to isolate intact high quality RNA from tissues with preserved morphology have been developed with the emergence of laser capture microdissection (Cox et al., 2005). Formaldehyde and paraformaldehyde fixation of tissues severely compromises analysis of biomolecules, particularly mRNA and proteins due to extensive cross-linking. Formaldehyde reacts with RNA forming an N-methylol (N-CH₂OH), followed by an electrophilic attack to form a methylene bridge between amino acid groups (Srinivasan et al., 2002; Perlmutter et al., 2004; Su et al., 2004). RNA becomes fragmented, chemically altered and difficult to isolate in quantity from formalin fixed and paraffin embedded samples (Goldsworthy et al., 1999). A comparison of frozen tissues, paraffin embedded tissues and precipitative fixatives (ethanol and acetone) revealed that these fixatives produce more RT-PCR product than paraffin embedded samples. Furthermore, frozen tissues produce a better yield than precipitative fixatives (Goldsworthy et al., 1999). Therefore, in order to protect the integrity of the RNA within the cells of the foetal sheep skin and ensure efficient reverse transcription, the samples analysed herein were snap-frozen in OCT using a cold block on dry ice. Frozen OCT blocks were then maintained at -80°C to ensure the RNA was protected during storage.

Analysis of RNA quality, after varying times of air drying with varying periods of fixation (Figure 5-2) and after optimising the staining protocol (Figure 5-3), revealed that the shorter the time period that the fresh frozen sections were exposed to room temperature, aqueous solutions and extreme changes in temperature, the better the RNA quality. These experiments also showed that sections stored overnight in an air tight container at -80°C in the presence of silica beads produced a higher quality and quantity of RNA as seen from the intensity of the 28S and 18S ribosomal RNA bands (Figure 5-2). Fixing the sections in 90% and 70% ethanol was trialled, but it was determined that higher ethanol concentrations or longer fixation times actually hardened the tissue. This made staining less efficient and

caused the tissue to fragment during laser pressure microdissection and catapulting. It was determined that the best method to prepare the OCT sections for LCM and qRT-PCR analysis was to remove the room temperature air drying step and maintain the slides at -20°C inside the cryostat (in the presence of silica beads) whilst the sectioning was completed. The slides were not fixed in ethanol; they were simply transferred to the -80°C freezer and stored overnight with silica beads. The next day, the slides were removed from -80°C and submerged directly in 80% ethanol for 30sec before the first step of the haematoxylin staining protocol. Upon completion of the staining protocol, the slides were allowed to drip dry in a container with dry ice and silica beads until required for laser capture. Slides were finally dipped in 100% ethanol at room temperature before being carefully blotted to remove the excess ethanol, and placed on the stage for immediate microdissection and laser pressure catapulting. Dipping the slides in ethanol prevented condensation accumulating on the slide as it equilibrated to room temperature on the stage of the laser capture apparatus. All aqueous steps in the staining protocol were kept to a minimum time frame and all solutions were made with DEPC treated autoclaved MQ or RO water to remove RNases.

Assessment of RNA integrity has been greatly improved through the use of highly sensitive gel analysis systems, such as the 2100 Bioanalyser technology (*Agilent Technologies*). Without access to this equipment, the integrity of the RNA post sectioning, staining and upon completion of the microdissection process was assessed by scraping the remaining sections from the microscope slide (termed “remnant tissue” herein) once the entire LCM process was complete. Due to the relative large number of cells present (compared to the microdissected regions), the amount of RNA extracted from this “remnant tissue” sample could be visualised using electrophoresis in a 1% agarose gel with a longer ethidium bromide staining procedure (Figure 5-3). Both the 28S and 18S bands were clearly intact and no significant degradation of the RNA sample was evident. This confirmed that the quality of the RNA had been maintained during sectioning and staining, and had not been compromised

due to the time the slides spent on the stage of the PALM laser pressure catapulting apparatus. Comparisons between the RNA extracted from non-embedded, OCT-embedded and laser-microdissected tumour tissue demonstrated varying degrees of RNA degradation, with the most degradation occurring after microdissection with the Arcturis PixCell microdissector (Sanchez-Carbayo et al., 2003). This study also indicated that the expression profiles generated from microdissected samples of lower RNA integrity may differ from their comparable non-laser-microdissected samples. Therefore, in order to generate comparable expression profiles, care must be taken during the sectioning, staining, microdissection and extraction to ensure RNA integrity is maintained.

The total RNA harvested from a single cell is estimated to be approximately 0.1-1.0pg and is not sufficient for standard RNA extraction procedures (Ginsberg, 2005). Therefore, in order to conduct downstream analysis of laser capture microdissected specimens, the RNA must be amplified or several captures performed and combined prior to extraction. Antisense RNA amplification (aRNA), a method for the linear amplification of the mRNA population of a sample was first described in 1990 (Van Gelder et al., 1990). It involves the use of a reverse transcriptase and poly(T) primers modified with the T7 RNA polymerase promoter sequence at the 5'end to produce an antisense cDNA strand. Following the subsequent second strand cDNA synthesis, T7 polymerase is used to generate up to a 2000-fold amplification of the antisense RNA (Phillips and Eberwine, 1996). Because the amplification of mRNA involves priming from the polyA tail, the process may not produce equal quantities of all transcripts, particularly those with extended 3'UTR regions. Analysis of the reliability and reproducibility of gene expression profiles generated from amplified RNA samples from breast cancer tissue showed that nanogram quantities of RNA isolated using laser capture microdissection generated reliable and reproducible gene expression profiles. However, these profiles did not mirror those obtained from microgram amounts of RNA that were not amplified (King et al., 2005). It is for this reason that amplification of mRNA was not

employed in this study. Ten thousand laser shots were required to collect 100-500ng total RNA from 6 μ m sections of human arteries and veins using the Arcturis PixCell II™ system, with 50% of the RNA preparations showing a qRT-PCR profile indicative of high quality RNA and smooth cell enrichment (Stagliano et al., 2001). For the experiments herein, multiple captures were performed on numerous sections taken from the four animals sampled on day 60 and the captured regions of similar cellular types/regions from each animal were combined before being extracted as a single sample. This allowed enough RNA to be extracted to perform qRT-PCR on several endogenous controls, structural gene markers and selected members of the tumor necrosis factor pathway (Table 5-2).

Comparisons of the fidelity of amplified RNA, total RNA and mRNA preparations on gene expression profiling using cDNA microarrays indicate that some bias in RNA abundance can be introduced by the amplification procedure. However, this does not generally affect the ratio between two samples if both RNA samples are amplified (Li et al., 2004). However, since the purpose of the study herein was to analyse expression differences between two regions of foetal sheep skin using qRT-PCR, the RNA samples were not amplified as any selective change in mRNA abundance may have had an impact upon the abundance of specific genes, particularly those which have a long 3'UTR and many of the candidate genes analysed herein had 3'UTR regions up to 3Kb. Furthermore, the quantity of RNA could not be measured in the microdissected preparations, and therefore, the RT reactions could not be normalised for input RNA. Since RT efficiency is dependent on RNA concentration and integrity, where possible, it is important to normalise RT reactions for input RNA concentration. Amplifying the total RNA in these samples would have added a further level of complexity to the gene expression comparisons and could have potentially masked real differences or created artificial differences when comparing the expression of target genes in the follicle versus non-follicle regions.

LCM has been employed to analyse DNA sequence mutations in the p53 gene of histologically normal and dysplastic keratinocytes of human epidermis (Agar et al., 2003) and in combination with cDNA microarrays to analyse the gene expression profile of adjacent neural subtypes (Luo et al., 1999) and rat dopamine receptors (Li et al., 2004). LCM and downstream qRT-PCR analysis have also been used to quantitate stage specific changes in the expression of genes associated with rat spermatogenesis (Sluka et al., 2002). Interestingly, some of these studies have reported the use of archival paraffin-embedded tissues in laser capture microdissection experiments. Following a rigorous dehydration protocol, the DNA was extracted from the laser microdissected regions and combined with TaqMan™ qPCR probes to assess the quantitative alterations in gene dosage of breast cancer tissues (Lehmann et al., 2000). In skin, LCM was used in combination with real time-PCR and microarray analysis to analyse the effect of the over-expression of *Noggin* on anagen follicles (Sharov et al., 2006) and for transcription profiling of mouse hair follicle bulge cells (Cotsarelis, 2006b; Ohyama et al., 2006).

LCM has also been performed on the basal and suprabasal cells of the outer root sheath of mature mouse hair follicle sections and combined with sensitive TaqMan™ qPCR probes to assess differential *Cyclin D1* gene expression in the different layers of the outer root sheath. Preliminary studies showed that the concentration of *Cyclin D1* in cells from a single capture (approx 50-200 cells) varied considerably in the different outer root sheath areas, indicating that cells with similar morphological appearance may have different gene expression levels (Xu et al., 2003). Therefore, in the laser capture microdissection experiment conducted herein, the follicle regions and non-follicle regions of day 60 foetal sheep skin were collected in multiple captures from all four animals sampled. The microdissected material was then pooled prior to extraction to attain an overall estimation of the difference in the mRNA levels of the targeted TNF pathway genes between these two regions of the developing skin.

EDA mRNA levels were below the limit of detection in both the follicle and non-follicle regions. Therefore, a conclusion based on the importance of *EDA* signalling in wool follicle initiation cannot be drawn. However, evidence from mouse, rat and chicken indicates that *EDA* is a poor candidate for conveying positional information because *EDA* is expressed ubiquitously throughout the epidermis both before and after initiation (Laurikkala et al., 2002; Drew et al., 2007). Conversely, prior to follicle initiation in mouse, *EDAR* is expressed ubiquitously throughout the epidermis but as the pattern emerges *EDAR* becomes focally upregulated in placodes. Dynamic *EDAR* expression is also dependent on *EDARADD* signal transduction because it is not seen in *EDARADD* knockout embryos (Mou et al., 2006). Interestingly, *EDARADD* was detected at a slightly higher level in follicle regions than non-follicle regions. However, the control remnant tissue preparation did not form a product (Table 5-2), unfortunately casting doubt on the validity of this result. It appears that as patterning takes place, cells display one of three expression states: (1) those with a high level of *EDAR* are committed to a follicle fate, (2) those with moderate *EDAR* expression capable of either fate, and (3) those with undetectable levels of *EDAR*, committed to the interfollicular regions of the follicle pattern (Mou et al., 2006). The results observed herein support this hypothesis as the *EDAR* mRNA transcript was detected at 3.3x higher levels in follicle regions which is composed of cells committed to the follicle fate.

The mRNA transcript levels of *TRAF-6* and *XEDAR* were below the assays' limit of detection in both the follicle and non-follicle region samples. *XEDAR* is not thought to play an important role in follicle initiation because *XEDAR* knockout mice display apparently normal hair development (Newton et al., 2004). It can be hypothesised that when absent, *XEDAR*'s role in follicle initiation can be replaced by other signalling pathways or molecules. On the other hand, *TRAF-6* knockout mice display a phenotype similar to ectodermal dysplasia, indicating that *EDAR* signal transduction through *TRAF-6* signalling is vital for normal follicle initiation and pattern formation. The LCM and qRT-PCR approach

used herein were not sufficiently sensitive to detect potential differences in *TRAF-6* mRNA levels. Interestingly, *TROY* knockout mice do not exhibit any obvious physical abnormalities or alterations in behaviour, locomotion, or fecundity (Shao et al., 2005). This appears to be at odds with the present finding that *TROY* was detected in the follicle regions and in the control remnant tissue preparation but not in the non-follicle regions. Based on this result one could speculate that TNF receptor *TROY* activation plays an important, but perhaps not essential, role in wool follicle initiation.

During mouse hair follicle development, *SHH* is not required for the first epidermal signal and hence, formation of placodes and condensates. It is, however, required for subsequent signalling between the dermis and epidermis regulating proliferation and downgrowth of the hair germ (Chiang et al., 1999). One could argue that the detection of *PTCHI* (the *SHH* receptor) mRNA in the follicle region preparation only indicates the activation of this signalling pathway between the placodes and condensates of foetal sheep skin. However, the evidence from mouse studies indicates that it does not play a role in patterning but simply regulates proliferation and downgrowth of the hair germ, hence, explaining why it was detected in the follicle regions only.

The Ct results reported for the LCM and qRT-PCR analysis of follicle regions vs non-follicle regions were from a single qPCR measurement. There simply was not sufficient RNA extracted from the laser captured regions to perform more than a single qPCR assay for all of the required exogenous and endogenous controls, as well as the desired TNF signalling pathway target genes. The results reported herein demonstrate careful optimisation of the sectioning, staining, LPC, cDNA production and qPCR in foetal sheep skin and have focused on including exogenous and endogenous at key steps to ensure equal efficiency in both RNA extraction and cDNA production from the LPC tissue. Ideally, similar experiments should be repeated, with each LCM and qRT-PCR experiment focusing on only a couple of target genes, thereby allowing triplicate qPCR reactions to be performed to account for differences

in qPCR reaction efficiency between triplicates. Unfortunately, due to the time taken to optimise the qRT-PCR analysis of LPC material, these experiments could not be conducted herein.

The results of this study could have been strengthened by the inclusion of *in-situ* hybridisation (ISH) experiments in order to attempt to confirm the site(s) of mRNA expression of the selected targets. Traditional ISH experiments using non radioactive labelled probes, whilst only semi quantitative at best, can be a specific and reliable method for localising mRNA targets, often giving an indication of the number of cells expressing the selected mRNA transcript. However, the application of these methods can be very limited when trying to localise low copy number targets or transcripts expressed by a small population of cells. Immuno-histochemical experiments could also have been included to not only localise the site of protein expression, but also account for any post-translation modifications. However, sourcing antibodies specific to ovine proteins that have the specificity to distinguish between minor protein variants can often be difficult. Furthermore, optimisation of the technique would have added another level of complexity to the planned experiments and time constraints simply did not permit this avenue of investigation. In theory, LCM couple with highly specific qRT-PCR primers could have the potential to localise, quantify and distinguish between splice variants and was, therefore, the chosen method focused on herein.

Future work to be conducted should also focus on improving the sensitivity of the qRT-PCR analysis of LCM tissue. Although all but one of the optimised assays worked efficiently on whole skin RNA (higher copy number), when these assays were transferred to LCM tissue, the sensitivity of several assays were insufficient. Protocols that could greatly increase the specificity of qRT-PCR analysis of LCM tissue are available, however, time constraints did not permit incorporation and optimisation of such techniques herein. Alternatively, the use of commercial qPCR assays such as TaqMan® probes (*Applied*

Biosystems, NSW) could also increase the chance of detecting low copy number cDNA transcripts. These assays use combinations of primers coupled to fluorogenic dyes and quenchers in a master mix of extremely high magnesium concentration in order to decrease the stringency of the reaction, hence increasing the chance of obtaining a specific fluorescent signal from low copy number targets. Currently, ovine specific probes are not commercially available and the lack of annotated ovine cDNA sequence data limit the application of such a system. However, techniques such as RNA amplification (Yim et al., 2003; Upson et al., 2004), multiplexed preamplification (Denning et al., 2007), global DNA preamplification (Iavarone et al., 2003) and degenerate oligonucleotide PCR (Kasai et al., 2000) have been used to amplify whole RNA and DNA or to specifically amplify target regions of the cDNA profile for the detection of low copy number transcripts and microarray analysis of LCM tissue.

5.6 Conclusion

Laser capture microdissection used in combination with qRT-PCR is a powerful tool for studying the spatial and temporal differences responsible for initiating tissue development and ontogeny. Particular attention must be paid to the processing of histological specimens in order to preserve the RNA transcript quality. Differences in mRNA transcript concentration of particular TNF gene pathway members were detected between follicle and non-follicle regions of day 60 foetal sheep skin, indicating an important role for this pathway in the generation of the primary wool follicle pattern. Incorporation of a preamplification technique or a more specific qRT-PCR assay would further improve the results of investigations of this nature.

Chapter Six

General Discussion

Chapter 6 General Discussion

6.1 Introduction

Primary wool follicles are initiated at discrete sites in the skin of sheep foetuses at approximately day 50 of gestation as the result of complex reciprocal molecular interactions between the mesenchyme and overlying epithelium. Secondary follicles initiate in a similar process approximately 30 days later and then branch into secondary-derived follicles at around day 100 of gestation. The lifetime wool production potential and fibre diameter of the Merino sheep is dependent on the total number of follicles initiated *in utero*. The key drivers of profitability in a wool enterprise are fibre diameter, staple length, staple strength, crimp and clean fleece weight, all of which are determined *in utero*. Understanding the molecular events that surround primary wool follicle initiation may provide approaches to enhance or manipulate this process in order to maximise the profitability of wool production enterprises. Furthermore, due to both morphological and molecular conservation between human and sheep follicle initiation and cycling, wool research is highly relevant to the study of human hair follicle initiation as well as diseases affecting this dynamic self regulating organ.

In order to study the morphological and molecular changes occurring during early wool follicle development, a foetal skin series spanning primary follicle initiation was generated through artificial insemination and foetal tissue sampling at days 43, 47, 50, 53, 57, 60, 64 and 68 post AI. The exact age of embryos generated through AI can vary by up to 48 hrs so crown-rump length measurements were taken from the foetuses sampled. The crown rump length measurements were used to generate a new equation relevant to Merino foetuses for estimating foetal age based on crown rump length and foetal weight (Equation 2). The age of the foetuses, as determined by their crown rump lengths, not only showed strong correlations with previous studies (Joubert, 1956), but also showed similar trends to the weights and crown rump lengths in studies on northern Nigerian sheep and goats

(Sivachelvan et al., 1996) and Australian feral goats (McDonald et al., 1988). It was concluded that day of gestation was a reasonable representation of foetal age in this study.

Histological analysis of the foetal skin samples (Figure 3-7_A-H) showed that wool follicle initiation within these samples followed previously published timings for primary follicle initiation (Hardy and Lyne, 1956). Wool follicles are similar to human scalp follicles in that they are slow cycling, long anagen follicles. Although hair and wool fibres and feathers arose independently around 155-255 million years ago, they have evolved similar follicular structures, with localised growth zones at the proximal ends and dermal papillae residing at the base of the follicle that is essential for the life, growth and cycling of the follicle (Yue et al., 2005). Hair, wool and feather follicles show histological conservation in early morphogenesis, have similar timing during development and share conserved morphogenesis signalling pathways (Stenn and Paus, 2001; Watt, 2001; Millar, 2002; Botchkarev and Paus, 2003). However, the evolution of feathers (from reptiles to birds) and hairs/wool (from reptiles to mammals) were independent events and differences in their follicular structures have resulted from this divergent evolution (Yue et al., 2005).

Histological analysis of the skin samples collected at day 43 showed an undifferentiated epithelium, only 2-3 cells layers thick, overlying an undifferentiated mesenchyme (Figure 3-7A). Rather than assigning copy number or an absolute mRNA concentration to all qRT-PCR measurements, expression at all other time points was expressed relative to the mRNA detected at this first undifferentiated time point. Structural signs of follicle initiation were not evident from the histology until day 53 and therefore, as expected, there was little change in mRNA expression in all target genes on days 47 and 50. The emergence of epidermal placodes in the foetal skin samples at day 53 of gestation (Figure 3-7C) coincided with a significant increase in the mRNA transcript level of the TNF signalling molecule EDA and receptors EDAR and TROY as well as the SHH receptor PTCH1 (Figure 6-1). In mice, increased EDA signalling both *in vivo* and *in vitro* stimulates

placode enlargement by a mechanism not involving cell proliferation (Mustonen et al., 2004). In chickens, hyperactivation of the TNF receptors EDAR and TROY leads to widespread formation of feather placodes and conversely, suppressing their expression leads to destabilization of feather placodes (Drew et al., 2007). Furthermore, ectopic activation of β -catenin (transcription factor activated by WNT signalling) is enough to induce *EDAR* expression (Houghton et al., 2005). Interestingly, at day 14.5 in the skin of *EDA* knockout mice (when primary placodes form in wildtype animals), the expression of the placode markers *β -catenin*, *LEF-1*, *SHH*, *PTCHI* and *BMP* is absent, indicating an interaction of the TNF pathway with the WNT, SHH and BMP signalling pathways in normal hair follicle development (Laurikkala et al., 2002). Both *PTCHI* and *EDAR* showed significant increases in mRNA levels during epidermal placode, dermal condensate and hair germ formation demonstrating the potential interaction of the SHH and TNF signalling pathways in wool follicle initiation.

In mice, *EDA* and *EDAR* expression is activated only during placode formation of the primary (tylotrich guard) follicles (Schmidt-Ullrich and Paus, 2005; Drew et al., 2007). Such a result may indicate the importance of this pathway in determination of the primary follicle pattern. As the study herein spanned only primary follicle formation, a comment as to the expression pattern of the TNF members during secondary follicle initiation cannot be made. *EDA* is synthesised as a transmembrane protein but cell culture studies have revealed that it can be cleaved in the medium by furin-mediated cleavage into an extracellular site (Drew et al., 2007). However, *EDA* is a poor candidate for conveying positional information as it is widely expressed in the epidermis (Laurikkala et al., 2002) and allows normal pattern formation to occur when applied in a diffusible form, both *in vivo* and *in vitro* (Gaide and Schneider, 2003; Mustonen et al., 2004). *EDAR* presents a better candidate for conveying positional signals as it is evenly expressed throughout mouse skin prior to follicle initiation, but as the follicle pattern emerges, it becomes upregulated in follicle primordia and

downregulated in the surrounding cells (Mou et al., 2006). In contrast, expression of *EDA* mRNA herein, across the entire time series, was significantly higher in the midside compared to the rump ($p < 0.0001$), whereas *EDAR* was showed only a moderate significant difference between the midside and rump ($p = 0.01$). The site difference observed in this study may indicate that *EDA* signalling plays a role in primary follicle patterning across the body of sheep.

In humans, mutations in *EDA*, *EDAR* and *EDARADD* result in the congenital condition hypohidrotic ectodermal dysplasia, characterised by sparse hair, missing and malformed teeth, and the absence of sweat glands (Munoz et al., 1997). The causative genes were confirmed by the mouse gene mutant homologs of *Tabby*, *Downless* and *Crinkled* (Ferguson et al., 1997; Headon and Overbeek, 1999; Headon et al., 2001). These mice lack guard, zig-zag and, in most cases, awl hairs. Considering the similarities in TNF signalling in mice and sheep during follicle initiation and the hair cycle similarities between wool and hair (long anagen, slow cycling), one could speculate that sheep could be a more biologically relevant model of human hair initiation and disease.

$\beta 1$ -integrin mRNA levels were significantly higher at day 57 compared to day 53 (Figure 6-1), which coincided with the formation of epidermal placodes. The potential markers for hair follicle epidermal stem cells include: *$\beta 1$ -integrin*, *keratin19*, *$\alpha 6$ -integrin*, *CD71*, *p63*, and *CD34* (Gambardella and Barrandon, 2003; Kim et al., 2004). Many of these markers are expressed in high levels in hair follicle stem cells, but the difficulty in distinguishing hair follicle stem cells from their transit amplifying progeny remains (Blanpain and Fuchs, 2006). Hair follicle stem cells sorted by expression of these markers are far from pure (Jones et al., 1995). Furthermore, because hair follicle stem cells may have been activated after leaving the stem cell niche, *in vitro* stem cell markers may not be the same as those *in vivo* (Ma et al., 2004). Therefore, the increased *$\beta 1$ -integrin* mRNA levels observed

herein may be indicative of an increase in the epidermal stem cell niche or an increase in the number of transit amplifying cells as the stem cells begin terminal differentiation.

Dermal condensates or localised thickenings of the mesenchyme that formed beneath the epidermal placodes were visible from day 60 post AI. Formation of these structures coincided with a significant increase in the expression of the *SHH* receptor *PTCH1* mRNA (Figure 6-1). The increase in *PTCH1* mRNA as the time series progressed was expected because in mice *PTCH1* and *SHH* are expressed in both the follicular epithelium and in the dermal condensate (Dahmane et al., 1997) and because SHH signalling is required for progression past the hair germ stage (St-Jacques et al., 1998). Although expression of sonic hedgehog *SHH* mRNA transcripts could not be quantitated in this sample series, a similar yet broader study conducted in parallel with the study herein showed that *SHH* mRNA levels are extremely low prior to day 67 of gestation (S. Bawden, personal communication). *SHH* mRNA expression could not be quantified until day 63 before gradually increasing during secondary follicle placode initiation at approximately day 80. If a quantitative assay could have been optimised for *SHH* in this study, it would have been expected that the *SHH* mRNA levels would have followed a similar expression pattern as its receptor *PTCH1*. The *PTCH1* knockout is embryonic lethal in mice. Furthermore, mice expressing a *PTCH1* truncated C-terminal domain do not exhibit any abnormal follicle development. Therefore, it cannot be said that *PTCH1* signalling is required for follicle development, although the mRNA results of this study indicate that it may play an important role in wool follicle initiation, perhaps through interaction with the TNF pathway.

The most significant changes in mRNA expression were observed in the tumor necrosis factor (TNF) signalling pathway receptors *EDAR* and *TROY* and the *SHH* receptor *PTCH1*. *EDAR* and *TROY* showed a significant spike in expression at day 53, then a decrease at day 57 and a gradual increase to their highest expression at day 68, the final time point, albeit not by the same magnitude as each other. *EDAR* expression increased 6.5-fold from

day 50 to day 68 (Figure 6-1), further highlighting the potential importance of EDA:EDAR signalling in hair and wool follicle initiation. *PTCHI* expression doubled from day 63 to day 68 (Figure 4-19) coinciding with the downgrowth of the hair germ (Figure 3-7H). This correlates with mouse and human hair follicle initiation, where SHH signalling is required for progression past formation of the epidermal placode and dermal condensate (Chiang et al., 1999). It is thought that EDA:EDAR signalling activates SHH signalling as both *SHH* and *PTCHI* expression is absent in *Tabby* (*EDA*) and *Downless* (*EDAR*) mice. Furthermore it has been shown that *EDAR* activated *NFκβ* stimulates *SHH* and *Cyclin D1* signalling to affect post-initiation hair placode down growth and follicle fate (Schmidt-Ullrich et al., 2006). Marked significant increases in expression of the *EDAR* and *PTCHI* were observed herein once hair germs were visible in the skin, therefore it could be speculated that a similar signal transduction between SHH:PTCH1 and EDA:EDAR is being utilised during wool follicle initiation.


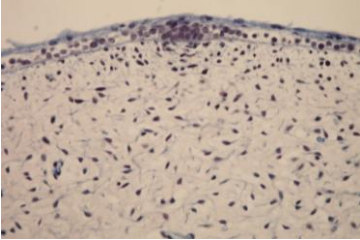
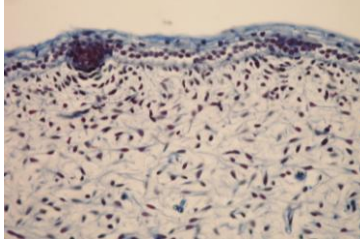
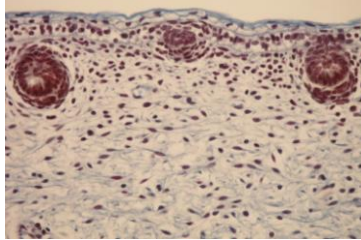
				
	day 43 Undifferentiated Epithelium	day 53 Epidermal placodes initiate	day 60 Dermal condensates initiate	day 68 Downgrowth of hair germ begins
RAC1		-	-	-
RHOA		-	-	-
β1-integrin		-	-	↑
Alkaline Phosphatase		-	-	↑↑
Cyclin B1		-	-	-
PCNA		-	-	-
EDA		↑	-	-
EDAR		↑	-	↑↑
TROY		↑	-	↑
XEDAR		-	-	-
EDARADD		-	-	-
TRAF6		-	-	↑
PTCH1		↑	↑	↑↑

Figure 6-1 Summary of the statistically significant mRNA expression changes (chapter four) at key histological timepoints. Arrows indicate the change in expression relative to the expression at day 43.

The qRT-PCR experiments reported (chapter four) were designed to address the proposed hypothesis that follicle dermal condensates form as the result of migration or proliferation of stem cell-like mesenchymal cells, or as a combination of both processes. The candidate genes selected were believed to exhibit differential mRNA expression during cell migration, proliferation and during rapid changes in stem cell number. Changes in the expression of these genes would, therefore, represent variation in these developmental processes. However, both the selected migration and proliferation markers showed no histologically discernible patterns in mRNA expression across the foetal skin time series. The migration markers, *RAC1* and *RHOa*, showed the lowest magnitude of variation in mRNA expression across the sample series of all the candidate and reference genes analysed. It was hypothesised that this may reflect the large number of cellular processes which involve the Rho-GTPases *RAC1* and *RHOa*, including polarisation, cell-cell and cell-matrix adhesion, membrane trafficking and transcriptional regulation (Hall, 1998; Jiang et al., 2006). Conversely, due to the complexity of the tissue remodelling occurring in both the follicular and inter-follicular regions of these foetal skin samples, the specific migration of the mesenchymal pre-papilla cells may not be detectable using whole skin qRT-PCR. One could also speculate that these migrating cells may not be using the Rho-GTPase pathway to facilitate their migration. It could also be said that the sheer magnitude of cell migration and proliferation, occurring in both the epidermis and dermis of foetal skin, as the organ thickens, expands to cover the growing foetus, and stratifies for protection from the elements from birth, has masked the proliferation of the target cell types, particularly when whole foetal skin was analysed using qRT-PCR.

The hypothesis, that dermal condensates initiate at discrete sites beneath the epidermis as a result of migration and arrangement of multipotent pre-papilla cells, could not be definitively addressed from the whole skin qRT-PCR results. A discernible pattern in expression of the selected proliferation and migration markers was not detected. One

explanation could be that the formation of dermal condensates actually involves both migration to the epidermal placodes and proliferation of the mesenchymal pre-papilla cells. *Cyclin B1* mRNA levels have been reported to increase by over 50-fold in somatic cycling mammalian cells as they progress through G1 and S into G2/M (Maity et al., 1995). The complexity and large number of the binding, phosphorylation and dephosphorylation events in which cyclin B1 is involved may have masked its importance in pre-papilla cell proliferation. PCNA, a nuclear homotrimer protein, is expressed late in G1 phase and early in S phase (Takahashi and Caviness, 1993), and has been implicated in cell proliferation as well as DNA replication and repair (Korgun et al., 2006). This perhaps explains why the significant changes in *PCNA* mRNA levels determined across the sample series did not coincide with the morphological changes observed in the histological characterisation. Furthermore, stem cells are known to undergo asymmetrical division in order to produce one daughter cell for expansion and terminal differentiation and one daughter cell to maintain stem cell compartment numbers. Therefore, tangible proliferation of the pre-papilla stem cell population may not actually occur.

The stem cell markers *β 1-integrin* (epidermal) and *alkaline phosphatase* (dermal) exhibited mRNA expression patterns that were consistent with the proposed hypothesis, that the number of pre-papilla cells in the skin is not the limiting factor in follicle initiation. However, not all the changes in mRNA concentrations correlated with the observed histology, perhaps because of the dynamic complexity of whole foetal skin, where the target cells (follicle regions) form only a small proportion of the total tissue sample from which the RNA was prepared.

No conclusions about whether a significant mesenchymal stem cell population is retained within the dermis after follicle initiation could be drawn, as the foetal skin series herein did not extend to secondary and secondary derived follicle initiation. The high levels of the stem cell markers *β 1-integrin* and *alkaline phosphatase* at day 68 could be indicative of

the expanding epidermal and dermal stem cell populations as the maturing primary follicle hair canals grow down into the dermis. In order to accommodate the downgrowth and begin maturation of the dermal papilla, the dermal stem cell population expands to invaginate the down growing hair germ. The skin could also be expanding both the epidermal and dermal stem cell populations in preparation for secondary follicle initiation, which begins at approximately day 80 of gestation (Hardy and Lyne, 1956). A more definitive conclusion may have been drawn if the foetal skin series had extended to and beyond secondary and secondary derived follicle initiation.

In previously published experiments using a Boyden's chamber, Akino et al. (2005) demonstrated that human mesenchymal stem cells showed "remarkable migration through an 8 μ m pore toward the lower chamber containing human aortic endothelial cells, dermal fibroblasts and epidermal keratinocytes". Of the cell types analysed, the human epidermal keratinocytes induced the most significant migration of human mesenchymal stem cells. Interestingly, the PKA pathway inhibitor H-89 inhibited this cell migration, indicating that this migration may be chemotactic in nature (Akino et al., 2005). Cells can also initiate migration in response to receptor signalling via integrins and the extracellular matrix or in response to soluble factors (Ray et al., 2003). These results supported the hypothesis that dermal papilla cells migrate to the basement membrane in response to signals from epidermal stem cells, perhaps in part through ectodysplasin signalling as significant changes in mRNA expression were detected for several of the TNF transcripts, corresponding histologically with formation of epidermal placodes (Figure 6-1).

Mathematical reaction-diffusion models have been suggested to describe formation of animal pigmentation patterns and distribution of epidermal appendages (Nagorcka, 1983; Nagorcka and Mooney, 1985 & 1992; Prum and Williamson, 2002). *In vivo* corroborations of the mathematical reaction diffusion system in hair follicle patterning involving WNT and DKK signalling (Sick et al., 2006; Schlake and Sick, 2007) and interactions between WNT/ β -

catenin and EDA/EDAR/NF κ B signalling (Narhi et al., 2008; Zhang et al., 2009) have been previously shown in mice. The results herein supported the idea of a reaction diffusion system controlling the size, density and spacing of initiating wool follicles in mammalian species other than mice. The qRT-PCR results in the laser capture microdissection experiment from the follicle regions vs non-follicle regions showed that the TNF receptor *EDAR*, a follicle promoting signal, was expressed higher in follicle regions than non-follicle regions, consistent with comparable studies in mice (Mou et al., 2006).

Now that a ligand that binds to TROY has been identified, LT α , the finding that *TROY* mRNA was detected in the follicle regions and not in the non-follicle regions warrants further investigation. Furthermore, *TROY* mRNA was expressed at significantly higher levels in midside samples than in rump samples ($p=0.0002$). One could hypothesise that expression of the receptor *TROY* is specifically involved in specification of wool fibre diameter and/or establishment of specific follicle types. A similar study such as the one herein could be conducted across different breeds of sheep with large variation in fibre diameter to ascertain if there is an expression difference in *TROY* and its newly identified ligand amongst these divergent animals.

Unexpected significant differences in mRNA expression between the midside and rump were observed in many of the transcripts assayed. One midside and one rump skin sample from each of four foetuses was included in the whole skin qRT-PCR analysis, accounting for biological variation both across and within animals. The variation in mRNA levels observed between the midside and rump may reflect the dynamic follicle patterning across the animal. Moreover, disparity in follicle density (and therefore, fibre diameter) between the midside and rump may also account for some of the observed variations in gene expression. Wool fibre diameter in Merino sheep can vary by up to one micron between the midside and rump (Figure 6-2), which equates to an approximate decrease of 20% in follicle density (Young and Chapman, 1958).

NOTE:
This figure is included on page 142
of the print copy of the thesis held in
the University of Adelaide Library.

Figure 6-2_Variation in fibre diameter (μm) across the body of Merino sheep (Young and Chapman, 1958)

Another potential explanation for these results may lie within the establishment of diverse follicle types that respond differently or at varying rates to changes in environmental conditions. It could be hypothesized that differences in gene expression or the signalling pathways (or more specifically the receptors within these pathways) utilised during follicle initiation may be responsible for establishing follicles that respond differently to environmental factors. The study herein is one of a few studies to demonstrate a spatial difference during follicle initiation between the midside and rump on a molecular level. Variation between fibres have been shown to occur temporally and spatially across the body of New Zealand Wiltshire sheep (Craven et al., 2007a), where it was speculated that this variation may arise due to differences between follicles that are determined by developmental processes *in utero*. Previous studies have also shown spatial variation in fibre diameter and morphology in response to nutritional stress (Lyne, 1964), both of which concur with this proposed hypothesis. Furthermore, a study looking at the bare breach score of ewes from 2004-2007 showed a change in the “wooliness” across the breach area, which correlated with

the ewes litter size (Edwards et al., 2009). Ewes that produced twins showed an increase in bare area compared to the single bearing ewes, which were in turn barer than dry ewes. This would suggest that nutritional and/or physiological stress (e.g. pregnancy, lactation demands) can affect follicle activity at least on the rear of the animal.

It has been previously hypothesised that discrete skin domains arise because fibroblasts that initiate wool follicles originate from different regions of the embryo and carry with them differing developmental programs for each type of follicle (Scobie et al., 2006). Expression of the follicle regulator *MSX1* mRNA was shown to have an increased expression in foetal sheep skin, in regions of eventual decreased follicle density (Craven et al., 2007b). It should be noted that these differences between body sites may complicate the interpretation of the data as follicle initiation occurs in waves, anterior → posterior, dorsal → ventral.

The objective of the LCM and qRT-PCR analysis of follicle and non-follicle regions was to identify the importance, if any, of TNF signalling in the generation of the primary wool follicle pattern. Of most interest was the fact that Troy was detected in the follicle regions but not in the non-follicle regions. When the experiments were completed, there was no known ligand that bound TROY. Subsequently though, a ligand that activates the transcription factor NF κ B by binding to TROY was published (Hashimoto et al., 2008). The immunomodulatory cytokine, lymphotoxin- α (LT α), was identified as a functional ligand of Troy by 3 biochemical approaches: (1) immunoprecipitation assays that revealed LT α binds to Troy, (2) co-transfection of LT α with Troy sharply upregulates NF κ B reporter transcription, and (3) recombinant LT α protein upregulates NF κ B activity through Troy in a dose-dependent manner. Furthermore, *LT α* is expressed in the dermal papillae of initiating hair follicles, whereas Troy was expressed in the adjacent matrix region. This suggests their involvement in mesenchyme-epithelium interactions during hair follicle development (Hashimoto et al., 2008). Notably, however, *TROY* mutant mice do not show significant alterations in hair composition or morphology (Shao et al., 2005). This would indicate that the newly identified

LT α -TROY pathway may have an additional, yet dispensible, action in hair and wool follicle initiation and patterning, which can be compensated by parallel EDA-EDAR signalling.

A new hypothesis addressing the role the TNF plays in patterning across the animal has emerged from this work. The fact that *EDA*, *EDAR* and *TROY* (Table 6-1) were expressed higher in the midside whereas *EDARADD*, *TRAF-6* and *XEDAR* (Table 6-1) were expressed higher in the rump is of particular interest. It can be hypothesised that modulation of gene expression or response to specific TNF molecules could be involved in the establishment of different follicle densities or various types of follicles that differ in response to environmental stress.

Table 6-1 *Significant differences in mRNA expression of target genes between the midside and rump in the skin of Merino foetuses.*

mRNA transcript	Midside	Rump
RAC1	*	
RHOa	***	
B1-integrin		***
Alkaline Phosphatase		***
Cyclin B1	No significant difference	
PCNA		**
EDA	***	
EDAR	**	
TROY	**	
XEDAR		*
EDARADD		*
TRAF6		*
PTCH1	No significant difference	

[* $p \leq 0.05$, ** $p \leq 0.001$, *** $p \leq 0.0001$]

The technical strengths in the study herein lie in the optimisation of RNA extraction and qRT-PCR analysis of laser capture microdissected tissues. This technique allowed analysis of distinct target cell populations, removing the “background noise” from non-target surrounding

tissues. Particular attention was paid to including exogenous and endogenous controls at key points within the experimental procedure to ensure efficient RNA extraction and cDNA production that could be compared across all samples. Although the LCM and qRT-PCR techniques were optimised for analysis of foetal skin herein, they could be adapted to other tissue types for a variety of downstream analyses including coupling these methods with microarray analysis for a wider investigation of mRNA signalling. The optimisation of RNA extraction, reverse transcription and qRT-PCR of laser capture microdissected tissues was substantially more time consuming than first anticipated, but was achieved. Unfortunately, the number and scope of laser capture microdissection experiments intended was consequently decreased, considerably reducing the ability to confirm the proposed hypotheses.

6.2 Future Work

Future work that could be completed to enhance the biological and industry relevance of this work include extending the laser capture microdissection analysis to compare expression of the candidate genes in the epidermal placodes and dermal condensates separately. One could also examine expression differences in varying regions and depths of the mesenchyme. These experiments may help to definitively determine whether the number of pre-papilla cells in the mesenchyme is the limiting factor to the number of wool follicles initiated or whether the patterning process is controlled by a more complex interaction of promoters and inhibitors of follicle initiation. Repeating the laser capture microdissection experiment on the follicle and non-follicle regions of both the midside and rump could help to explain the gene expression differences observed between these two body sites. Furthermore, by combining laser capture microdissection with mRNA amplification and microarray analysis on this sample series, a more gene discovery focused approach could be taken to determine the “first dermal signal(s)”.

The laser capture microdissection experiments were limited by the quality and orientation of the frozen OCT sections of foetal skin. Unlike formalin fixed and cover slipped sections, the frozen sections required for mRNA analysis are more fragile and show poorer contrast and resolution after staining, which made identification of the target structures difficult. Identifying and capturing follicle regions (placodes and condensates) from day 57 skin samples was first attempted but due to poor contrast from adjacent tissues, these structures could only be confidently recognised in the day 60 tissue sections. If placodes could be identified in day 53 or 57 sections, then the mesenchymal region beneath them could be microdissected and the tissue analysed using gene discovery methods (e.g. cDNA microarray analysis) to perhaps identify the first dermal signal(s). This approach could also be used to better understand how the epidermal placode signals to the mesenchyme to initiate formation of the underlying condensate. A question that could be addressed is: is a chemotactic signal released by the placodes inducing migration of the pre-papilla cells or is a proliferative signal sent to multipotent mesenchymal cells already residing beneath the basement membrane? Furthermore, by conducting a more rigorous LCM and qRT-PCT analysis of the developing follicle regions of midside and rump skin, the relationship between the differential spatial expression and the establishment of differing types of follicles, could be further explored. The results of such an investigation would be relevant to both current and on-going experiments on biological defleecing and developing alternatives to mulesing.

Laser capture microdissection is a powerful technique that has numerous applications in many tissue types. Once the target tissues are excised, DNA, RNA or proteomic analyses can be coupled with this technology to investigate the hypotheses. As new, more accurate markers are reported, and more sensitive quantitation technologies are developed, the breadth of the technology's applications will only increase.

Identification of the exact molecule(s) or at least, the specific pathways responsible for initiating the formation of wool follicles from an undifferentiated epithelium may provide the

wool industry with potential targets for nutritional or pharmaceutical intervention in order to manipulate the density of wool follicles initiated *in utero*. Although the results of the qRT-PCR experiments have demonstrated significant differences in the mRNA expression of TNF family members, it cannot be speculated that an increase in mRNA transcript levels will equate to a definitive increase in protein levels as signalling relies on a complex interaction of transcription factors, ligands and receptors. *In vivo* or *in vitro* assays that either increase or knock out the function protein products are required to assign definitive function of these mRNA transcripts in wool follicle initiation.

6.3 Conclusion

The molecular characterisation conducted herein has demonstrated that known regulators of mice and human hair follicle initiation are also expressed during wool follicle initiation in Merino sheep. Furthermore, spatial differences in expression of some of these regulators may be involved in initiating different types of follicles at specific locations on the animal. Biologically, the results of this study also demonstrate an important role for sheep in research into human hair conditions. Sheep show a high level of morphological conservation to human hair follicle development and cycling and sheep also share 85% genome sequence homology to humans. Furthermore, wool follicles are slow cycling, long anagen follicles, that are decidedly similar to human scalp follicles. The study conducted herein has also demonstrated that the TNF signalling pathway, as in mouse, rat and human, is important in wool follicle initiation and patterning. The TNF pathway expression data reported herein showed strong correlations to both the timing and fold changes reported in mouse hair follicle initiation, and are therefore, likely to reflect the same molecular signals involved in human follicle initiation. Consequently, sheep could be a more biologically relevant model of human hair initiation and disease (e.g. ectodermal dysplasia) than the currently used mice and rat models.

Appendices

Appendix I: General Solutions, Buffers and Stains

10mg/ml Ethidium Bromide Stock

100ml

Ethidium Bromide 1g

Adjust volume to 100ml with ddH₂O and store in light protected bottle at RT

Stock solution diluted 1:20,000 with MQ H₂O to a working concentration of 0.5µg/ml for agarose gel staining.

Formamide Loading Buffer (2X)

80% formamide, deionised

10mM EDTA

1mg/ml xylene cyanole

1mg/ml bromophenol blue

Routinely made at a volume of 1ml.

Glycerol Loading Buffer (10X)

10ml

Glycerol 5ml

0.2M EDTA (pH8.0) 5ml

SDS 0.01g

Bromophenol blue 0.01g

Xylene Cyanole 0.01g

Combine glycerol and EDTA and dissolve the remaining ingredients in the solution.

PBS (10X)

	1L
NaCl	80g
KCl	2g
Na ₂ HPO ₄ ·7H ₂ O	11.5g
KH ₂ PO ₄	2g

Dissolve in 500mls of MQ H₂O. Adjust to pH 8.0 and make up volume to 1L with MQ H₂O and autoclave. Dilute 1:10 with MQ H₂O to create 1X working solution.

20% Paraformaldehyde**TAE Buffer (20X)**

	1L
TRIS	96.8g
Glacial acetic acid	28.5mls
EDTA	14.6g

Dissolve in 500mls of MQ H₂O. Adjust to pH 8.0 and make up volume to 1L with MQ H₂O and autoclave. Dilute 1:20 with RO H₂O to create working solution.

1M Tris-HCl (pH 8.0)

	1L
Tris base	121.1g
HCL	42ml

Dissolve in 500mls of MQ H₂O and adjust to pH 8.0 with HCl. Adjust volume to 1L with MQ H₂O and autoclave. Store at RT. Diluted 1:1000 with nuclease free water to working concentration of 10mM.

Histology Stains and Solutions

Lillee Mayer's Haematoxylin

Haematoxylin	5g
Aluminium ammonium sulphate	50g
Glycerol	300ml
RO water	700ml
Sodium Iodate (NaIO ₃)	1g
Glacial acetic acid	20ml

Dissolve haematoxylin in a few mls of ethanol and dissolve aluminium ammonium sulphate in water with gentle heating. Combine the two solutions and add the rest of the ingredients. Filter the solution before use.

Acid Ethanol

1% (v/v) in 70% ethanol

Eosin (1% and 0.5% (LCM))

Aqueous Eosin Yellowish (1% or 0.5%)	50mls
95% ethanol	390mls
1% aqueous phloxine	5mls
Glacial Acetic Acid	2mls

Saturated Picric Acid (ethanol)

Saturation point is approximately 9% in absolute ethanol at 30°C. Best made by adding excess picric acid to absolute ethanol and stirring until no more picric acid will go into solution (i.e. granules settle at the bottom of the bottle).

Krause's Picro-Indigo Carmine

Indigo Carmine 1g
Saturated Picric Acid (aq) 300mls

Dissolve indigo carmine in the saturated picric acid.

Winiwater's SafraninStock Solution

Safrinin 10g
95% ethanol 15mls
RO H₂O 145mls

Dissolve safranin in the ethanol and combine with RO H₂O.

Working Solution

Stock Solution 25mls
50% ethanol 80mls

Filter the solution before use.

Appendix II: Primers*Table II-1_ Oligo dTVN primers for reverse transcription*

Oligo Name	Sequence 5'-3'
oligo_dAA	TTTTTTTTTTTTTTAA
oligo_dAT	TTTTTTTTTTTTTTAT
oligo_dAG	TTTTTTTTTTTTTTAG
oligo_dAC	TTTTTTTTTTTTTTAC
oligo_dCA	TTTTTTTTTTTTTTCA
oligo_dCT	TTTTTTTTTTTTTTCT
oligo_dCG	TTTTTTTTTTTTTTCG
oligo_dCC	TTTTTTTTTTTTTTCC
oligo_dGA	TTTTTTTTTTTTTTGA
oligo_dGT	TTTTTTTTTTTTTTGT
oligo_dGG	TTTTTTTTTTTTTTGG
oligo_dGC	TTTTTTTTTTTTTTGC

Table II-2_qRT-PCR Oligonucleotides

Gene	Oligo Name	Sequence 5'-3'
RAC1	Rac1_F2	GACACCATTGTCCCAACAC
	Rac1_R2	GGATCGCCTCATCAAACACT
RHOa	RhoA_F2	CGAAACGACGAGCACACa
	RhoA_R2	CAAAAACCTCCCTCACTCCA
PCNA	PCNAF3	CTGCAAGTGGAGAACTTGGA
	PCNAR2	CCTCAGTGCAAAAGTTAGCTG
CYCB1	CyclinB1_F2	CTTTCCCCCGAGCCTATTT
	CyclinB1_R2	TTGGTTTGACTGCTTGCTCTT
β1-Integrin	IntegB1_F4	CGAGTGTGGTGCCTGTAAGTG
	IntegB1_R4	AGTCGTCAACGTCCTTCTCCTT
ALP	AlkPhosF6	CCCCCGTGGCAACTCTAT
	AlkPhosR6	TCACCACCCACCACCTTGTA
EDA	Eda-A1_F3	AAGCTGGAACCTCGAGAAAAC
	Eda-A1_R2	ATGCGAGACCAGTCATTGAG
EDAR	EDARfwd5	CGAGAAGGACGAATTCGAGA
	EDARrev6	GCAGCTGCTCCTTCTCTGAT
EDARADD	EDARADDfwd4	CAGGGAGAAGAAAATGGCTTT
	EDARADDrev4	CGGATCCAGCTTTATCCTGA
TROY	TNF19fwd1	GAGTGTGTGCCTTGTGGAGA
	TNF19rev2	ATCCTCACCAGGTTGACCTT
XEDAR	TNF27fwd2	TGGATTGCCAAGAAAATGAGT
	TNF27rev1	CTCCACCCTCTCCATAACCA
TRAF-6	Traf6fwd1	TGCAATACCATGCTCATCAGA
	Traf6rev1	GGCAACCAAAAAGCACTGAA
KRT5	Krt5F3	CAGGAGCTGATGAACACCAA
	Krt5R3	TCCAACCTCCTTCTCCACTCA
COL11A1	CollF3	TGATGGGGTCAAATGAAGGT
	CollR2	CCCATTCCCAGTGTGTTT
In house qRT-PCR reference gene primers		
RPL19	ovRPL19F1	CAACTCCCGCCAGCAGAT
	ovRPL19R1	CCGGGAATGGACAGTCACA
GAPDH	ovGAPDHF1	ATGCCTCCTGCACCACCA
	ovGAPDHF1	AGTCCCTCCACGATGCCAA

References

- Adelson, D. L., Hollis, D. E., and Brown, G. H. (2002). Wool fibre diameter and follicle density are not specified simultaneously during wool follicle initiation. *Australian Journal of Agricultural Research* **53**, 1003-1009.
- Adelson, D. L., Hollis, D. E., Merchant, J. C., and Kelley, B. A. (1997). In vivo effects of epidermal growth factor on epidermal pattern formation and hair follicle initiation in the marsupial bandicoot *Isodon macrourus*. *Reprod Fertil Dev* **9**, 493-500.
- Adolphe, C., Narang, M., Ellis, T., Wicking, C., Kaur, P., and Wainwright, B. (2004). An in vivo comparative study of sonic, desert and Indian hedgehog reveals that hedgehog pathway activity regulates epidermal stem cell homeostasis. *Development* **131**, 5009-19.
- Agar, N. S., Halliday, G. M., Barnetson, R. S., and Jones, A. M. (2003). A novel technique for the examination of skin biopsies by laser capture microdissection. *J Cutan Pathol* **30**, 265-70.
- Alibardi, L. (2004). Comparative aspects of the inner root sheath in adult and developing hairs of mammals in relation to the evolution of hairs. *J Anat* **205**, 179-200.
- Alonso, L., and Fuchs, E. (2003a). Stem cells in the skin: waste not, wnt not. *Genes and Development* **17**, 1189-1200.
- Alonso, L., and Fuchs, E. (2003b). Stem cells of the skin epithelium. *PNAS* **100**, 11830-11835.
- Andl, T., Reddy, S. T., Gaddapara, T., and Millar, S. E. (2002). WNT signals are required for the initiation of hair follicle development. *Dev Cell* **2**, 643-53.

References

- Athar, M., Tang, X., Lee, J. L., Kopelovich, L., and Kim, A. L. (2006). Hedgehog signalling in skin development and cancer. *Experimental Dermatology* **15**, 667-677.
- Austin, C. R. (1972). "1 Germ Cells and Fertilization," 1st/Ed. Cambridge University Press, Cambridge.
- Bailly, E., Pines, J., Hunter, T., and Bornens, M. (1992). Cytoplasmic accumulation of cyclin B1 in human cells: association with a detergent-resistant compartment and with the centrosome. *J Cell Sci* **101 (Pt 3)**, 529-45.
- Barton, S. A., Purvis, I. W., and Brewer, H. G. (2001). Are wool follicle characteristics associated with wool quality and production in hogget and adult sheep? *Proceedings of the Australian Association of Animal Breeding and Genetics* **14**, 289-291.
- Bianco, P., and Boyde, A. (1993). Confocal images of marrow stromal (Westen-Bainton) cell. *Histochemistry* **100**, 93.
- Blanpain, C., and Fuchs, E. (2006). Epidermal stem cells of the skin. *Annu Rev Cell Dev Biol* **22**, 339-73.
- Bloom, W., and Fawcett, D. W. (1962). The Skin. In "A Textbook of Histology", pp. 372-391. W.B. Saunders Company, London.
- Botchkarev, V. A., Botchkareva, N. V., Roth, W., Nakamura, M., Chen, L. H., Herzog, W., Lindner, G., McMahon, J. A., Peters, C., and Lauster, R. (1999). Noggin is a mesenchymal derived stimulator of hair follicle induction. *Nature Cell Biology* **1**.
- Botchkarev, V. A., Botchkareva, N. V., Sharov, A. A., Funa, K., Huber, O., and Gilchrist, B. A. (2002). Modulation of BMP signaling by noggin is required for induction of the secondary (nontylotrich) hair follicles. *J Invest Dermatol* **118**, 3-10.

- Botchkarev, V. A., and Fessing, M. Y. (2005). Edar Signalling in the Control of Hair Follicle Development. *Journal of Investigative Dermatology Symposium Proceedings* **10**, 247-251.
- Botchkarev, V. A., and Paus, R. (2003). Molecular biology of hair morphogenesis: Development and cycling. *Development and Cycling* **298B**, 164-180.
- Bray, M. (1997). The Location of Stem Cell Population in the Hair and Wool Follicles. Honours, University of Adelaide, Adelaide.
- Brouard, M., and Barrandon, Y. (2003). Controlling skin morphogenesis: hope and despair. *Current Opinions in Biotechnology* **14**, 520-525.
- Brunner, A. M., Yakovlev, I. A., and Strauss, S. H. (2004). Validating internal controls for quantitative plant gene expression studies. *BMC Plant Biol* **4**, 14.
- Bryden, M. M., Evans, H. E., and Binns, W. (1972). Embryology of the Sheep I: Extraembryonic Membranes and the Development of Body Form. *Journal of Morphology* **138**, 169-186.
- Bullock, T. E., Wen, B., Marley, S. B., and Gordon, M. Y. (2007). Potential of CD34 in the regulation of symmetrical and asymmetrical divisions by hematopoietic progenitor cells. *Stem Cells* **25**, 844-51.
- Bumcrot, D. A., and McMahon, A. P. (1996). Sonic hedgehog: making the gradient. *Chem Biol* **3**, 13-6.
- Bustin, S. A. (2000). Absolute quantification of mRNA using real-time reverse transcription polymerase chain reaction assays. *J Mol Endocrinol* **25**, 169-93.

- Bustin, S. A. (2002). Quantification of mRNA using real-time reverse transcription PCR (RT-PCR): trends and problems. *J Mol Endocrinol* **29**, 23-39.
- Castilho, R. M., Squarize, C. H., Patel, V., Millar, S. E., Zheng, Y., Molinolo, A., and Gutkind, J. S. (2007). Requirement of Rac1 distinguishes follicular from interfollicular epithelial stem cells. *Oncogene* **26**, 5078-85.
- Chiang, C., Swan, R. Z., Grachtchouk, M., Bolinger, M., Litingtung, Y., Robertson, E. K., Cooper, M. K., Gaffield, W., Westphal, H., Beachy, P. A., and Dlugosz, A. A. (1999). Essential role for Sonic hedgehog during hair follicle morphogenesis. *Dev Biol* **205**, 1-9.
- Chuong, C. M., Patel, N., Lin, J., Jung, H. S., and Widelitz, R. B. (2000). Sonic hedgehog signaling pathway in vertebrate epithelial appendage morphogenesis: perspectives in development and evolution. *Cell Mol Life Sci* **57**, 1672-81.
- Chuong, C. M., Widelitz, R. B., Ting-Berreth, S., and Jiang, T. X. (1996). Early events during avian skin appendage regeneration: dependence on epithelial-mesenchymal interaction and order of molecular reappearance. *J Invest Dermatol* **107**, 639-646.
- Coelho, C. M., and Zucoloto, S. (1999). Proliferative activity of denture-induced fibrous inflammatory hyperplasia analyzed by proliferating cell nuclear antigen labeling index. *Int J Prosthodont* **12**, 73-7.
- Cognie, Y. (1990). Current Technologies for Synchronisation and Artificial Insemination of Sheep. In "Reproductive Physiology of Merino Sheep" (C. M. Oldham, G. B. Martin and I. W. Purvis, eds.), pp. 207-216. University of Western Australia, Perth.

- Corbett, J. L. (1979). Variation in wool growth with physiological state. *In* "Physiological and environmental limitations to wool growth" (J. L. Black and P. J. Reis, eds.), pp. 79-95. University of New England, Lueria, NSW.
- Cotsarelis, G. (2006a). Epithelial Stem Cells: A Folliculocentric View. *Journal of Investigative Dermatology* **126**, 1459-1468.
- Cotsarelis, G. (2006b). Gene expression profiling gets to the root of human hair follicle stem cells. *J Clin Invest* **116**, 19-22.
- Cottle, D. J. (1991). Sheep Breeds. *In* "Australian Sheep and Wool Handbook" (D. J. Cottle, ed.), pp. 54-61. Inkata Press, Melbourne, Australia.
- Craven, A. J., Ashby, M.G, Scobie, D. R., and Nixon, A. J. (2007a). Variation of wool characteristics across the body of New Zealand Wiltshire sheep. *Proceedings of the New Zealand Society of Animal Production* **67**, 339-344.
- Craven, A. J., Rufaut, N. W., Scobie, D. R., and Nixon, A. J. (2007b). Expression of the developmental regulators Msx1 and Msx2 in sheep skin varies with body region and wool growth pattern. *Proceedings of the New Zealand Society of Animal Production* **67**.
- Dahmane, N., Lee, J., Robins, P., Heller, P., and Ruiz i Altaba, A. (1997). Activation of the transcription factor Gli1 and the Sonic hedgehog signalling pathway in skin tumours. *Nature* **389**, 876-81.
- DasGupta, R., and Fuchs, E. (1999). Multiple roles for activated LEF/TCF transcription complexes during hair follicle development and differentiation. *Development* **126**, 4557-4568.

References

- Deans, R. J., and Moseley, A. B. (2000). Mesenchymal stem cells: Biology and potential clinical uses. *Experimental Hematology* **28**, 875-884.
- Denning, K. M., Smyth, P. C., Cahill, S. F., Finn, S. P., Conlon, E., Li, J., Flavin, R. J., Aherne, S. T., Guenther, S. M., Ferlinz, A., O'Leary, J. J., and Sheils, O. M. (2007). A molecular expression signature distinguishing follicular lesions in thyroid carcinoma using preamplification RT-PCR in archival samples. *Mod Pathol* **20**, 1095-102.
- Domen, J., and Weissman, I. L. (1999). Self renewal, differentiation or death: Regulation and manipulation of hematopoietic stem cell fate. *Molecular Medicine Today* **5**, 201-208.
- Drew, C. F., Lin, C. M., Jiang, T. X., Blunt, G., Mou, C., Chuong, C. M., and Headon, D. J. (2007). The Edar subfamily in feather placode formation. *Dev Biol* **305**, 232-45.
- Edwards, N. M., Hebart, M., and Hynd, P. I. (2009). Phenotypic and genotypic analysis of a barebrech trait in Merino sheep as a potential replacement for surgical mulesing. *Journal of Animal Production Science* **49**, 56-64.
- Ellis, T., Smyth, I., Riley, E., Bowles, J., Adolphe, C., Rothnagel, J. A., Wicking, C., and Wainwright, B. J. (2003). Overexpression of sonic hedgehog suppresses embryonic hair follicle morphogenesis. *Developmental Biology* **263**, 203-215.
- Emmert-Buck, E. R., Bonner, R. F., Smith, P. D., Chauqui, R. F., Zhuang, Z., Goldstein, S. R., Weiss, R. A., and Liotta, L. A. (1996). Laser Capture Microdissection. *Science* **274**, 998-1001.
- Evans, M. J., and Kaufmann, M. (1981). Establishment of pluripotential cells from mouse embryos. *Nature* **292**, 154-156.

- Evans, T., Rosenthal, E. T., Youngbloom, J., Distal, D., and Hunt, T. (1983). Cyclin: A protein specified by maternal mRNA in sea urchin eggs that is destroyed at each cleavage division. *Cell* **33**, 389-396.
- Ferguson, B. M., Brockdorff, N., Formstone, E., Ngyuen, T., Kronmiller, J. E., and Zonana, J. (1997). Cloning of Tabby, the murine homolog of the human EDA gene: evidence for a membrane-associated protein with a short collagenous domain. *Hum Mol Genet* **6**, 1589-94.
- Fleige, S., Walf, V., Huch, S., Prgomet, C., Sehm, J., and Pfaffl, M. W. (2006). Comparison of relative mRNA quantification models and the impact of RNA integrity in quantitative real-time RT-PCR. *Biotechnol Lett* **28**, 1601-13.
- Foitzik, K., Paus, R., Doetschman, T., and Dotto, G. P. (1999). The TGF-beta2 isoform is both a required and sufficient inducer of murine hair follicle morphogenesis. *Dev Biol* **212**, 278-289.
- Fraser, A. S. (1954). Development of the skin follicle population in merino sheep. *Australian Journal of Agricultural Research* **5**, 737-744.
- Gaide, O., and Schneider, P. (2003). Permanent correction of an inherited ectodermal dysplasia with recombinant EDA. *Nat Med* **9**, 614-8.
- Gambardella, L., and Barrandon, Y. (2003). The multifaceted adult epidermal stem cell. *Current Opinions in Biotechnology* **15**, 771-777.
- Garcia-Crespo, D., Juste, R. A., and Hurtado, A. (2005). Selection of ovine housekeeping genes for normalisation by real-time RT-PCR; analysis of PrP gene expression and genetic susceptibility to scrapie. *BMC Vet Res* **1**, 3.

References

- Gharzi, A., Reynolds, A. J., and Jahoda, C. A. B. (2003). Plasticity of hair follicle dermal cells in wound healing and induction. *Experimental Dermatology* **12**, 126-136.
- Ginsberg, S. D. (2005). RNA amplification strategies for small sample populations. *Methods* **37**, 229-37.
- Goldsworthy, S. M., Stockton, P. S., Trempus, C. S., Foley, J. F., and Maronpot, R. R. (1999). Effects of fixation on RNA extraction and amplification from laser capture microdissected tissue. *Mol Carcinog* **25**, 86-91.
- Greeff, J. C., Lewer, R. P., Ponzoni, R. W., and Purvis, I. W. (1995). Staple Strength:Progress Towards Elucidating Its Place in Merino Breeding. *Proceedings of the Australian Association of Animal Breeding and Genetics* **11**, 595-302.
- Grubor, B., Gallup, J. M., Ramirez-Romero, R., Bailey, T. B., Crouch, E. C., Brogden, K. A., and Ackermann, M. R. (2004). Surfactant protein D expression in normal and pneumonic ovine lung. *Vet Immunol Immunopathol* **101**, 235-42.
- Gwatkin (1977). "Fertilization Mechanisms in Man and Mammals," Plenum Press, New York.
- Hall, A. (1998). Rho GTPases and the actin cytoskeleton. *Science* **279**, 509-14.
- Handjiski, B. K., Eichmuller, S., Hofmann, U., Czarnetzki, B. M., and Paus, R. (1994). Alkaline phosphatase activity and localization during the murine hair cycle. *Br J Dermatol* **131**, 303-10.
- Hardy, M. (1992). The secret life of the hair follicle. *Trends in Genetics* **8**, 55-60.
- Hardy, M. H., and Lyne, A. G. (1956). Pre-natal development of wool follicles in Merino sheep. *Australian Journal of Biological Science* **9**, 423-441.

- Hashimoto, T., Cui, C. Y., and Schlessinger, D. (2006). Repertoire of mouse ectodysplasin-A (EDA-A) isoforms. *Gene* **371**, 42-51.
- Hashimoto, T., Schlessinger, D., and Cui, C. Y. (2008). Troy binding to lymphotoxin-alpha activates NF kappa B mediated transcription. *Cell Cycle* **7**, 106-11.
- Headon, D. J., Emmal, S. A., Ferguson, B. M., Tucker, A. S., Justice, M. J., Sharpe, P. T., Zonana, J., and Overbeek, P. A. (2001). Gene defect in ectodermal dysplasia implicates a death domain adapter in development. *Nature* **414**, 913-6.
- Headon, D. J., and Overbeek, P. A. (1999). Involvement of a novel Tnf receptor homologue in hair follicle induction. *Nat Genet* **22**, 370-4.
- Hebart, M., Penno, N., and Hynd, P. I. (2006). Undersanding the bare breech phenotype. *In* "8th World Congress of Genetics Applied to Livestock", Brazil.
- Hein, W. R., Barber, T., Cole, S. A., Morrison, L., and Pernthaner, A. (2004). Long-term collection and characterization of afferent lymph from the ovine small intestine. *J Immunol Methods* **293**, 153-68.
- Higuchi, R., Fockler, C., Dollinger, G., and Watson, R. (1993). Kinetic PCR analysis: real-time monitoring of DNA amplification reactions. *Biotechnology (N Y)* **11**, 1026-30.
- Hocking Edwards, J. E. (1999). Reduction in wool follicles prior to birth in Merino sheep. *Reproductive and Fertility Development* **11**, 229-234.
- Hocking Edwards, J. E., Birtles, M. J., Harris, M. J., Parry, A., Paterson, E., Wickham, G. A., and McCutcheon, S. N. (1996). Pre- and post-natal wool follicle development and density in sheep of five genotypes. *Journal of Agricultural Science (Camb.)* **126**, 363-370.

References

- Houghton, L., Lindon, C., and Morgan, B. A. (2005). The ectodysplasin pathway in feather tract development. *Development* **132**, 863-72.
- Huggett, J., Dheda, K., Bustin, S., and Zumla, A. (2005). Real-time RT-PCR normalisation; strategies and considerations. *Genes Immun* **6**, 279-84.
- Hwang, A., Maity, A., McKenna, W. G., and Muschel, R. J. (1995). Cell cycle-dependent regulation of the cyclin B1 promoter. *J Biol Chem* **270**, 28419-24.
- Hynd, P. I. (1995). Skin and Follicle-Based Selection for Wool Production and Quality. *Wool Technology and Sheep Breeding* **43**, 15-23.
- Hynd, P. I., and Masters, D. G. (2002). Nutrition and Wool Growth. In "Sheep Nutrition" (M. Freer and H. Dove, eds.), pp. 165-189. CSIRO Publishing, Melbourne, Australia.
- Hynes, R. O. (1987). Integrins: A Family of Cell Surface Receptors. *Cell* **48**, 549-554.
- Iavarone, M., Trabut, J. B., Delpuech, O., Carnot, F., Colombo, M., Kremendorf, D., Brechot, C., and Thiers, V. (2003). Characterisation of hepatitis B virus X protein mutants in tumour and non-tumour liver cells using laser capture microdissection. *J Hepatol* **39**, 253-61.
- Iida, M., Ihara, S., and Matsuzaki, T. (2007). Hair cycle-dependent changes of alkaline phosphatase activity in the mesenchyme and epithelium in mouse vibrissal follicles. *Dev Growth Differ* **49**, 185-95.
- Iseki, S., Araga, A., Ohuchi, H., Nohno, T., Yoshioka, H., Hayashi, F., and Noji, S. (1996). Sonic hedgehog is expressed in epithelial cells during development of whisker, hair, and tooth. *Biochem Biophys Res Commun* **218**, 688-93.

- Jahoda, C. A. B. (2003). Cell movement in the hair follicle dermis-More than a two-way street? *Journal of Investigative Dermatology* **121**, ix-xi.
- Jahoda, C. A. B., and Reynolds, A. J. (2001). Hair follicle dermal sheath cells: unsung participants in wound healing. *LANCET* **358**, 1445-1448.
- Jahoda, C. A. B., Whitehouse, C. J., Reynolds, A. J., and Hole, N. (2003). Hair follicle dermal cells differentiate into adipogenic and osteogenic lineages. *Experimental Dermatology* **12**, 849-859.
- Jensen, U. B., Lowell, S., and Watt, F. (1999). The spatial relationship between stem cells and their progeny in the basal layer of human epidermis: a new view based on whole-mount labelling and lineage analysis. *Development* **126**, 2409-2418.
- Jiang, H., Sha, S. H., and Schacht, J. (2006). Rac/Rho pathway regulates actin depolymerization induced by aminoglycoside antibiotics. *J Neurosci Res* **83**, 1544-51.
- Jiang, T. X., Jung, H. S., Widelitz, R. B., and Chuong, C. M. (1999). Self-organization of periodic patterns by dissociated feather mesenchymal cells and the regulation of size, number and spacing of primordia. *Development* **126**, 4997-5009.
- Johnson, D. G., and Walker, C. L. (1999). Cyclins and cell cycle checkpoints. *Annu Rev Pharmacol Toxicol* **39**, 295-312.
- Jones, P. H., Harper, S., and Watt, F. (1995). Stem cell patterning in the human epidermis. *Cell* **80**, 83-93.
- Joubert, D. M. (1956). A study of pre-natal growth and development in the sheep. *Journal of Agricultural Science* **47**, 382-427.

- Jung, H. S., Oropeza, V., and Thesleff, I. (1999). Shh, Bmp-2, Bmp-4 and Fgf-8 are associated with initiation and patterning of mouse tongue papillae. *Mech Dev* **81**, 179-82.
- Jung, M., Ramankulov, A., Roigas, J., Johannsen, M., Ringsdorf, M., Kristiansen, G., and Jung, K. (2007). In search of suitable reference genes for gene expression studies of human renal cell carcinoma by real-time PCR. *BMC Mol Biol* **8**, 47.
- Junqueira, L. C. U., Carneiro, J., and Kelley, R. O. (1998). "Basic histology," 9th/Ed. Appleton & Lange, Stamford, Conn.
- Kakino, S., Sasaki, K., Kurose, A., and Ito, H. (1996). Intracellular localization of cyclin B1 during the cell cycle in glioma cells. *Cytometry* **24**, 49-54.
- Kasai, T., Shimajiri, S., and Hashimoto, H. (2000). Detection of SYT-SSX fusion transcripts in both epithelial and spindle cell areas of biphasic synovial sarcoma using laser capture microdissection. *Mol Pathol* **53**, 107-10.
- Kelly, R. W., and Newnham, J. P. (1989). Estimation of Gestational Age in Merino Ewes by Ultrasound Measurement of Fetal Head Size. *Australian Journal of Agricultural Research* **40**, 1293-1299.
- Kim, D. S., Cho, H. J., Choi, H. R., Kwon, S. B., and Park, K. C. (2004). Isolation of human epidermal stem cells by adherence and the reconstruction of skin equivalents. *Cell Mol Life Sci* **61**, 2774-81.
- King, C., Guo, N., Frampton, G. M., Gerry, N. P., Lenburg, M. E., and Rosenberg, C. L. (2005). Reliability and reproducibility of gene expression measurements using amplified RNA from laser-microdissected primary breast tissue with oligonucleotide arrays. *J Mol Diagn* **7**, 57-64.

- Kollar, E. J. (1970). The induction of hair follicles by embryonic dermal papillae. *J Invest Dermatol* **55**, 374-8.
- Korgun, E. T., Celik-Ozenci, C., Acar, N., Cayli, S., Desoye, G., and Demir, R. (2006). Location of cell cycle regulators cyclin B1, cyclin A, PCNA, Ki67 and cell cycle inhibitors p21, p27 and p57 in human first trimester placenta and deciduas. *Histochem Cell Biol* **125**, 615-24.
- Kratochwil, K., Dull, M., Farinas, I., Galceran, J., and Grosschedl, R. (1996). Lef-1 expression is activated by BMP-4 and regulates inductive tissue interactions in tooth and hair development. *Genes and Development* **10**, 1382-1394.
- Lajtha, L. G. (1979). Stem cell concepts. *Differentiation* **14**, 23-34.
- Lako, M., Armstrong, L., Cairns, P. M., Harris, S., Hole, N., and Jahoda, C. A. B. (2002). Hair follicle dermal cells repopulate the mouse haematopoietic system. *Journal of Cell Science* **115**, 3967-3974.
- Laud, K., Hornez, L., Gourdou, I., Belair, L., Arnold, A., Peyrat, J. P., and Djiane, J. (2001). Expression of BRCA1 gene in ewe mammary epithelial cells during pregnancy: regulation by growth hormone and steroid hormones. *Eur J Endocrinol* **145**, 763-70.
- Laurikkala, J., Pispala, J., Jung, H. S., Nieminen, P., Mikkola, M., Wang, X., Saarialho-Kere, U., Galceran, J., Grosschedl, R., and Thesleff, I. (2002). Regulation of hair follicle development by the TNF signal ectodysplasin and its receptor Edar. *Development* **129**, 2541-53.
- Lavker, R. M., Sun, T. T., Oshima, H., Barrandon, Y., Akiyama, M., Ferraris, C., Chevalier, G., Favier, B., Jahoda, C. A. B., Dhouailly, D., Panteleyev, A. A., and Christiano, A.

- M. (2003). Hair Follicle Stem Cells. *Journal of Investigative Dermatology Symposium Proceedings* **8**, 28-38.
- Le Borgne, R., and Schweisguth, F. (2003). Unequal segregation of neutralized biases notch activation during asymmetric cell division. *Dev Cell* **5**, 139-148.
- Lehmann, U., Glockner, S., Kleeberger, W., von Wasielewski, H. F., and Kreipe, H. (2000). Detection of gene amplification in archival breast cancer specimens by laser-assisted microdissection and quantitative real-time polymerase chain reaction. *Am J Pathol* **156**, 1855-64.
- Leung, A. Y., Leung, J. C., Chan, L. Y., Ma, E. S., Kwan, T. T., Lai, K. N., Meng, A., and Liang, R. (2005). Proliferating cell nuclear antigen (PCNA) as a proliferative marker during embryonic and adult zebrafish hematopoiesis. *Histochem Cell Biol* **124**, 105-11.
- Li, Y., Li, T., Liu, S., Qiu, M., Han, Z., Jiang, Z., Li, R., Ying, K., Xie, Y., and Mao, Y. (2004). Systematic comparison of the fidelity of aRNA, mRNA and T-RNA on gene expression profiling using cDNA microarray. *J Biotechnol* **107**, 19-28.
- Libus, J., and Storchova, H. (2006). Quantification of cDNA generated by reverse transcription of total RNA provides a simple alternative tool for quantitative RT-PCR normalization. *Biotechniques* **41**, 156, 158, 160 passim.
- Limat, A., Breitkreutz, D., Thiekoetter, G., Klein, C. E., Braathen, L. R., Hunziker, T., and Fusenig, N. E. (1995). Formation of a regular neo-epidermis by cultured human outer root sheath cells grafted on nude mice. *Transplantation* **59**, 1032-8.

- Luo, L., Salunga, R. C., Guo, H., Bittner, A., Joy, K. C., Galindo, J. E., Xiao, H., Rogers, K. E., Wan, J. S., Jackson, M. R., and Erlander, M. G. (1999). Gene expression profiles of laser-captured adjacent neuronal subtypes. *Nat Med* **5**, 117-22.
- Lyne, A. G. (1964). Effect of adverse nutrition on the skin and wool follicles in Merino sheep. *Australian Journal of Agricultural Research* **15**, 788-801.
- Lyon, M. F., Rastan, S., and Brown, S. D. M. (1996). "Genetic Variants and Strains of the Laboratory Mouse," 3rd/Ed. Oxford University Press, Oxford.
- Ma, D. R., Yang, E. N., and Lee, S. T. (2004). A review: the location, molecular characterisation and multipotency of hair follicle epidermal stem cells. *Ann Acad Med Singapore* **33**, 784-8.
- Maity, A., McKenna, W. G., and Muschel, R. J. (1995). Evidence for post-transcriptional regulation of cyclin B1 mRNA in the cell cycle and following irradiation in HeLa cells. *Embo J* **14**, 603-9.
- Marigo, V., Laufer, E., Nelson, C. E., Riddle, R. D., Johnson, R. L., and Tabin, C. (1996). Sonic hedgehog regulates patterning in early embryos. *Biochem Soc Symp* **62**, 51-60.
- Maxwell, W. M. C., Szell, A., Hunton, J. R., and Ryan, J. P. (1990). Artificial Breeding: Embryo Transfer and Cloning. In "Reproductive Physiology of Merino Sheep" (C. M. Oldham, G. B. Martin and I. W. Purvis, eds.), pp. 217-237. The University of Western Australia, Perth.
- McDonald, B. J., O'Rourke, P. K., Connell, J. A., and Hoey, W. A. (1988). Prenatal Growth and Estimation of Fetal Age in the Australian Feral Goat. *Australian Journal of Agricultural Research* **39**, 729-734.

- McElwee, K. J., Kissling, S., Wenzel, E., Huth, A., and Hoffmann, R. (2003). Cultured peribulbar dermal sheath cells can induce hair follicle development and contribute to the dermal sheath and dermal papilla. *J Invest Dermatol* **121**, 1267-75.
- Michno, K., Boras-Granic, K., Mill, P., Hui, C. C., and Hamel, P. A. (2003). Shh expression is required for embryonic hair follicle but not mammary gland development. *Dev Biol* **264**, 153-65.
- Millar, S. E. (2002). Molecular mechanisms controlling hair follicle development. *Journal of Investigative Dermatology* **118**, 216-225.
- Mills, A. A., Zheng, B., Wang, X. J., Vogel, H., Roop, D. R., and Bradley, A. (1999). p63 is a p53 homologue required for limb and epidermal morphogenesis. *Nature* **398**, 708-713.
- Montagna, W. (1962). "Eccrine sweat glands and eccrine sweating," Pergamon, Oxford.
- Montagna, W., and Parakkal, P. F. (1974). "The structure and function of skin," Academic Press, New York.
- Moore, A. G., and Moore, G. P. M. (2001). Extracellular matrix molecules and follicle morphogenesis in ovine skin. *Reproductive and Fertility Development* **13**, 143-149.
- Moore, G. P., Jackson, N., Isaacs, K., and Brown, G. (1998). Pattern and morphogenesis in skin. *J Theor Biol* **191**, 87-94.
- Morgan, B. A., Orkin, R. W., Noramly, S., and Perez, A. (1998). Stage-specific effects of sonic hedgehog expression in the epidermis. *Dev Biol* **201**, 1-12.
- Mou, C., Jackson, B., Schneider, P., Overbeek, P. A., and Headon, D. J. (2006). Generation of the primary hair follicle pattern. *Proc Natl Acad Sci U S A* **103**, 9075-80.

- Munoz, F., Lestringant, G., Sybert, V., Frydman, M., Alswaini, A., Frossard, P. M., Jorgenson, R., and Zonana, J. (1997). Definitive evidence for an autosomal recessive form of hypohidrotic ectodermal dysplasia clinically indistinguishable from the more common X-linked disorder. *Am J Hum Genet* **61**, 94-100.
- Murray, A. W. (2004). Recycling the cell cycle: cyclins revisited. *Cell* **116**, 221-34.
- Mustonen, T., Limonen, M., Pummila, M., Kangas, A. T., Laurikkala, J., Jaatinen, R., Pispä, J., Gaide, O., Schneider, P., Thesleff, I., and Mikkola, M. L. (2004). Ectodysplasin A1 promotes placodal cell fate during early morphogenesis of ectodermal appendages. *Development* **131**, 4907-4919.
- Nagorcka, B. N. (1983). Evidence for a reaction-diffusion system as a mechanism controlling mammalian hair growth. *Biosystems* **16**, 323-32.
- Nagorcka, B. N., and Mooney, J. R. (1985). The role of a reaction-diffusion system in the initiation of primary hair follicles. *J Theor Biol* **114**, 243-72.
- Nagorcka, B. N., and Mooney, J. R. (1992). From stripes to spots: prepatterns which can be produced in the skin by a reaction-diffusion system. *IMA J Math Appl Med Biol* **9**, 249-67.
- Naito, A., Yoshida, H., Nishioka, E., Satoh, M., Azuma, S., Yamamoto, T., Nishikawa, S., and Inoue, J. (2002). TRAF6-deficient mice display hypohidrotic ectodermal dysplasia. *Proc Natl Acad Sci U S A* **99**, 8766-71.
- Narhi, K., Jarvinen, E., Birchmeier, W., Taketo, M. M., Mikkola, M. L., and Thesleff, I. (2008). Sustained epithelial beta-catenin activity induces precocious hair development but disrupts hair follicle down-growth and hair shaft formation. *Development* **135**, 1019-28.

- Newton, K., French, D. M., Yan, M., Frantz, G. D., and Dixit, V. M. (2004). Myodegeneration in EDA-A2 transgenic mice is prevented by XEDAR deficiency. *Mol Cell Biol* **24**, 1608-13.
- Nieuwenhuisa, E., Barnfielda, P. C., Makinoa, S., and Hui, C. (1997). Epidermal hyperplasia and expansion of the interfollicular stem cell compartment in mutant mice with a C-terminal truncation of Patched1. *Developmental Biology* **308**, 547-560.
- Nixon, A. J. (1993). A Method for Determining the Activity State of Hair Follicles. *Biotechnic and Histochemistry* **68**, 316-325.
- Nolan, T., Hands, R. E., and Bustin, S. A. (2006). Quantification of mRNA using real-time RT-PCR. *Nat Protoc* **1**, 1559-82.
- Noramly, S., Freeman, A., and Morgan, B. A. (1999). Beta-catenin signaling can initiate feather bud development. *Development* **126**, 3509-3521.
- Ohyama, M., Terunuma, A., Tock, C. L., Radonovich, M. F., Pise-Masison, C. A., Hopping, S. B., Brady, J. N., Udey, M. C., and Vogel, J. C. (2006). Characterization and isolation of stem cell-enriched human hair follicle bulge cells. *J Clin Invest* **116**, 249-60.
- Pantaloni, D., Le Clainche, C., and Carlier, M. F. (2001). Mechanism of actin-based motility. *Science* **292**, 1502-6.
- Paus, R. (1998). Principles of hair cycle control. *J Dermatol* **25**, 793-802.
- Paus, R., Muller-Rover, S., Van Der Veen, C., Maurer, M., Eichmuller, S., Ling, G., Hofmann, U., Foitzik, K., Mecklenburg, L., and Handjiski, B. (1999). A

- comprehensive guide for the recognition and classification of distinct stages of hair follicle morphogenesis. *J Invest Dermatol* **113**, 523-32.
- Peirson, S. N., Butler, J. N., and Foster, R. G. (2003). Experimental validation of novel and conventional approaches to quantitative real-time PCR data analysis. *Nucleic Acids Res* **31**, e73.
- Pera, M. F., Reubinoff, B., and Trounson, A. (2000). Human Embryonic Stem Cells. *Journal of Cell Science* **113**, 5-10.
- Perlmutter, M. A., Best, C. J., Gillespie, J. W., Gathright, Y., Gonzalez, S., Velasco, A., Linehan, W. M., Emmert-Buck, M. R., and Chuaqui, R. F. (2004). Comparison of snap freezing versus ethanol fixation for gene expression profiling of tissue specimens. *J Mol Diagn* **6**, 371-7.
- Phillips, J., and Eberwine, J. H. (1996). Antisense RNA Amplification: A Linear Amplification Method for Analyzing the mRNA Population from Single Living Cells. *Methods* **10**, 283-8.
- Pons, S., and Marti, E. (2000). Sonic hedgehog synergizes with the extracellular matrix protein vitronectin to induce spinal motor neuron differentiation. *Development* **127**, 333-42.
- Powell, B. C., Passmore, E. A., Nesci, A., and Dunn, S. M. (1998). The notch signalling pathway in hair growth. *Mechanisms of Development* **78**, 189-192.
- Powell, B. C., and Rodgers, G. E. (1997). The role of keratin proteins and their genes in the growth, structure and properties of hair. In "Formation and structure of human hair" (P. Jolles, H. Zahn and H. Hooker, eds.), pp. 59-148. Birkhauser Verlag Basel, Basel.

- Powell, B. C., and Rogers, G. E. (1994). Differentiation in hard keratin tissues: hair and related structures. *In* "The keratinocyte handbook" (I. Leigh, B. Land and F. Watt, eds.), pp. 401-436. Cambridge University Press, New York.
- Prum, R. O., and Williamson, S. (2002). Reaction-diffusion models of within-feather pigmentation patterning. *Proc Biol Sci* **269**, 781-92.
- Purvis, I. W., and Swan, A. A. (1997). Can follicle density be used to enhance the rate of genetic improvement in Merino flocks? *Proceedings of the Australian Association of Animal Breeding and Genetics* **12**, 512-515.
- Raghavan, S., Bauer, C., Mundschau, G., Li, Q., and Fuchs, E. (2000). Conditional ablation of beta1 integrin in skin. Severe defects in epidermal proliferation, basement membrane formation, and hair follicle invagination. *J Cell Biol* **150**, 1149-60.
- Randonic, A., Thulke, S., Mackay, I., Landt, O., Siegert, W., and Nitsche, A. (2004). Guideline for reference gene selection for quantitative real-time PCR. *Biomedical and Biophysical Research Communications* **313**, 856-862.
- Ray, R. M., McCormack, S. A., Covington, C., Viar, M. J., Zheng, Y., and Johnson, L. R. (2003). The requirement for polyamines for intestinal epithelial cell migration is mediated through Rac1. *J Biol Chem* **278**, 13039-46.
- Reddy, S., Andl, T., Bagasra, A., Lu, M. M., Epstein, D. J., Morrisey, E. E., and Millar, S. E. (2001). Characterisation of *Wnt* gene expression in developing and postnatal hair follicles and identification of *Wnt5a* as a target of Sonic Hedgehog in hair follicle morphogenesis. *Mechanisms of Development* **107**, 69-82.
- Rendl, M., Lewis, L., and Fuchs, E. (2005). Molecular dissection of mesenchymal-epithelial interactions in the hair follicle. *PLoS Biol* **3**, e331.

References

- Reynolds, A. J., and Jahoda, C. A. B. (2004). Cultured human and rat tooth papilla cells induce hair follicle regeneration and fiber growth. *Differentiation* **72**, 566-575.
- Reynolds, A. J., Lawrence, C., Cserhalmi-Friedman, P. B., Christiano, A. M., and Jahoda, C. A. (1999). Trans-gender induction of hair follicles. *Nature* **402**, 33-4.
- Ridley, A. J., and Hall, A. (1992). The small GTP-binding protein rho regulates the assembly of focal adhesions and actin stress fibers in response to growth factors. *Cell* **70**, 389-99.
- Rogers, G., and Hynd, P. I. (2001). Animal models and culture methods in the study of hair growth. *Clinics in Dermatology* **19**, 105-119.
- Rogers, G. E. (2006). Biology of the wool follicle: an excursion into a unique tissue interaction system waiting to be re-discovered. *Exp Dermatol* **15**, 931-49.
- Rubin, M. A. (2001). Use of laser capture microdissection, cDNA microarrays, and tissue microarrays in advancing our understanding of prostate cancer. *J Pathol* **195**, 80-6.
- Sanchez-Carbayo, M., Saint, F., Lozano, J. J., Viale, A., and Cordon-Cardo, C. (2003). Comparison of gene expression profiles in laser-microdissected, nonembedded, and OCT-embedded tumor samples by oligonucleotide microarray analysis. *Clin Chem* **49**, 2096-100.
- Schiller, I., Lu, Z. H., Vaughan, L., Weilenmann, R., Koundrioukoff, S., and Pospischil, A. (2003). Establishment of proliferative cell nuclear antigen gene as an internal reference gene for polymerase chain reaction of a wide range of archival and fresh mammalian tissues. *J Vet Diagn Invest* **15**, 585-8.

- Schinckel, P. G. (1955). The post-natal development of the skin follicle population in a strain of merino sheep. *Australian Journal of Agricultural Research* **6**, 68-76.
- Schinckel, P. G., and Ferguson, K. A. (1953). Skin Transplantation in the Foetal Lamb. *Australian Journal of Biological Science* **6**, 533-546.
- Schinckel, P. G., and Short, B. F. (1961). The influence of nutritional level during pre-natal and early post-natal life in adult Merino sheep. *Australian Journal of Agricultural Research* **12**, 176-202.
- Schlake, T., and Sick, S. (2007). Canonical WNT signalling controls hair follicle spacing. *Cell Adh Migr* **1**, 149-51.
- Schmidt-Ullrich, R., and Paus, R. (2005). Molecular principles of hair follicle induction and morphogenesis. *Bioessays* **27**, 247-61.
- Schmidt-Ullrich, R., Tobin, D. J., Lenhard, D., Schneider, P., Paus, R., and Scheidereit, C. (2006). NF-kappaB transmits Eda A1/EdaR signalling to activate Shh and cyclin D1 expression, and controls post-initiation hair placode down growth. *Development* **133**, 1045-57.
- Scobie, D. R., Nixon, A. J., and Rufaut, N. W. (2006). The biological basis of variation in sheep's fleece cover. *Proceedings of the New Zealand Society of Animal Production* **66**, 124-128.
- Sengel, P. (1975). Feather pattern development. *Ciba Found Symp* **0**, 51-70.
- Shao, Z., Browning, J. L., Lee, X., Scott, M. L., Shulga-Morskaya, S., Allaire, N., Thill, G., Levesque, M., Sah, D., McCoy, J. M., Murray, B., Jung, V., Pepinsky, R. B., and Mi,

- S. (2005). TAJ/TROY, an orphan TNF receptor family member, binds Nogo-66 receptor 1 and regulates axonal regeneration. *Neuron* **45**, 353-9.
- Sharov, A. A., Sharova, T. Y., Mardaryev, A. N., Tommasi di Vignano, A., Atoyian, R., Weiner, L., Yang, S., Brissette, J. L., Dotto, G. P., and Botchkarev, V. A. (2006). Bone morphogenetic protein signaling regulates the size of hair follicles and modulates the expression of cell cycle-associated genes. *Proc Natl Acad Sci U S A* **103**, 18166-71.
- Shi, C. M., Cheng, T. M., Su, Y. P., Mai, Y., Qu, J. F., and Ran, X. Z. (2004). Transplantation of dermal multipotent cells promotes the hematopoietic recovery in sub-lethally irradiated rats. *Journal of Radiation Research (Tokyo)* **45**, 19-24.
- Short, B. F. (1955). Development of the secondary follicle population in sheep. *Australian Journal of Agricultural Research* **6**, 62-67.
- Sick, S., Reinker, S., Timmer, J., and Schlake, T. (2006). WNT and DKK determine hair follicle spacing through a reaction-diffusion mechanism. *Science* **314**, 1447-50.
- Sivachelvan, M. N., Ghali Ali, M., and Chibuzo, G. A. (1996). Foetal Age Estimation in Sheep and Goats. *Small Ruminant Research* **19**, 69-76.
- Sluka, P., O'Donnell, L., and Stanton, P. (2002). Stage specific expression of genes associated with rat spermatogenesis: Characterisation by laser-capture microdissection and real time PCR. *Biology of Reproduction* **67**, 820-828.
- Soria, J. C., Jang, S. J., Khuri, F. R., Hassan, K., Liu, D., Hong, W. K., and Mao, L. (2000). Overexpression of cyclin B1 in early-stage non-small cell lung cancer and its clinical implication. *Cancer Res* **60**, 4000-4.

References

- Srinivasan, M., Sedmak, D., and Jewell, S. (2002). Effect of fixatives and tissue processing on the content and integrity of nucleic acids. *Am J Pathol* **161**, 1961-71.
- Stagliano, N. E., Carpino, A. J., Ross, J. S., and Donovan, M. (2001). Vascular gene discovery using laser capture microdissection of human blood vessels and quantitative PCR. *Ann N Y Acad Sci* **947**, 344-9.
- Stenn, K. S., and Paus, R. (2001). Controls of hair follicle cycling. *Physiological Reviews* **81**, 449-494.
- St-Jacques, B., Dassule, H. R., Karavanova, I., Botchkarev, V. A., Li, J., Danielian, P. S., McMahon, J. A., Lewis, P. M., Paus, R., and McMahon, A. P. (1998). Sonic hedgehog signaling is essential for hair development. *Curr Biol* **8**, 1058-68.
- Strausfeld, U. P., Howell, M., Descombes, P., Chevaleir, S., Rempel, R. E., Maller, J. L., Hunt, T., and Blow, J. J. (1996). Both cyclin A and cyclin E have S-phase promoting activity in *Xenopus* eggs extracts. *Journal of Cell Science* **109**, 1555-1563.
- Su, J. M., Perlaky, L., Li, X. N., Leung, H. C., Antalffy, B., Armstrong, D., and Lau, C. C. (2004). Comparison of ethanol versus formalin fixation on preservation of histology and RNA in laser capture microdissected brain tissues. *Brain Pathol* **14**, 175-82.
- Swan, A. A., Lax, J., and Purvis, I. W. (1995). Genetic Variation in Objectively Measured Wool Traits in CSIRO's Fine Wool Flock. *Proceedings of the Australian Association of Animal Breeding and Genetics* **11**, 516-520.
- Takahashi, T., and Caviness, V. S., Jr. (1993). PCNA-binding to DNA at the G1/S transition in proliferating cells of the developing cerebral wall. *J Neurocytol* **22**, 1096-102.

- Thomas, N. (2002). Bone Morphogenetic Proteins and Hair and Wool Follicle Morphogenesis. Ph.D., University of Adelaide, Adelaide.
- Trempus, C. S., Morris, R. J., Bortner, C. D., Cotsarelis, G., Faircloth, R. S., Reece, J. M., and Tennant, R. W. (2003). Enrichment for living murine keratinocytes from the hair follicle bulge with the cell surface marker CD34. *Journal of Investigative Dermatology* **120**, 501-511.
- Tucker, A. S., Headon, D. J., Courtney, J. M., Overbeek, P., and Sharpe, P. T. (2004). The activation level of the TNF family receptor, Edar, determines cusp number and tooth number during tooth development. *Dev Biol* **268**, 185-94.
- Upton, J. J., Stoyanova, R., Cooper, H. S., Patriotis, C., Ross, E. A., Boman, B., Clapper, M. L., Knudson, A. G., and Bellacosa, A. (2004). Optimized procedures for microarray analysis of histological specimens processed by laser capture microdissection. *J Cell Physiol* **201**, 366-73.
- Van Gelder, R. N., von Zastrow, M. E., Yool, A., Dement, W. C., Barchas, J. D., and Eberwine, J. H. (1990). Amplified RNA synthesized from limited quantities of heterogeneous cDNA. *Proc Natl Acad Sci U S A* **87**, 1663-7.
- Vandesompele, J., De Preter, K., Pattyn, F., Poppe, B., Van Roy, N., De Paepe, A., and Speleman, F. (2002). Accurate normalization of real-time quantitative RT-PCR data by geometric averaging of multiple internal control genes. *Genome Biol* **3**, RESEARCH0034.
- Verfaillie, C. M. (2002). Adult stem cells: assessing the case for pluripotency. *Trends in Cell Biology* **12**, 502-508.

References

- Wang, Y. L. (1985). Exchange of actin subunits at the leading edge of living fibroblasts: possible role of treadmilling. *J Cell Biol* **101**, 597-602.
- Watt, F. (2001). Stem cell fate and patterning in mammalian epidermis. *Current Opinion in Genetics and Development* **11**, 410-417.
- Webb, A., Li, A., and Kaur, P. (2004). Location and phenotype of human adult keratinocyte stem cells of the skin. *Differentiation* **72**, 387-95.
- Weed, M., Mundlos, S., and Olsen, B. R. (1997). The role of sonic hedgehog in vertebrate development. *Matrix Biol* **16**, 53-8.
- Wennerberg, K., and Der, C. J. (2004). Rho-family GTPases: it's not only Rac and Rho (and I like it). *J Cell Sci* **117**, 1301-12.
- Widelitz, R. B., Jiang, T. X., Yu, M., Shen, T., Shen, J. Y., Wu, P., Yu, Z., and Chuong, C. M. (2003). Molecular biology of feather morphogenesis: a testable model for evo-devo research. *J Exp Zool B Mol Dev Evol* **298**, 109-22.
- Xu, X., Lyle, S., Lui, Y., Solky, B., and Cotsarelis, G. (2003). Differential expression of cyclin D1 in the human hair follicle. *American Journal of Pathology* **163**, 969-978.
- Yang, A., Schweitzer, R., Sun, D., Kaghad, M., Walker, N., Bronson, R. T., Tabin, C., Sharpe, A., Caput, D., and Crum, C. (1999). p63 is essential for regenerative proliferation in limb, cranofacial and epithelial development. *Nature* **398**, 714-718.
- Yasuda, M., Takesue, F., Inutsuka, S., Honda, M., Nozoe, T., and Korenaga, D. (2002). Overexpression of cyclin B1 in gastric cancer and its clinicopathological significance: an immunohistological study. *J Cancer Res Clin Oncol* **128**, 412-6.

- Yim, S. H., Ward, J. M., Dragan, Y., Yamada, A., Scacheri, P. C., Kimura, S., and Gonzalez, F. J. (2003). Microarray analysis using amplified mRNA from laser capture microdissection of microscopic hepatocellular precancerous lesions and frozen hepatocellular carcinomas reveals unique and consistent gene expression profiles. *Toxicol Pathol* **31**, 295-303.
- Young, S. S. Y., and Chapman, R. E. (1958). Fleece characters and their influence on wool production per unit area in skin of Merino sheep. *Australian Journal of Agricultural Research* **9**, 363-372.
- Yuan, J., Yan, R., Kramer, A., Eckerdt, F., Roller, M., Kaufmann, M., and Strebhardt, K. (2004). Cyclin B1 depletion inhibits proliferation and induces apoptosis in human tumor cells. *Oncogene* **23**, 5843-52.
- Yue, Z., Jiang, T. X., Widelitz, R. B., and Chuong, C. M. (2005). Mapping Stem Cell Fate in the Feather Follicle. *Nature* **438**, 1026-1029.
- Zhang, M., Brancaccio, A., Weiner, L., Missero, C., and Brissette, J. L. (2003). Ectodysplasin regulates pattern formation in the mammalian hair coat. *Genesis* **37**, 30-7.
- Zhang, Y., Tomann, P., Andl, T., Gallant, N. M., Huelsken, J., Jerchow, B., Birchmeier, W., Paus, R., Piccolo, S., Mikkola, M. L., Morrisey, E. E., Overbeek, P. A., Scheidereit, C., Millar, S. E., and Schmidt-Ullrich, R. (2009). Reciprocal requirements for EDA/EDAR/NF-kappaB and Wnt/beta-catenin signaling pathways in hair follicle induction. *Dev Cell* **17**, 49-61.
- Zhu, Q., Tipoe, G. L., and White, F. H. (1999). Proliferative activity as detected by immunostaining with Ki-67 and proliferating cell nuclear antigen in benign and

References

malignant epithelial lesions of the human parotid gland. *Anal Quant Cytol Histol* **21**, 336-42.

Zwaka, T. P., and Thomson, J. A. (2005). Differentiation of human embryonic stem cells occurs through symmetric cell division. *Stem Cells* **23**, 146-9.